NUREG/CR-6198
TMI V(94)EG01
EGG-2735

TMI-2 Nozzle Examinations Performed at the Idaho National Engineering Laboratory

Manuscript Completed: February 1994
Date Published: March 1994

Prepared by D. W. Akers, B. K. Schuetz

Idaho National Engineering Laboratory
Managed by the U.S. Department of Energy

EG&G Idaho, Inc.
Idaho Falls, ID 83415

Prepared for
Division of Systems Research
Office of Nuclear Regulatory Research
U.S. Nuclear Regulatory Commission
Washington, DC 20555-0001
NRC FIN L1004
Under DOE Contract No. DE-AC07-76ID01570

ABSTRACT

As part of the Three Mile Island Unit 2 (TMI-2) Vessel Investigation Project, under the auspices of the Organization for Economic Cooperation and Development, examinations were performed at the Idaho National Engineering Laboratory on eight nozzles and one guide tube from the TMI-2 reactor vessel. This document describes the examination methodology, summarizes the examination results, and presents interpretations of the results as they relate to the damage to the reactor vessel and to the development of a core relocation scenario. Not all examinations originally proposed as part of this program were completed due to facility problems at the INEL. Consequently, only the results of completed aspects of the examination program are presented.

CONTENTS

LIST OF FIGURES

LIST OF TABLES

EXECUTIVE SUMMARY

The accident at the Three Mile Island Unit 2 (TMI-2) reactor resulted in the relocation of about 19,000 kg of molten core material to the lower head of the reactor vessel. The Vessel Investigation Project (VIP) was formed as a cooperative effort by the Organization for Economic Cooperation and Development (OECD) to assess potential damage to the lower head of the reactor vessel. As part of this project, 14 nozzles and two guide tube segments were removed from the TMI-2 lower head for detailed inspection and microstructural evaluation. The objectives of these examinations were to assess the peak nozzle temperatures near the lower head and to define the mechanisms and extent of nozzle degradation needed to evaluate the challenge to the lower head of the reactor vessel.

Six nozzles were examined at Argonne National Laboratory-East (ANL-E), and eight nozzles and a guide tube were examined at the Idaho National Engineering Laboratory (INEL). The remaining guide tube segment was undamaged and was not examined. In addition, several sections of the INEL nozzles were shipped to CEA-CEN in Saclay, France for examination. Examinations performed at the INEL included visual characterization, gamma spectrometry, sectioning, and optical metallography. Due to facility problems, the examination program was not as extensive as originally planned.

Conclusions of the completed examinations are that some nozzles were melted off, whereas others were only thermally affected by contact with the molten debris. The elevations at which the nozzles were melted off suggests that the molten core debris was on top of a crust of solidified material that apparently insulated the reactor vessel from the hottest debris. The pattern of nozzle degradation was consistent with the location of a hot spot in the TMI-2 vessel at the E7-8/F7-8 location as determined by metallurgical examination of the vessel steel samples.

Evidence of the interaction of molten fuel and the stainless steel and Inconel core structures was found. Interaction phases contained U, Zr, Fe, and other structural materials. Both thermal and chemical interaction products were identified. The finding of significant quantities of control assembly materials (Ag, Cd, In, Zr, Fe, and Cr without U) in the nozzle material and on nozzle surfaces indicates their presence on the lower head prior to the massive relocation of core debris 226 minutes into the accident. This relocation probably occurred as loose debris, which relocated after fuel failure in the upper core region and before the fuel relocation event.

FOREWORD

The contents of this report were developed as part of the Three Mile Island Unit 2 Vessel Investigation Project. This project is jointly sponsored by eleven countries under the auspices of the Nuclear Energy Agency of the Organization for Economic Cooperation and Development. The twelve sponsoring organizations are:

* The Centre d'Etudes d'Energie Nucléaires of Belgium,
* The Säteilyturvakeskus of Finland,
* The Institute de Protection et de Sûreté Nucléaire of the Commissariat à l'Energie Atomique of France,
* The Gesellschaft für Reaktorsicherheit mbH of Germany,
* The Comitato Nazionale per La Ricerca e per Lo Sviluppo Dell' Energia Nucleare e Delle Energie Alternative of Italy,
* The Japan Atomic Energy Research Institute,
* The Consejo de Seguridad Nuclear of Spain,
* The Statens Kärnkraftinspektion of Sweden,
* The Office Fédéral de l'Energie of Switzerland,
* AEA Technology of the United Kingdom,
* The United States Nuclear Regulatory Commission, and
* The Electric Power Research Institute.

The primary objectives of the Nuclear Energy Agency (NEA) are to promote cooperation between its Member governments on the safety and regulatory aspects of nuclear development, and on assessing the future role of nuclear energy as a contributor to economic progress.

This is achieved by:

- encouraging harmonisation of governments' regulatory policies and practices in the nuclear field, with particular reference to the safety of nuclear installations, protection of man against ionising radiation and preservation of the environment, radioactive waste management, and nuclear third party liability and insurance;

- keeping under review the technical and economic characteristics of nuclear power growth and of the nuclear fuel cycle, and assessing demand and supply for the different phases of the nuclear fuel cycle and the potential future contribution of nuclear power to overall energy demand;

- developing exchanges of scientific and technical information on nuclear energy, particularly through participation in common services;

- setting up international research and development programmes and undertakings jointly organized and operated by OECD countries.

In these and related tasks, NEA works in close collaboration with the International Atomic Energy Agency in Vienna, with which it has concluded a Cooperation Agreement, as well as with other international organizations in the nuclear field.

TMI-2 Nozzle Examinations Performed at the INEL

1. INTRODUCTION

The accident at the Three Mile Island Unit 2 (TMI-2) reactor resulted in the relocation of about 19,000 kg of molten core material to the lower head of the reactor vessel. Relocation occurred at about 224 minutes after the reactor scrammed and lasted for about 2 minutes. The Vessel Investigation Project (VIP), a cooperative effort by the Organization for Economic Cooperation and Development (OECD), has the objective of assessing the potential damage to the lower head of the reactor vessel. As part of the VIP, 14 nozzles and two guide tube segments were removed from the lower head for detailed inspection and metallurgical evaluation.

Six nozzles were examined at Argonne National Laboratory-East (ANL-E).[1] Eight nozzles and a guide tube were examined at the Idaho National Engineering Laboratory (INEL). Samples from several INEL nozzles and a guide tube were also examined by CEA-CEN in Saclay, France.[2] The distribution of samples between ANL-E and the INEL was selected so that both laboratories had comparable samples from all sections of the lower head. The purpose of this report is to document the results of the examinations of the INEL nozzles; however, the work performed and results from the INEL samples were limited due to the temporary shutdown of the INEL hotcell facility.

The general objectives of the examinations were to (a) determine peak temperatures of the nozzle materials near the lower head, and (b) assess the mechanisms, and extent of nozzle degradation needed to provide information on the challenge to the lower head of the reactor vessel.

Specific objectives of the examinations were to:

- Determine the nature and extent (axial and radial) of fuel/debris ingress into a nozzle
- Evaluate the nature and degree of chemical and thermal interaction between fuel, debris, and nozzles
- Assess thermal-related metallurgical changes in the nozzle as a function of axial position to evaluate the axial temperature distribution and attempt to quantify temperatures near the vessel
- Determine the position and composition of debris adhering to nozzle surfaces to establish the depth of the debris bed.

The following sections discuss the examination methodology, a summary of the examination results, and the interpretation of the results as they relate to the damage to the reactor vessel.

2. SAMPLE PREPARATION AND EXAMINATION METHODOLOGY

After the nozzles and guide tube samples were removed from the TMI-2 reactor, they were shipped to the INEL, and the nozzles were divided between the INEL and ANL-E. The locations of the nozzle samples on the lower head of the reactor vessel are shown in Figure 1, and Figure 2 shows a schematic of a TMI-2 in-core nozzle. Six nozzles, located at core locations M-9, L-6, H-5, H-8, D-10, and E-11, were examined at ANL-E,[1] and eight nozzles, located at core locations M-10, H-9, L-11, R-7, K-11, K-12, G-5, and E-7, and a guide tube (located at K-5) were examined at the INEL. In addition to the INEL examinations, samples from nozzles E-7, G-5, and R-7, and guide tube K-5 were examined by CEA-CEN in Saclay, France.[2] At both INEL and ANL-E, each nozzle was visually examined and photographed to identify notable areas of damage prior to sectioning. Photographs were taken of the entire external surface, including the bottom and top surfaces. Appendix A describes the photographic method.

Following the visual examinations, each nozzle was characterized using gamma spectrometry to determine the location of radionuclides in the nozzles and to identify locations for sectioning and microstructural examinations. The experimental arrangement for the gamma spectrometry measurements is shown in Appendix A. Spectra were obtained at 0.6-cm intervals from top to bottom of each nozzle using a collimated intrinsic germanium detector system. The Cs-137 activity profile was measured because this activity is expected to be representative of the distribution of UO_2 fuel present in the nozzles. In addition, both Co-60 and gross activity profiles were measured. The Co-60 measurements were performed to determine the location of activated metals that may have relocated from the reactor core to the lower head.

The following criteria were used to determine the sectioning locations for nozzles for destructive analysis:

- Top and bottom locations to obtain information on the hottest (sometimes molten) and coldest (nearest the vessel) temperature extremes in a nozzle
- Fuel/nozzle interaction areas (to assess nozzle degradation mechanisms)
- Indications from gamma scans of fuel penetration into the nozzle
- Obvious locations of surface layers on a nozzle
- Locations of surface cracking (possible nozzle degradation mechanism).

After the nozzle sectioning diagrams were developed and reviewed, the nozzles were placed in tubes and vacuum-impregnated with cold-setting epoxy resin. This was done to stabilize loose surface debris, fragile solidified masses, and internal components. Additional vacuum-impregnation was performed during sectioning if significant voids were found in the epoxy and if there was a possibility of material falling out. After sectioning, microstructural specimens were placed in Bakelite or other mounts, vacuum-impregnated with epoxy resin, and polished. Appendix A describes the examination techniques used.

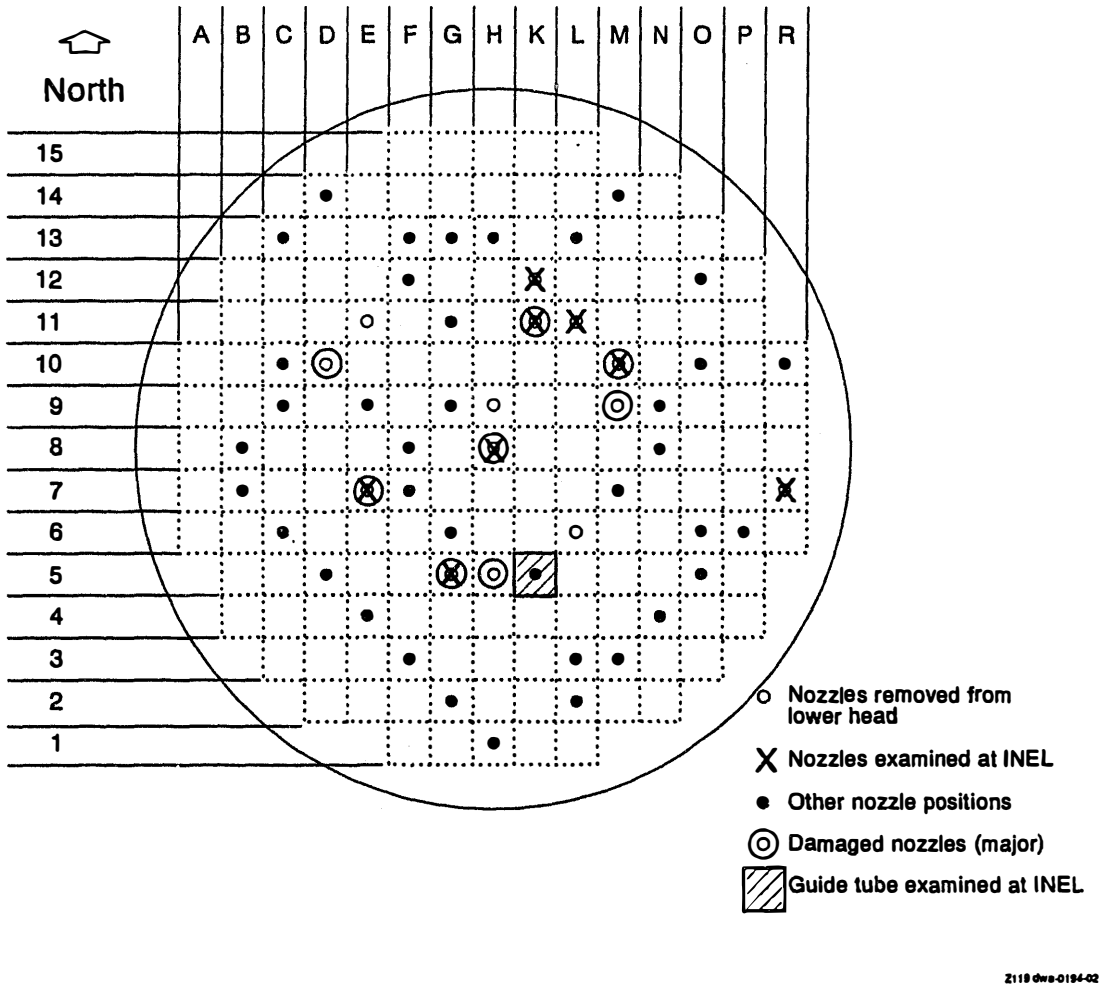

Figure 1. TMI-2 grid locations showing the positions of the lower head nozzles.

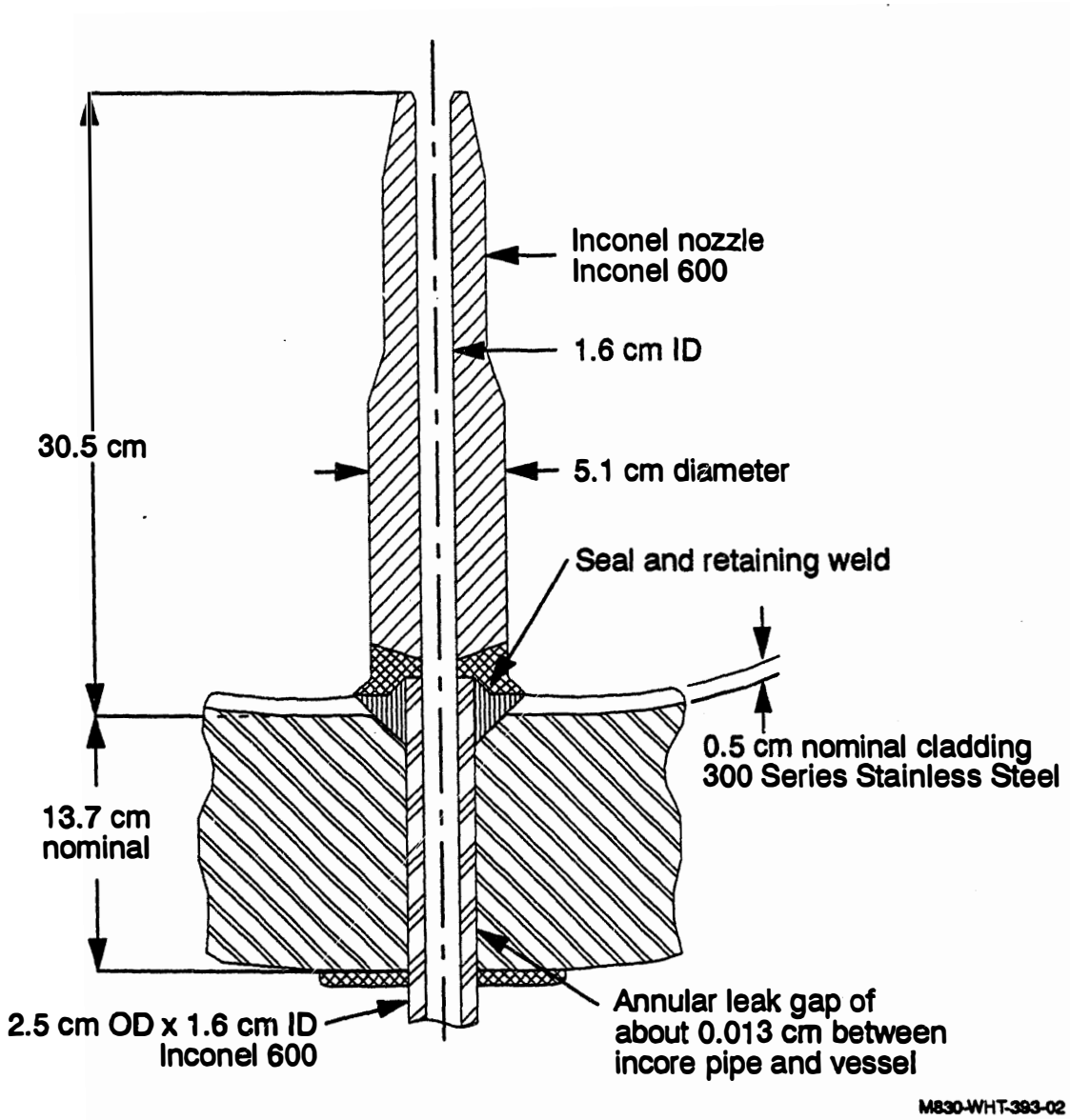

Figure 2. Schematic of a TMI-2 lower head nozzle.

Following destructive sample preparation, the primary analysis techniques used were optical metallography and scanning electron microscopy (SEM) with energy dispersive x-ray (EDS) or wavelength dispersive x-ray (WDS) analyses. The optical metallography analyses were performed to assess the microstructure of deposited fuel debris and the damage to the nozzles. SEM analyses were performed to better assess the microstructure and to determine the distribution of elements and the composition of different phases formed by the interaction of the fuel debris with the nozzle and guide tube material.

3. EXAMINATION RESULTS

The TMI-2 nozzle examinations results that were completed include the photographic examinations, radioactive materials distribution, and some microstructural examinations. Table 1 summarizes the observed damage to each nozzle, nozzle segment lengths, and probing results. Each nozzle was probed with a wire to determine the location of blockages. Detailed photographic and radioactivity distribution data for the nozzles are listed in Appendix B. In addition, Appendix B displays the sectioning diagrams for the nozzles.

Because of the extensive amount of information available from the nozzle and guide tube examinations, only representative data are shown and discussed in this report. Photographs of all samples are shown in Appendix B. Photographs of nozzles R-7, K-11, and E-7 are shown in Figures 3 through 5, and are ordered from the least damage to the most. The K-5 guide tube sample is shown in Figure 6.

Figure 3 shows the R-7 nozzle, on which the instrument string was melted off and a bulb of previously molten fuel was found attached to the instrument string. Visual examination of the R-7 nozzle shows little damage except for the top edge. The gamma spectroscopy results for this sample indicate a high-activity region near the top of the nozzle; however, the probing examinations indicated that there were no blockages in the nozzle. As a consequence, only the bulb on the instrument string and the top of the nozzle were sectioned for examination. The top bulb proved to be composed of U-, Zr-, and Fe-rich interaction phases that are probably representative of the interaction zone between the molten fuel material and the guide tube or instrument string material. A quarter section of the bulb was sent to CEA-CEN for examination. As will be discussed, microstructural examinations of the R-7 bulb indicate apparent interaction between the fuel debris and the instrument string material. Formation of a number of intermediate phases composed of fuel material and constituents of the instrument string are indicated.

Figure 4 shows the K-11 nozzle and the extensive damage to the middle portion with lesser damage to the top and bottom of the nozzle. The nozzle was approximately 235 mm (9.3 in.) long. The major region of damage extends from about 19 mm (0.75 in.) from the bottom to within 76 mm (3 in.) of the top of the nozzle. Gamma spectroscopy analysis of K-11 indicated the presence of high-activity material (fuel) at several locations near the bottom of the nozzle: 20–63 mm (0.8–2.5 in.), 70–100 mm (2.8–4 in.), and 200–230 mm (8–9 in.). These data suggest that fuel penetrated through most of the nozzle. A probe of the nozzle was performed from both the top and the bottom. Both probes were able to penetrate to the breach near the center of the nozzle. Sections were removed from the K-11 nozzle from the locations indicated in the gamma

Table 1. Nozzle and Guide Tube Descriptions.

Location	Length (cm)	Description
E-7	1.3 to 1.6 (variable)	Nozzle E-7 was severely damaged. A thin section of nozzle was partially molten. In Figure 5, it can be seen that a crack extends all the way through one wall of the nozzle. Probe results: Not applicable.
G-5	4.4	Only a short section of the nozzle remained, with melt ingress into the instrument string hole. Instrument string visible. Probe results: The nozzle was completely filled with melt. It could not be determined if melt penetration ends above or below the original cut location.
H-9	23.5	The H-9 nozzle exhibits very little damage. The instrument core string is still intact. Probe results: No blockage discovered.
K-11	23.5	The K-11 nozzle sustained major damage. The entire thickness of the wall was melted away on one side, and it exhibits slumping (bending) at about mid-length of the nozzle. It was the only nozzle found showing undercutting (see Figure B-32). Probe results: A wire probe was performed from both ends of the nozzle section, and although narrowing of the interior diameter was noted, no blockage was encountered.
K-12	24.4 25.7 (w/string)	The K-12 nozzle exhibited almost no visible damage. The activity profile shows that K-12 exhibits twice the relative activity along almost the entire length than does any other nozzle. Probe results: No blockages were detected.
L-11	22.9	Nozzle L-11 was undamaged, except for a 51-mm (2-in.) region that showed minor damage at the shoulder of the nozzle. Probe results: No blockages were detected.

Table 1. (continued).

Location	Length (cm)	Description
M-10	17.1	The M-10 nozzle exhibited severe melt damage to the top 64 mm (2.5 in.) of the nozzle. The uppermost portion of nozzle appears to have been sheared off. Probe results: An assay of the melt penetration depth determined the blockage to exist to within 57 mm (2.25 in.) from the bottom (butt) end. The base of the melt blockage was of varying depths. Examination of Figure B-8 reveals melt interaction with the interior wall and the instrument core string of the nozzle.
R-7	23.2 (with melt bulb removed)	The initial nozzle condition showed a melt bulb [~16-mm (~0.625-in.) diameter] attached to the instrument core string and minor melt damage to the top of the nozzle. Probe results: No blockages were detected.
K-5 (guide tube) (MPR-5-24)	23.8 (maximum) 14.9 (minimum)	The K-5 guide tube sustained severe bottom end damage. The edges indicate extensive melt interaction, being deformed outwards. Guide tube material was much harder than the as-fabricated stainless steel. Probe results: Not applicable.

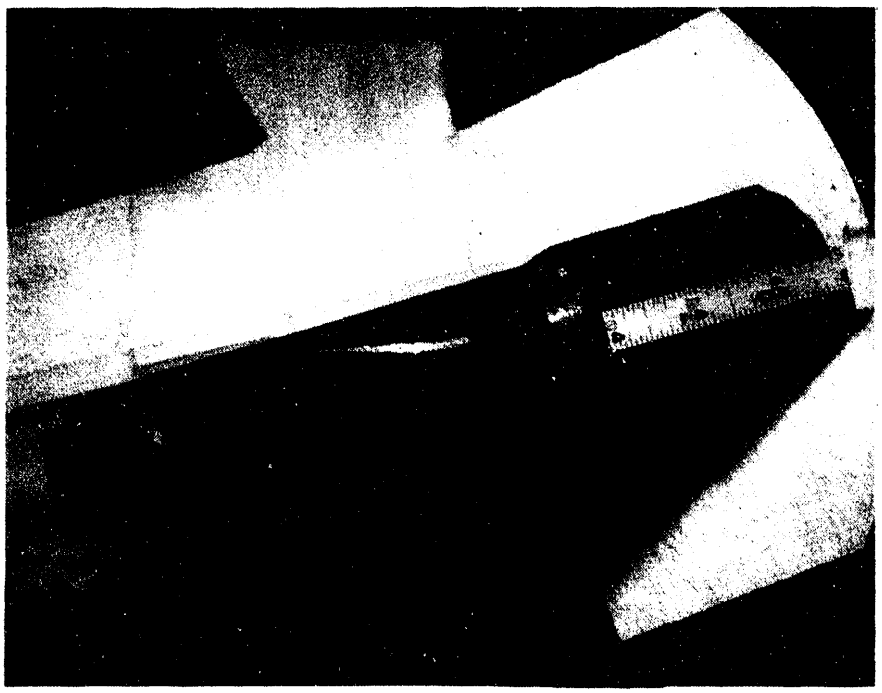

Figure 3. R-7 nozzle sample.

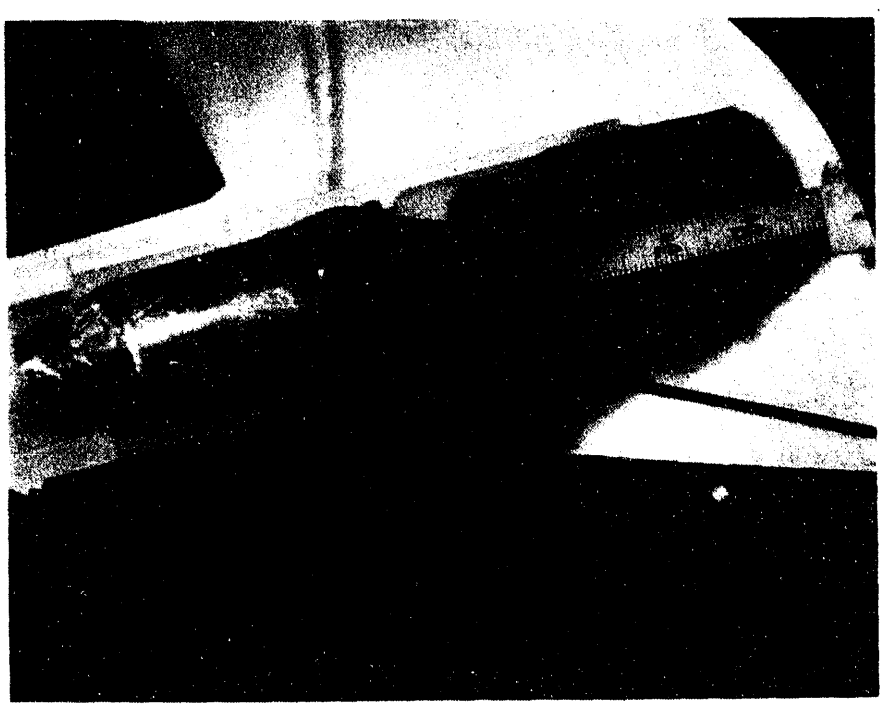

Figure 4. K-11 nozzle sample.

Figure 5. E-7 nozzle sample.

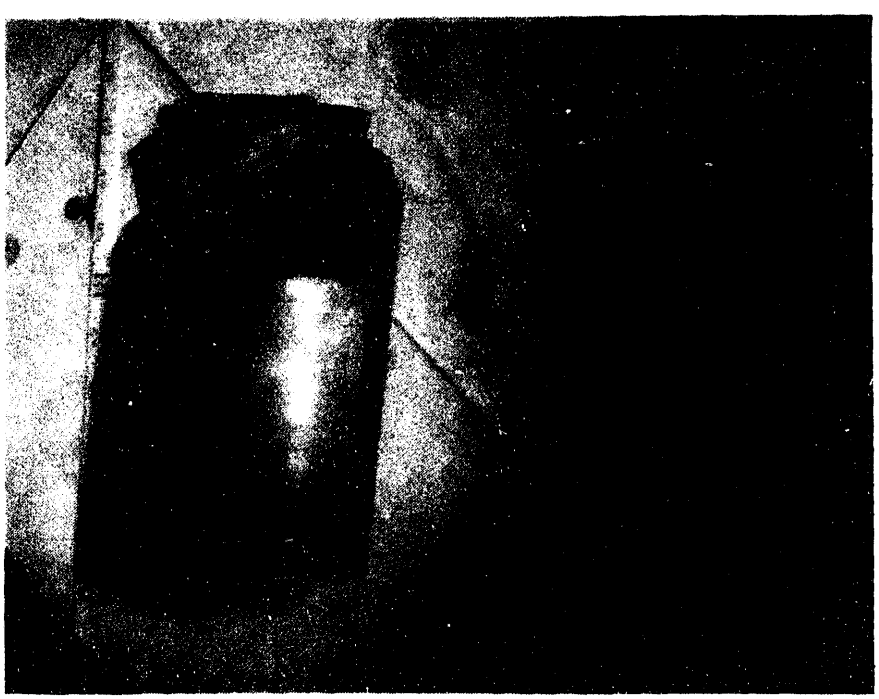

Figure 6. K-5 guide tube sample.

scan analyses (i.e., near the bottom, the mid-plane, and the top of the nozzle). Fuel probably entered the nozzle through holes near the midplane.

Very little of the E-7 nozzle, as shown in Figure 5, remained after being removed from the lower head. The original length of the nozzle stub was about 51 mm (2 in.); however, after the stub was cut, it was about 16 mm (0.63 in.) long. Under close examination, it can be seen that a crack extends entirely through one side of the nozzle. Gamma spectroscopy was not performed on this nozzle because sectioning locations did not need to be determined. One section of this nozzle was sent to CEA-CEN for examination.

As shown in Figure 6, the K-5 guide tube suffered substantial damage at the lower end. The damaged edges created by melt interaction are slightly twisted outward. The original diameter of the guide tube was about 117 mm (4.6 in.); the remaining length on the longest side was 238 mm (9.4 in.), while the remaining length on the shortest side was only 149 mm (5.9 in.). The K-5 guide tube did not need to be gamma scanned or probed because the sample location was determined from visual examination of the nozzle section. As discussed in Appendix C, apparent molten fuel material interacted with the stainless steel of the guide tube and melted into its surface. In most cases, the clear separation between the stainless steel and the fuel material phases suggests that the mechanism for this interaction appears to be melting of the stainless steel with no apparent chemical interaction. However, Figure C-8 shows the presence of an apparent intermediate phase that may be the result of a dissolution of the stainless steel by the fuel debris.

The very bottom of the guide tube was cut transversely, at a depth of approximately 19 mm (0.75 in.). It was very difficult to section this sample, and an MPR Associates technician indicated that the damaged guide tube material was much harder to cut than as-fabricated stainless steel.

In all cases, where nozzle or guide samples were obtained, they were subjected to a series of optical and SEM EDX/WDX examinations. The microstructural data are shown in Appendix C. Observations from these measurements are the following:

- Melt was attached to many surfaces and had interacted with the K-5 guide tube material
- Interactions occurred between liquid fuel material and the R-7 nozzle material.

Only limited SEM/EDX/WDX work was performed. Samples that were examined consisted of surface material from the tops of nozzles R-7, E-7, G-5, and M-10. A wide range of interactions between these materials was observed. Some SEM/WDX dot map data from these samples are shown in Appendix D.

4. CONCLUSIONS

The results of the examinations indicate that some nozzles were melted off by interaction with molten core debris, whereas others were only thermally affected by contact with core debris, some of which attached themselves to nozzle surfaces. The elevations at which the nozzles were melted off suggest that the liquid core debris was on top of a crust of solidified material that apparently insulated the reactor vessel from the hottest debris. The pattern of nozzle degradation was consistent with the location of a hot spot in the TMI-2 vessel at the E7-8/F7-8 location as

determined by metallurgical examination of the vessel steel samples.[3] The basal crust of the material insulated the vessel and the lower portions of the nozzles. The finding of significant quantities of control assembly materials (Ag, Cd, In, Zr, Fe, and Cr without U) in the nozzle material and on nozzle surfaces indicates their presence on the lower head prior to the massive relocation of core debris 226 minutes into the accident.

5. REFERENCES

1. L. A. Neimark, T. L. Shearer, A. Purohit, and A. G. Hins, *TMI-2 Instrument Nozzle Examinations at Argonne National Laboratory*, TMI V(93)AL01, OECD-NEA-TMI-2 Vessel Investigation Project, February 1993.

2. M. Trotabas, M. Perrot, and P. Winter, "TMI-2 Instrument Nozzle and Guide Tube Examinations at Saclay," Presentation to the TMI-2 Project Review Group, Bethesda, MD, November 12-13, 1992, TMI V(92)FO01, OECD-NEA-TMI-2 Vessel Investigation Project, CEA/DRN/DMT 93/479.

3. G. E. Korth, *Metallographic and Hardness Examinations of TMI-2 Lower Pressure Vessel Head Samples*, TMI V(92)EG01, OECD-NEA-TMI-2 Vessel Investigation Project, January 1992.

Appendix A

Examination Techniques

Appendix A

Examination Techniques

This appendix presents a brief overview of techniques used during examination of the TMI-2 nozzle and guide tube samples, including physical, optical metallography, scanning electron microscopy, chemical, and radiochemical examinations.

A.1 Physical Examinations

Physical examinations included visual/photographic and radiation field examinations, each of which are discussed in this section.

A.1.1 Visual/Photographic

Each nozzle and guide tube was examined, and its appearance and size were recorded. A 35-mm single lens reflex camera body was attached to a Kollmorgen periscope at the camera port. A "data back" as part of the camera door was used to record a number on the negative, and a camera log was used to track each photograph. A scale was placed alongside each sample to determine the magnification of the photograph. In some cases, the samples were photographed from different orientations to give an overall view of the damage sustained.

A.1.2 Radiation Field

Beta/gamma and gamma radiation levels on the nozzles and guide tubes were measured with a teletector probe during a transfer from one cell to another. Most of the nozzles exhibited high radiation levels, with initial readings ranging from 1 to 100 R/hr beta-gamma at contact.

A.2 Microstructural Examinations

Optical metallography was used and involved viewing highly polished samples with a light microscope at magnifications up to 500x. The samples were often treated with etchants to highlight grain boundaries and second phases.

Small samples were mounted in 31.8-mm (1.25-in.) brass mounts. A brass holder (shown in Figure A-1) was used to contain each sample in a lead/bismuth alloy. The alloy was melted (melting point 123.9°C) in a metal beaker and then poured into a preheated brass mount. Each sample was positioned so that its examination surface was held level with the lead/bismuth surface and allowed to set up for 24 hours.

Large samples that did not fit in a brass mount were mounted on an aluminum plate with a 127-mm (5-in.) ID aluminum ring (see Figure A-2). The samples were then placed with the examination surface facing the plate. Epoxy resin, mixed with hardener [Jeffamine (polyoxpropulene diamine)], was poured around the samples. The mounts were then inserted into

a vacuum chamber to impregnate the samples with epoxy. The epoxy was allowed to cure for approximately 72 hours.

The following grinding and polishing sequence was used for the TMI-2 lower head nozzles and guide tubes:

1. Course grind with water-lubricated silicon carbide 120-grit paper with a whirlamat.

2. Medium grind with 240- and 400-grit paper. Wash the sample between grit sizes.

3. Final grind with 600-grit paper.

4. Initial polish with 6-μm diamond grit in mineral oil-type fluid on a hard paper with a whirlamat.

5. Final polish with 3-μm diamond grit in mineral oil on a short nap nylon cloth.

In general, a swab-etching was used, with the etching time varying, depending on whether a heavy or light etch was appropriate. A fuel etchant of 85% H_20_2 and 15% H_2S0_4 was used because most of the damage observed from nozzle and guide tube examinations involved a ceramic melt with urania content.

A.3 Scanning Electron Microscopy

Scanning electron microscopy (SEM) examinations were performed to determine the physical and chemical states of the lower head components. The high-image resolution and small scanning area of the SEM analysis complemented the optical metallography, allowing detailed examination of specific sample areas that were identified from the metallographic analysis to be important. Energy dispersive x-ray (EDS) and wavelength dispersive x-ray (WDS) analyses were used to acquire elemental composition data, which identify core thermodynamic properties (e.g., peak temperatures).

In SEM, a finely focused electron beam is swept in a raster across the surface of a sample. The types of signals include secondary electrons, backscattered electrons, and characteristic x-rays. The primary signal of interest is the variation in secondary electron emission that occurs from differences of the surface topography. The secondary electrons are collected by a scintillator-photomultiplier system, and the resultant signal is displayed on a cathode-ray tube. The scanning electron beam is synchronized with the scanning of the cathode-ray tube such that images can be presented on a storage oscilloscope or a monitor oscilloscope for photographing.

This procedure was also used for backscattered electron (BSE) images. Backscattered electrons are electrons that undergo elastic collisions within the sample and ultimately escape. A significant portion (~30%) of the beam electrons escape, resulting in the backscattered electron signal. These electrons, because of their higher energy, originate from deeper in the material than do secondary electrons. Because the efficiency of the scattering process is dependent on the electron density (atomic number), the primary advantage of BSE images is that they contain information on the relative densities of phases in the examined material. This differentiates

between elements of low and high atomic numbers by the brightness displayed on the screen. Those phases with high average atomic numbers are displayed as light areas, while phases with low atomic numbers appear as dark areas.

A.3.1 Energy-Dispersive X-Ray Spectroscopy

Energy-dispersive x-ray spectroscopy (EDS) analysis is performed by measuring characteristic detectable x-rays from elements above atomic number 10 that are excited by a scanning electron beam. The beam is typically 1 μm in diameter, but scattering produces x-rays over a region up to 10 times wider. SEM/EDS systems are very convenient for quickly surveying areas for elemental content and spectral uniformity, and produce high-quality images and photographic records. Other advantages include the low beam energy and the relatively low operating vacuum, both of which limit the absorption of deposited molecules. However, the usefulness of this instrument is reduced by its susceptibility to background radiation, its inability to detect oxygen and carbon, and its inability to provide binding energy information.

The limit of detection for most elements for the SEM/EDS is between 0.5 and 5 wt% under ideal conditions; however, radioactivity can drastically affect the signal-to-noise ratio for the SEM analysis, depending on the magnitude of the radiation field present. Therefore, elements that exist in the sample at concentrations of less than 1 to 2 wt% may not be detected by SEM analysis.

A.3.2 Wavelength-Dispersive X-ray Spectroscopy

Wavelength-dispersive x-ray spectroscopy (WDS) is similar to EDS except that the x-rays generated by the electron beam are separated by wavelength through a diffracting crystal, and a gas-filled proportional counter is used as the detector. The detector is physically scanned across the spectrum of diffracted x-rays and generates a signal on a point-by-point basis. Acquisition is slow, but WDS provides a very high resolution spectrum.

WDS was used to provide elemental data of two types: qualitative x-ray dot maps, and spectra for quantitative analysis. Dot maps are produced by tuning the spectrometer to the element signal peak of interest and rastering the electron beam across the area. Spectrometer output is correlated to beam position, and a picture of the area is constructed in which relative brightness corresponds to beam-generated x-ray intensity, and thereby to the concentration of the element. The images show the relative distribution of elements in the area.

WDS can be used to ascertain precise elemental compositions in very small (<10 μm) regions of the sample. The procedure for obtaining quantitative information from WDS spectra consists of comparing, for a given element in a phase of unknown composition, the intensity of the characteristic x-ray against a well-characterized standard. However, the atomic processes of electron beam/material and x-ray/material interaction are extremely complex, and accurate quantitative analyses can be achieved only by correcting for these effects. This is especially important for material of highly dissimilar constituents such as heavy metal oxides.

A.4 Gamma Spectrometry Examinations

Gamma spectrometry was used to scan along the length of six TMI nozzles (H-9, K-11, K-12, L-11, M-10, and R-7) to determine radioactivity profiles and to identify locations of fuel interactions in or on the nozzles. Based on the presence of any high concentrations of radioactivity, sectioning was performed.

The equipment used consisted of an ORTEC intrinsic germanium detector, a Davidson multichannel analyzer, and a lead collimator. The scanning apparatus was completely surrounded by 102 mm (4 in.) of lead shielding, reducing the transmission of gamma rays beyond the shield and to the operator to approximately 0.1% (for Cs-137). The procedure for the TMI-2 nozzle gamma scanning was the following:

1. Establish a Zone III at the rear of Cell #2.

2. Construct the gamma scanning setup as illustrated in Figure A-3. This setup alleviates the need for any entries into Zone III during the scanning process and reduces or eliminates any radiation/contamination exposure.

3. After the gamma scanning setup is assembled, open the rear port and insert the square aluminum pipe into the cell. With the pipe in place, insert the sample holder into the pipe and push it into the cell using the push rod.

4. From the front of Cell #2, identify and remotely place the TMI-2 nozzle into the push rod.

5. From outside the cell, pull the pushrod, dragging the sample holder through the square aluminum pipe until it reaches the detector/sample shield. Once in the shield, it may take a few minutes to verify the alignment of the nozzle with the collimator in the detector assembly.

The nozzles were scanned with a germanium detector (PG-3) and a Davidson multichannel analyzer. Regions of interest were selected for the Cs-137 photopeak, the region that includes the two Co-60 photopeaks, and the entire spectrum from approximately 400–1,350 KeV. Each position was scanned for 60 seconds, live time. After scanning each position of each nozzle, the gross counts for each region of interest were tabulated. The tabulated data were then background subtracted and plotted with no decay corrections included. All six nozzles were scanned in the same geometry, from the base (large-diameter end closest to the lower head) to the tip, in 6.4-mm (0.25-in.) increments. The data points associated with the scan position of each nozzle are within 3.2 mm (0.125 in.) of the actual position.

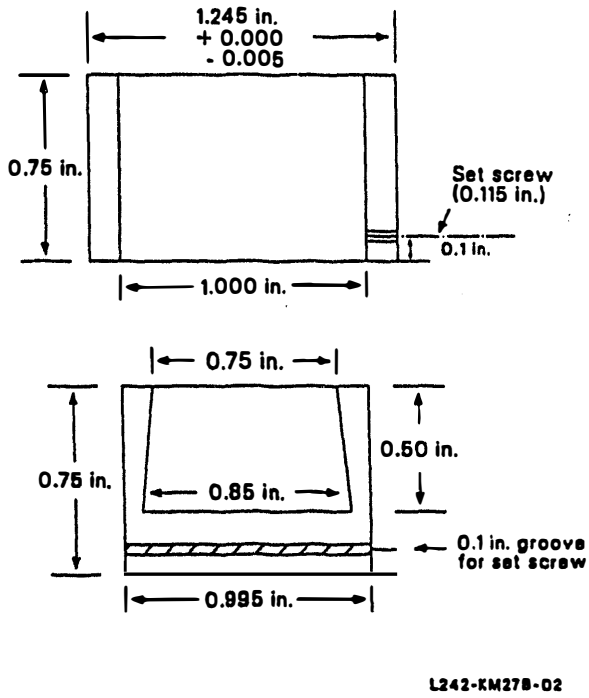

Figure A-1. Schematic drawing of 1-1/4-in. metallographic mount.

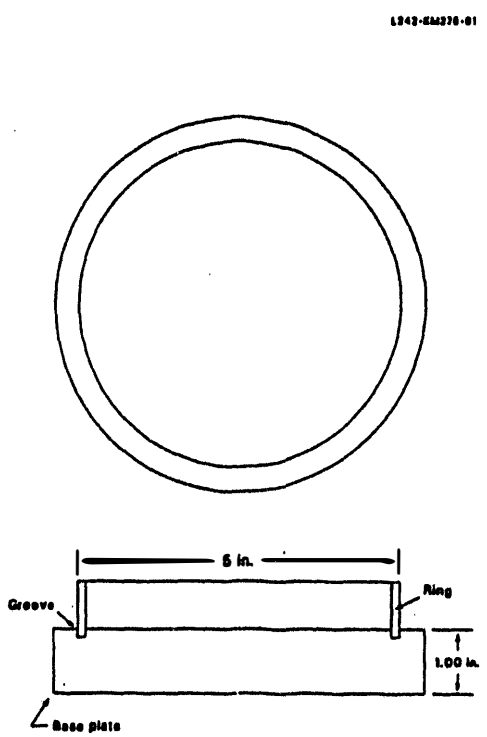

Figure A-2. Schematic drawing of 5-in. metallographic mount.

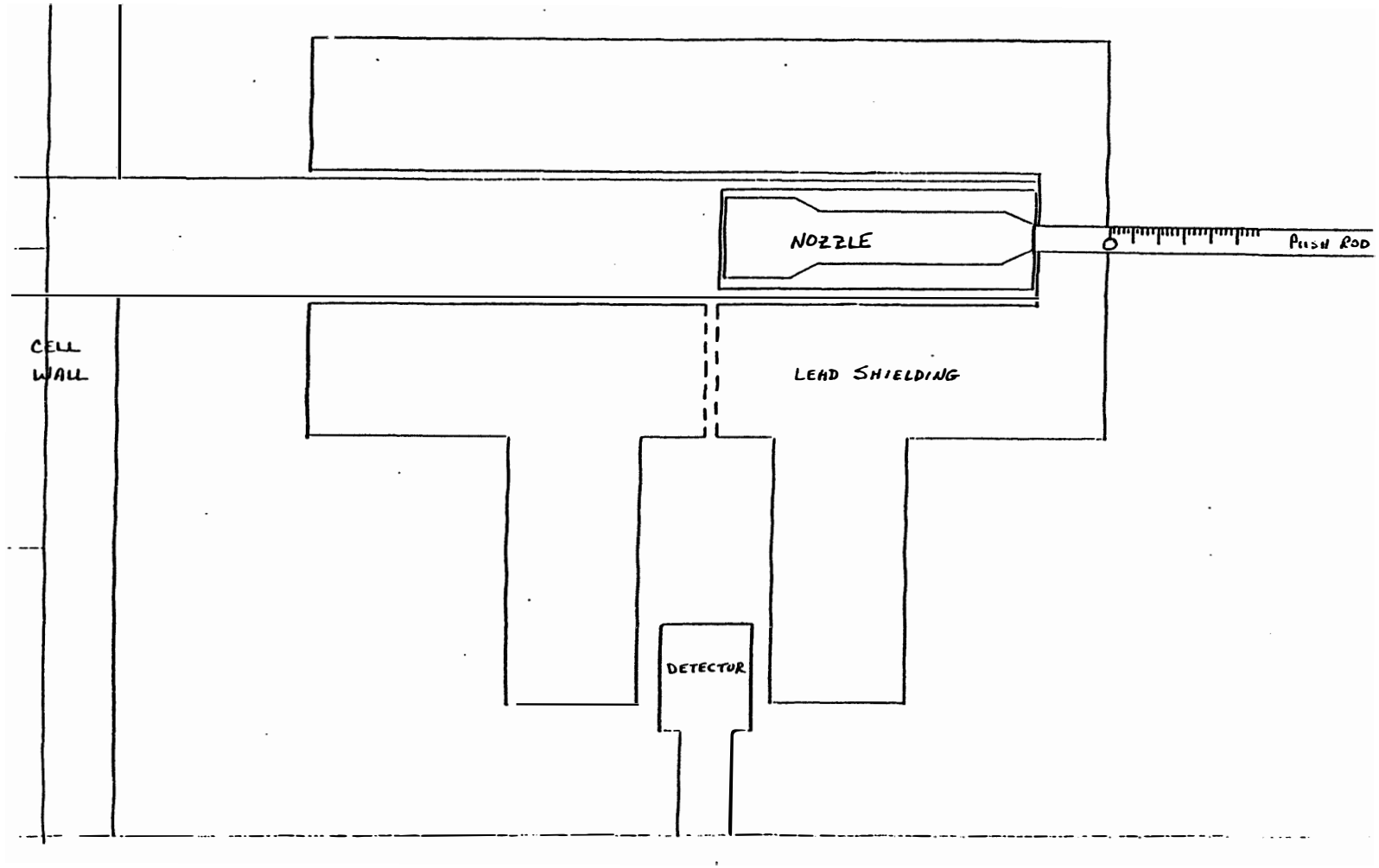

Figure A-3. Sketch of TMI-2 nozzle gamma-scanning apparatus.

Appendix B

Visual and Gamma Spectrometry

Appendix B

Visual and Gamma Spectrometry

Visual examinations and activity profiles are addressed in this appendix. The TMI-2 nozzles were examined visually to determine the overall damage they sustained, including melt interaction, melt penetration, cracking, and shearing. Various perspectives and angles of rotation were used during macrophotography.

Radioactivity profiles were obtained for six of the TMI-2 nozzles (H-9, K-11, K-12, L-11, M-10, and R-7). Each nozzle was loaded into the detector assembly with its base aligned with the collimator, and was counted in 1.9-cm (0.75-in.) increments for a specified period of time. As each nozzle advanced through the assembly, the gross area counts of the Cs-137, Co-60, and full-spectrum photopeaks were recorded for each position. Activity profiles were developed using the gamma scan data by plotting nozzle position (x-axis) versus the gross area counts (y-axis).

For the sectioning examinations, cutting locations on each nozzle were determined by using the photopeaks of activity profiles and observations of damaged regions and melt interaction zones noted in the visual examinations.

B.1 M-10 Nozzle

An initial examination of the M-10 nozzle was performed on a small fragment broken from its tip, where the material and melt interaction were greatest. This fragment was mounted in brass and subjected to analysis by SEM. The results from this analysis are reported in Appendix D.

Figure B-1 is a full-length view of the M-10 nozzle. It was measured to be 17.1 cm (6.75 in.) long. Figure B-2 is a magnified view of the material and melt interaction on the tip of the nozzle.

The activity profiles for the M-10 nozzle, which were obtained by plotting the data found in Table B-1, indicated high activity regions at approximately 5.7 cm (2.25 in.) and 15.2 cm (6 in.) (see Figures B-3 through B-5). It is interesting to note that Cs-137 is high at the lower elevation, whereas Co-60 is high at the upper elevation.

A probe test of M-10 was conducted by inserting a wire into the bottom end of the nozzle. The result of the test indicated that melt had plugged the nozzle to within 5.7 cm (2.25 in.) of the bottom end. Using the gamma scan data and penetration test information to identify regions of interest, the nozzle was sectioned as shown in Figure B-6. A transverse cut was made at the nozzle tip creating a section 1.9 cm (0.75 in.) thick. This section was then cut longitudinally, creating two samples, M-10-1A and M-10-1B. The second transverse cut was made in a location 4.8 cm (1-7/8 in.) from the bottom end. After this section was cut from the nozzle, the instrument core string was inspected; it appeared to be undamaged. Interior damage, however, was noted on the upper surface. A third transverse cut was made at a distance of 6.7 cm

(2-5/8 in.) from the bottom end. This created a 1.9-cm (0.75-in.) section, sample M-10-2, for which a top and 0-degree reference was maintained.

After examination of these unpolished sample sections, it was determined that both samples M-10-1A (see Figure B-7) and M-10-1B (see Figures B-8 and B-9) would yield more information if they were mounted and polished longitudinally. Section M-10-2 was mounted and polished on the transverse surface (see Figures B-10 and B-11). The results of these examinations are discussed in Appendix C.

B.2 H-9 Nozzle

A visual examination of the H-9 nozzle (see Figure B-12) showed that it was approximately 241 mm (9.5 in.) long and had sustained very little obvious damage. Inspection of the top of the nozzle showed that the instrument core string was still intact, as shown in Figure B-13. Figures B-12 and B-13 show the front (0 degrees) and back surface (180 degrees) of the nozzle, respectively.

The gamma scan data listed in Table B-2 were used to obtain the activity profile plots shown as Figures B-14 through B-16. The differences between the first and last scan positions seen on the full-spectrum plot (Figure B-16) are probably due to improper alignment in the sample holder. Inspection of the activity profiles indicates high activity regions at approximately 5.1 cm (2 in.) and 14 cm (5.5 in.) from the base.

A probe test was performed on the H-9 nozzle, but no blockage was discovered. Using the indications obtained from the gamma scan results, sectioning was performed on the nozzle as shown in Figure B-17. A transverse cut was made 13.3 cm (5.25 in.) from the bottom of the nozzle. The second transverse cut was located about 15 cm (6 in.) from the bottom, creating a transverse section approximately 0.75 in. (1.9 cm) thick. A top reference was maintained. This transverse section was then cut longitudinally, producing sample H-9-1, which was mounted to examine the transverse (cross-sectional) surface, and producing sample H-9-2, which was mounted to examine the longitudinal surface with the top reference being maintained.

B.3 Nozzle L-11

The L-11 nozzle (see Figure B-18) was about 22.9 cm (9 in.) long and appeared to be undamaged except for a 5.1-cm (2-in.) region at the shoulder of the nozzle. The high activity region extended from 5.1 cm (2 in.) to 10 cm (4 in.) at the bottom end.

The activity profile plots (see Figures B-19 through B-21), which were obtained from the L-11 gamma scan data in Table B-3, indicate a high activity region 5.1 cm (2 in.) to 10 cm (4 in.) from the bottom end of the nozzle.

A probe of the nozzle was conducted, but no blockage was found. From a comparison of the gamma scan results and the visual inspection, the cutting locations were determined, as shown in Figure B-22. The first transverse cut was made 7.6 cm (3 in.) from the bottom end of the nozzle. The nozzle was cut again to produce a section 1.9 cm (0.75 in.) thick. While maintaining

the identification of the top surface, another cut was made longitudinally, producing sample L-11-A, which was mounted to show the longitudinal surface, and sample L-11-B, which was mounted and polished to show the transverse surface (cross section) of the nozzle.

B.4 Nozzle R-7

Figure B-23 shows a full-length view of the R-7 nozzle with the melt bulb and instrument core string intact. A visual examination of the nozzle indicated that it had sustained little damage except on the top surface of the nozzle as shown in Figure B-24.

Initially, a small sample from the melt bulb at the top of the instrument core string on the R-7 nozzle was submitted for SEM analysis. The results from this analysis can be found in Appendix D. A full-length photo of the nozzle after the bulb had been removed for examination is shown in Figure B-25. The detached melt bulb was submitted for optical metallography and SEM analysis. A one-quarter section of the melt bulb was cut and sent to CEA-CEN in France.

Although the base of the nozzle had an uneven surface, it was 23.2 cm (9-1/8 in.) long (after melt bulb removal). Gamma scan data for the nozzle, listed in Table B-4, were used to plot the activity profiles (Figures B-26 through B-28). These showed high activity regions at approximately 11.4 cm (4.5 in.) and at 19 to 23 cm (7.5 to 9 in.) from the base.

No blockages were found during the probe of the nozzle. Based on the visual and gamma scan data, the nozzle was sectioned at 1.9 cm (0.75 in.) from the top surface, as shown in Figure B-29. The resulting 1.9-cm (0.75-in.) sample was then cut longitudinally. The top surface reference was maintained. One-half of the sample was mounted to show the longitudinal surface.

B.5 Nozzle K-11

A visual examination and measurement of the K-11 nozzle showed that it was 23.5 cm (9-1/4 in.) long and suffered extensive damage to the majority of its surface. Figures B-30 and B-31 are full-length views of the front (0-degree) and back (180-degree) surface, respectively. They give an overall view of the K-11 nozzle. The major damage extends from about 1.9 cm (0.75 in.) from the bottom end to within 7.6 cm (3 in.) of the top of the nozzle. A magnified view of the top of the nozzle shows cracking and melt interaction (see Figures B-32 and B-33, which show the 0- and 180-degree reference views, respectively).

The gamma scan data listed in Table B-5 were used to plot the activity profiles, which are shown in Figures B-34 through B-36. Analysis of these plots indicates regions of interest at locations 1.9 to 5.7 cm (0.75 to 2.25 in.), 6.4 to 10 cm (2.5 to 4 in.), and 20 to 23 cm (8 to 9 in.) from the bottom of the nozzle.

The nozzle was probed for blockage from the bottom end. Although narrowing of the interior diameter was noted, the wire could be seen in the exposed center of the nozzle, and no blockage was found. A penetration test was also performed from the top end of the nozzle, and no blockage was found.

Gamma scan data and visual inspection were used to determine cutting locations on the K-11 nozzle as shown in Figure B-37. A white marker line extending the length of the nozzle was used to maintain a 0-degree reference. The first cut was made 3.2 cm (1-1/4 in.) from the bottom end, and the second cut was made 1.5 cm (0.6 in.) above the first cut, creating sample K-11-1. A third cut was made 7.6 cm (3 in.) from the bottom, followed by a fourth cut, which produced a 19-mm (0.75-in.) section identified as K-11-2. A fifth cut created sample K-11-3. The remaining nozzle section was rotated, and two more cuts were made approximately 4.1 cm (1.6 in.) and 5.7 cm (2.25 in.) from the tip of the nozzle, creating sample K-11-4.

Each of the above samples, K-11-1, -2, -3, and -4, were sectioned longitudinally along the 0-degree reference line. Zero-degree and top-reference orientations were maintained throughout the process by using rough sketches of the sample sections to record cutting details. Sample K-11-1 was cut to produce sample K-11-1A, which was not mounted, and sample K-11-1B, which was mounted and polished to show the longitudinal surface. Sample K-11-2 was cut into sample K-11-2A (see Figure B-38), which was mounted to show the longitudinal surface, and sample K-11-2B (see Figure B-39), which was mounted to show the transverse surface. Sample K-11-3 was cut longitudinally, creating sample K-11-3A (see Figure B-40), which was mounted to show the transverse surface, and sample K-11-3B (see Figure B-41), which was mounted to show the longitudinal surface. One-half of sample K-11-4 was mounted to show the longitudinal surface (sample K-11-4A).

B.6 Nozzle G-5

The G-5 nozzle (see Figure B-42) was approximately 4.4 cm (1.75 in.) long and was severely damaged. As shown in Figure B-43, melt was attached to the nozzle and its center was completely plugged with melt.

This nozzle was not subjected to gamma spectroscopy because it was so short. Since the nozzle was completely plugged with melt, any cutting location would have provided melt interaction information. As shown in Figure B-44, the first cut was transverse, approximately 1.9 cm (0.75 in.) from the top of the sample. The resulting segment was then cut longitudinally. One-half was mounted to show the longitudinal surface; the other half was cut into a rectangular-shaped section and shipped to CEA-CEN in France.

B.7 Nozzle E-7

As shown in Figure B-45, approximately 5.1 cm (2 in.) of the E-7 nozzle was all that remained on the lower head after the shearing that occurred during the accident. The sample section removed was only 0.5 to 0.6 in. (1.3 to 16 cm) long. A crack extending entirely through one side of the nozzle was also observed.

Gamma spectrometry was not performed on this nozzle because it was so short. After the sample was cut longitudinally, one of the halves split in two because of the crack that extended through the nozzle, leaving three sections. A pie-shaped segment was cut from the second largest of the three portions and shipped to CEA-CEN in France. The largest of the samples was cut twice longitudinally, creating sample E-7-1, which was mounted to show the longitudinal surface,

and sample E-7-2, which was prepared for examination of the transverse (top) surface. A sectioning diagram for nozzle E-7 is shown in Figure B-46.

B.8 Nozzle K-12

The K-12 nozzle sustained very little damage, as illustrated in Figures B-47 and B-48, (0- and 180-degree rotation, respectively). An identifying notch can be seen at the base of the nozzle in Figure B-47. The nozzle was 25.7 cm (10-1/8 in.) long with the instrument string and 24.4 cm (9-5/8 in.) long without the string.

The activity profiles plotted from the gamma scan data in Table B-6 show high levels of activity along the entire length of the K-12 nozzle. Activity peaks at greater than 1,400,000 counts (see Figures B-49 through B-51) are almost double the relative activity of any other nozzles that were gamma-scanned. The possible explanation for this high activity is that there is a significant amount of surface-deposited activity.

A probe wire was inserted into the bottom end of the nozzle, and no blockages were detected. Since no specific regions of interest were indicated by examination, random sectioning locations were chosen, as seen in Figure B-52. The first transverse cut was made 5.1 cm (2 in.) from the bottom end of the nozzle. A second cut was made 7.0 cm (2.75 in.) from the bottom, producing sample K-12-1. This sample was then sectioned longitudinally, producing sample K-12-1A, which was mounted to show the transverse surface, and sample K-12-1B, which was mounted to show the longitudinal surface. A top reference was maintained during the cutting process.

B.9 Guide Tube K-5

The K-5 guide tube, which was damaged by melt interaction, was found to be twisted and slightly misshapen (see Figure B-53). Its approximated diameter was determined to be 117 mm (4-5/8 in.). Length measurements around the guide tube varied from 23.9 cm (9.4 in.) to only 15 cm (5.9 in.).

Gamma spectroscopy was not performed on the K-5 guide tube because there was no visible significant difference in the deposition of material on the nozzle.

The guide tube was sectioned as shown in Figure B-54. Several cutting blades were destroyed in the effort to perform the first transverse cut at approximately 1.9 cm (0.75 in.) from the bottom of the guide tube. MPR Associates reported this same difficulty during the removal of the guide tube samples from the reactor, stating that the damaged guide tube material was much harder than the as-fabricated stainless steel. A second cut was made longitudinally on one end of the primary section, creating sample K-5-1, which was polished longitudinally after it had been stabilized with sample supports. The same end was cut again longitudinally, and the resulting sample was shipped to France. A fourth cut was made on the opposite end of the primary section, again longitudinally, creating sample K-5-2. It was stabilized against another sample and polished transversely.

Table B-1. Gamma scan data for nozzle M-10 (from base of cut nozzle)

Position (in./cm)	Cs-137 (ROI #1)	Co-60 (ROI #2)	Spectrum (ROI #3)
0.00/0.0	3973	281	16337
0.25/0.6	7069	282	26288
0.50/1.2	9949	0	35378
0.75/1.9	12598	394	44168
1.00/2.5	14077	0	51441
1.25/3.2	17409	19	65291
1.50/3.8	38498	282	127205
1.75/4.4	55000	0	178721
2.00/5.1	71925	812	232359
2.25/5.7	90693	1322	283614
2.50/6.4	46051	1367	160392
2.75/7.0	13298	1246	69638
3.00/7.5	6826	1159	47691
3.25/8.2	4898	1105	39887
3.50/8.9	5468	1033	45134
3.75/9.5	7151	1529	56983
4.00/10.2	7071	4683	79261
4.25/10.8	5906	7354	99153
4.50/11.4	6899	5471	89845
4.75/12.1	8817	4174	88036
5.00/12.7	10651	3964	95578
5.25/13.3	12302	3737	99209
5.50/14.0	15973	3456	116808
5.75/14.6	40098	4346	200127
6.00/15.2	48075	3602	200205
6.25/15.9	14983	1106	63594

Table B-2. Gamma scan data for nozzle H-9 (from base of cut nozzle)

Position (in./cm)	Cs-137 (ROI #1)	Co-60 (ROI #2)	Spectrum (ROI #3)
0.00/0.0	278	0	50950
0.25/0.6	3502	517	64036
0.50/1.2	6078	1336	84505
0.75/1.9	6892	895	88133
1.00/2.5	7477	544	88719
1.25/3.2	7239	490	97311
1.50/3.8	8623	1600	127313
1.75/4.4	9846	1412	164493
2.00/5.1	105608	1075	525158
2.25/5.7	153039	1011	709598
2.50/6.4	27467	537	247593
2.75/7.0	11573	704	150678
3.00/7.5	16683	1071	161245
3.25/8.2	22154	1642	189771
3.50/8.9	22486	2044	174764
3.75/9.5	21928	1336	168268
4.00/10.2	22041	1181	170899
4.25/10.8	24411	1130	176717
4.50/11.4	21065	758	167139
4.75/12.1	15667	849	163131
5.00/12.7	18414	1090	194633
5.25/13.3	60335	1553	370085
5.50/14.0	148972	1745	704230
5.75/14.6	145853	2099	734036
6.00/15.2	65678	10222	519421
6.25/15.9	30966	15364	413730
6.50/16.5	27509	6842	301934
6.75/17.1	29942	2202	256029
7.00/17.8	40365	1979	289724
7.25/18.4	58496	5399	375165
7.50/19.0	63477	4478	383288
7.75/19.7	30536	1264	223491
8.00/20.3	19212	1085	159151
8.25/21.0	17820	450	143022
8.50/21.6	12538	803	116257
8.75/22.2	11240	331	104811
9.00/22.9	23287	495	141968
9.25/23.4	18539	135	121073
9.50/24.1	18566	602	120879
9.75/24.8	6003	175	74091
110.0/25.4	1777	0	55289

Table B-3. Gamma scan data for nozzle L-11 (from base of cut nozzle)

Position (in./cm)	Cs-137 (ROI #1)	Co-60 (ROI #2)	Spectrum (ROI #3)
0.00/0.0	3586	167	17375
0.25/0.6	15486	83	54283
0.50/1.2	19338	444	69446
0.75/1.9	17991	625	70900
1.00/2.5	15695	380	67390
1.25/3.2	14591	256	63702
1.50/3.8	12550	825	59743
1.75/4.4	9233	349	53839
2.00/5.1	8316	1382	61624
2.25/5.7	15285	2440	99817
2.50/6.4	51626	5050	242161
2.75/7.0	89559	12291	468767
3.00/7.5	130133	8367	608715
3.25/8.2	188563	6991	766811
3.50/8.9	156708	6289	617241
3.75/9.5	88749	7534	384800
4.00/10.2	41032	7759	222712
4.25/10.8	14570	2473	93358
4.50/11.4	11090	1266	64192
4.75/12.1	11474	930	59927
5.00/12.7	13680	1149	64910
5.25/13.3	15562	679	72125
5.50/14.0	27748	1486	117119
5.75/14.6	27810	1519	114370
6.00/15.2	17968	85	70969
6.25/15.9	18677	426	68790
6.50/16.5	20654	401	72013
6.75/17.1	20026	63	70243
7.00/17.8	20269	521	7234
7.25/18.4	21149	239	70084
7.50/19.0	19217	0	62320
7.75/19.7	14085	80	47813
8.00/20.3	16420	382	53609
8.25/21.0	13146	176	42828
8.50/21.6	11363	518	37899
8.75/22.2	11066	201	37147
9.00/22.9	10445	308	32793
9.25/23.4	2724	155	9741

Table B-4. Gamma scan data for nozzle R-7 (from base of cut nozzle)

Position (in./cm)	Cs-137 (ROI #1)	Co-60 (ROI #2)	Spectrum (ROI #3)
0.00/0.0	474	0	2674
0.25/0.6	563	273	2969
0.50/1.2	547	0	3244
0.75/1.9	322	284	3215
1.00/2.5	266	40	2348
1.25/3.2	302	121	2872
1.50/3.8	626	417	3945
1.75/4.4	750	0	5232
2.00/5.1	1276	310	7063
2.25/5.7	1161	72	7860
2.50/6.4	1474	0	9864
2.75/7.0	2302	183	11922
3.00/7.5	3755	62	16809
3.25/8.2	5346	89	22360
3.50/8.9	8147	429	32602
3.75/9.5	12180	588	44707
4.00/10.2	19205	143	64206
4.25/10.8	24799	313	77974
4.50/11.4	22986	0	72784
4.75/12.1	18715	285	61234
5.00/12.7	14384	220	49012
5.25/13.3	11554	0	40917
5.50/14.0	9458	556	35700
5.75/14.6	8917	523	35020
6.00/15.2	8065	0	32226
6.25/15.9	7814	405	31792
6.50/16.5	8200	371	34206
6.75/17.1	13516	511	51234
7.00/17.8	21623	777	77528
7.25/18.4	29052	229	103240
7.50/19.0	33193	1348	120855
7.75/19.7	57722	795	209275
8.00/20.3	92136	1626	310636
8.25/21.0	91205	1642	303881
8.50/21.6	82096	1593	275752
8.75/22.2	65962	1925	222634
9.00/22.9	35006	1132	120317
99.25/23.0	2372	605	16291

Table B-5. Gamma scan data for nozzle K-11 (from base of cut nozzle)

Position (in./cm)	Cs-137 (ROI #1)	Co-60 (ROI #2)	Spectrum (ROI #3)
0.00/0.0	213	324	11150
0.25/0.6	5785	142	38097
0.50/1.2	12253	597	97800
0.75/1.9	27643	907	203175
1.00/2.5	89243	1088	472481
1.25/3.2	128463	1953	650506
1.50/3.8	105058	2279	566874
1.75/4.4	82641	1937	479256
2.00/5.1	75657	3013	445515
2.25/5.7	67473	3294	404138
2.50/6.4	55696	3062	359474
2.75/7.0	53551	3211	348205
3.00/7.5	63250	3681	388749
3.25/8.2	74224	3900	430172
3.50/8.9	67191	4597	382262
3.75/9.5	51030	3445	289803
4.00/10.2	35356	1884	201844
4.25/10.8	24371	1077	140340
4.50/11.4	26534	1836	136121
4.75/12.1	31615	1699	152175
5.00/12.7	26466	2626	138202
5.25/13.3	25537	2098	135753
5.50/14.0	28582	2241	150533
5.75/14.6	29819	2018	161135
6.00/15.2	35725	1595	178035
6.25/15.9	28338	2465	150174
6.50/16.5	21072	1901	112842
6.75/17.1	20845	1273	105688
7.00/17.8	29836	1547	134394
7.25/18.4	26385	1263	117408
7.50/19.0	14337	613	68085
7.75/19.7	10000	247	49768
8.00/20.3	11022	504	54884
8.25/21.0	26744	950	112439
8.50/21.6	33889	1037	139049
8.75/22.2	21665	667	87234
99.00/22.	12773	846	49014
99.25/23.4	6243	382	23393
9.5/24.1	1267	0	6498

Table B-6. Gamma scan data for nozzle K-12 (from base of cut nozzle)

Position (in./cm)	Cs-137 (ROI #1)	Co-60 (ROI #2)	Spectrum (ROI #3)
0.00/0.0	3073	774	35992
0.25/0.6	6185	676	60754
0.50/1.2	8892	922	86004
0.75/1.9	9404	603	126221
1.00/2.5	29494	1536	273328
1.25/3.2	125766	2056	750672
1.50/3.8	174354	3097	1100302
1.75/4.4	171651	3282	1202616
2.00/5.1	170350	6810	1242939
2.25/5.7	155164	9726	1256498
2.50/6.4	161628	9713	1337884
2.75/7.0	150716	7790	1266698
3.00/7.5	148602	7993	1222078
3.25/8.2	135025	8115	1152459
3.50/8.9	125771	11658	1144313
3.75/9.5	164194	9280	1307605
4.00/10.2	178728	7823	1367460
4.25/10.8	147140	7942	1214165
4.50/11.4	146224	9219	1190455
4.75/12.1	155335	8655	1245091
5.00/12.7	162761	10014	1289928
5.25/13.3	169861	8759	1333474
5.50/14.0	172724	8481	1356308
5.75/14.6	168834	9759	1325592
6.00/15.2	163305	9949	1291440
6.25/15.9	163228	8329	1270380
6.50/16.5	162087	10185	1264342
6.75/17.1	163130	10812	1271003
7.00/17.8	164521	10804	1290088
7.25/18.4	169640	12399	1314631
7.50/19.0	173156	7447	1341323
7.75/19.7	169504	8325	1338725
8.00/20.3	171698	11147	1331725
8.25/21.0	167810	8907	1302177
8.50/21.6	176604	8997	1337375
8.75/22.2	209646	9503	1438863
9.00/22.9	186166	8867	1139391
9.25/23.4	86016	4919	554483
9.50/24.1	12176	1845	157095
9.75/24.8	7848	808	82568
10.0/25.4	5372	1002	52655
10.3/26.0	1133	176	30983

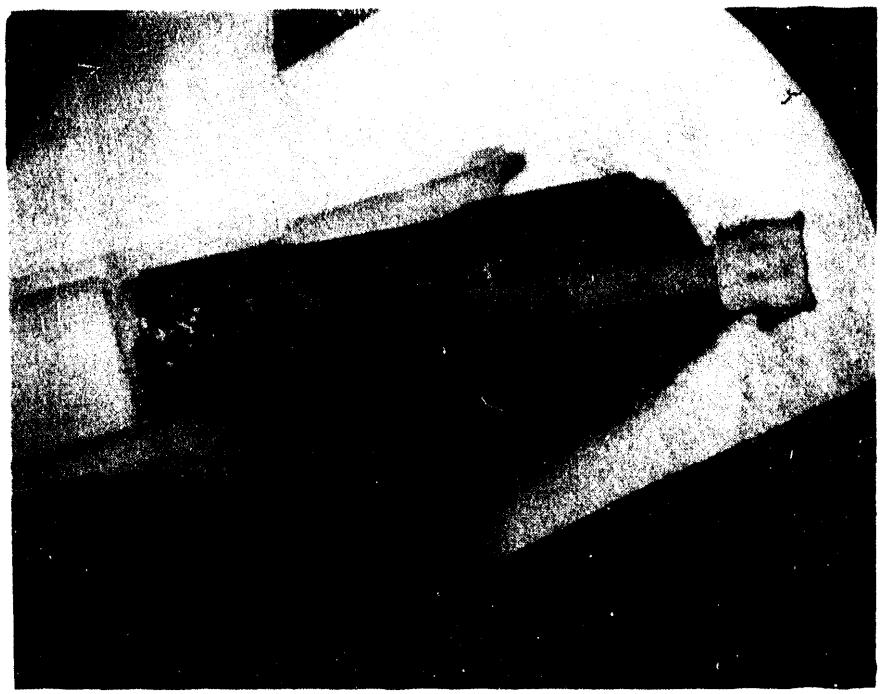

Figure B-1. Photograph of the entire M-10 nozzle (the extrapolated length is 6-3/8 in.).

Figure B-2. Closeup view of the melt interaction zone on the top edge (tip) of nozzle M-10.

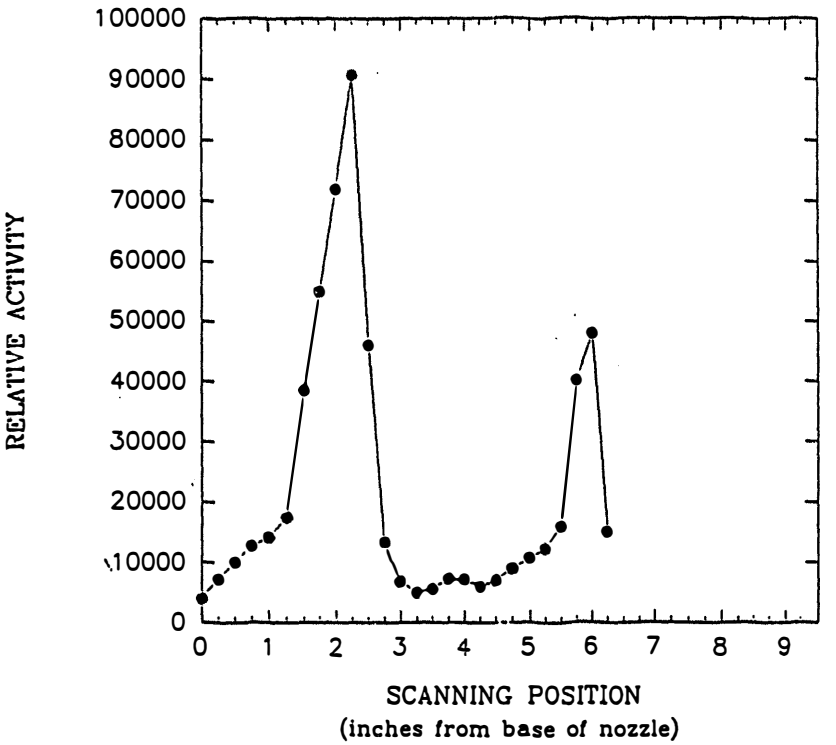

Figure B-3. The Cs-137 activity profile of nozzle M-10.

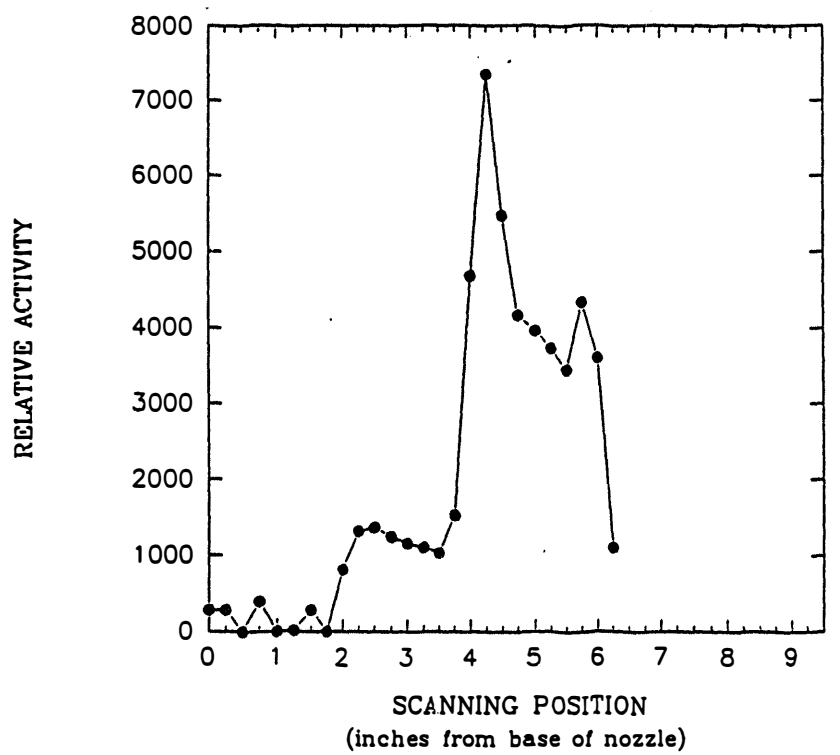

Figure B-4. The Co-60 activity profile of nozzle M-10.

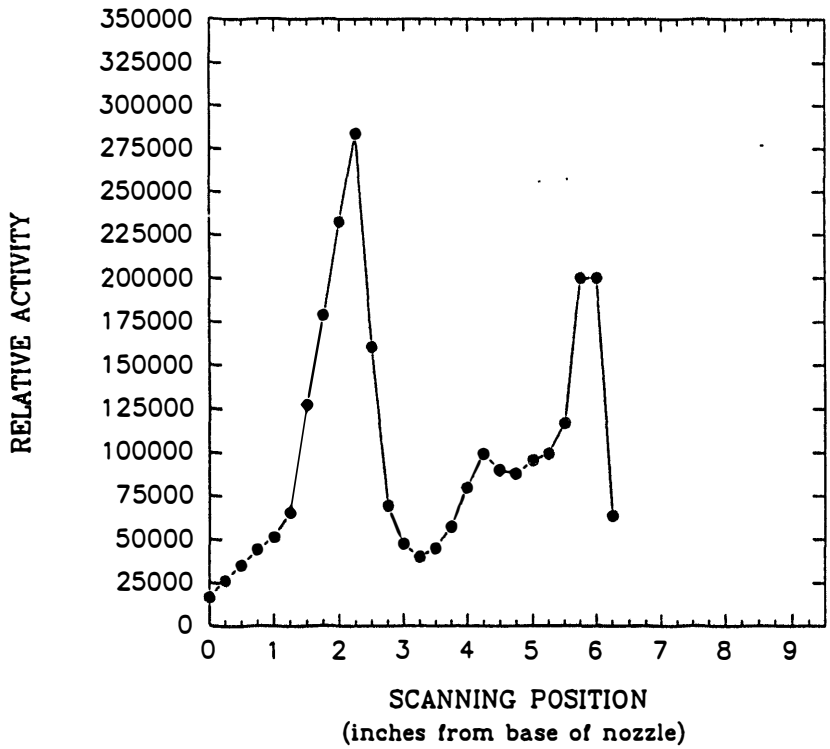

Figure B-5. The full-spectrum activity profile of nozzle M-10.

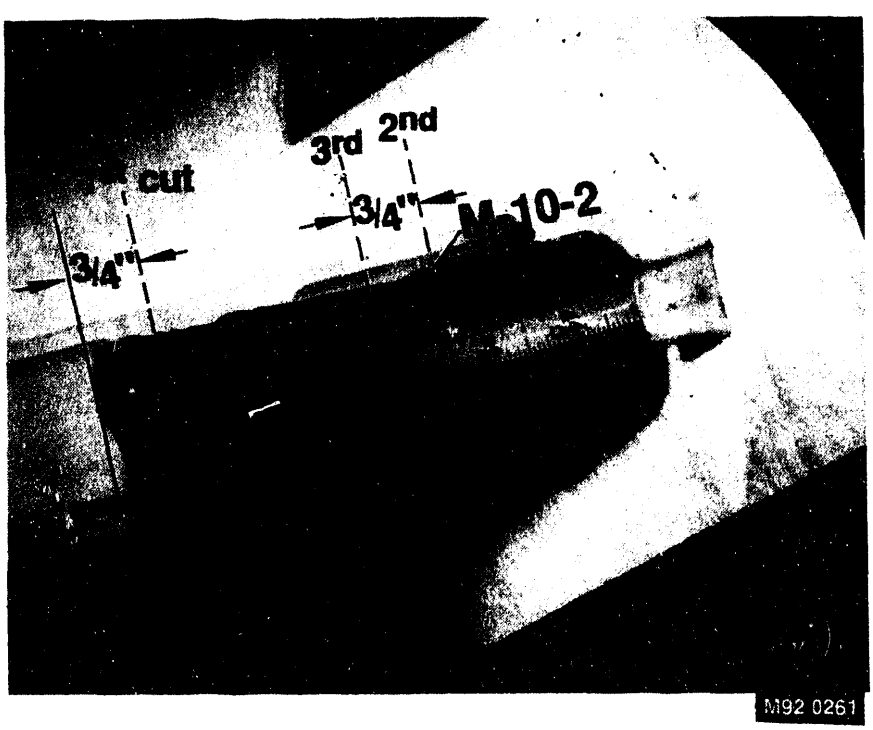

Figure B-6. Sectioning diagram of the M-10 nozzle.

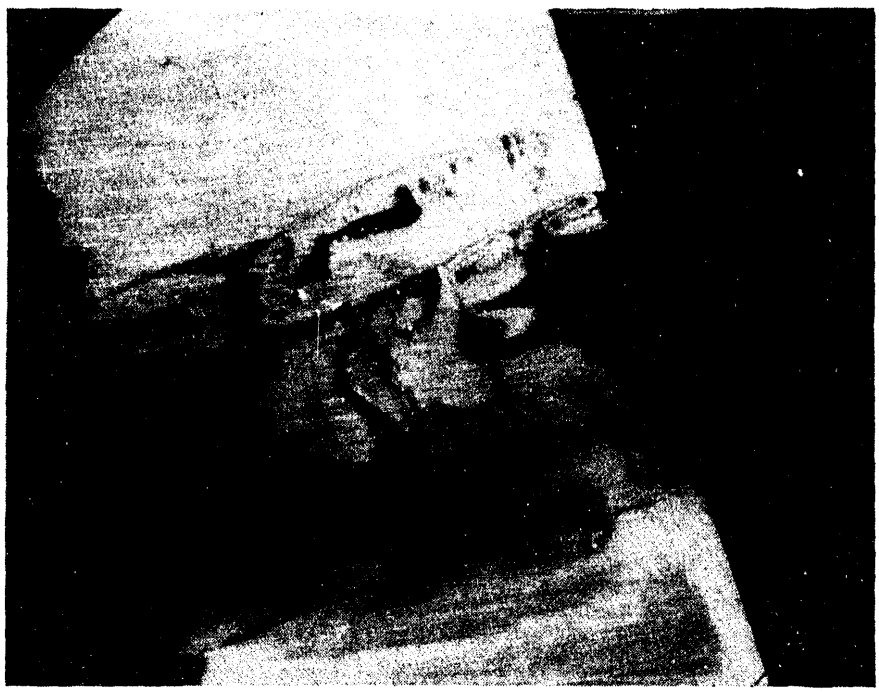

Figure B-7. Sample M-10-1A, from a longitudinal cut of M-10-1.

Figure B-8. Sample M-10-1B, showing melt/instrument string interaction.

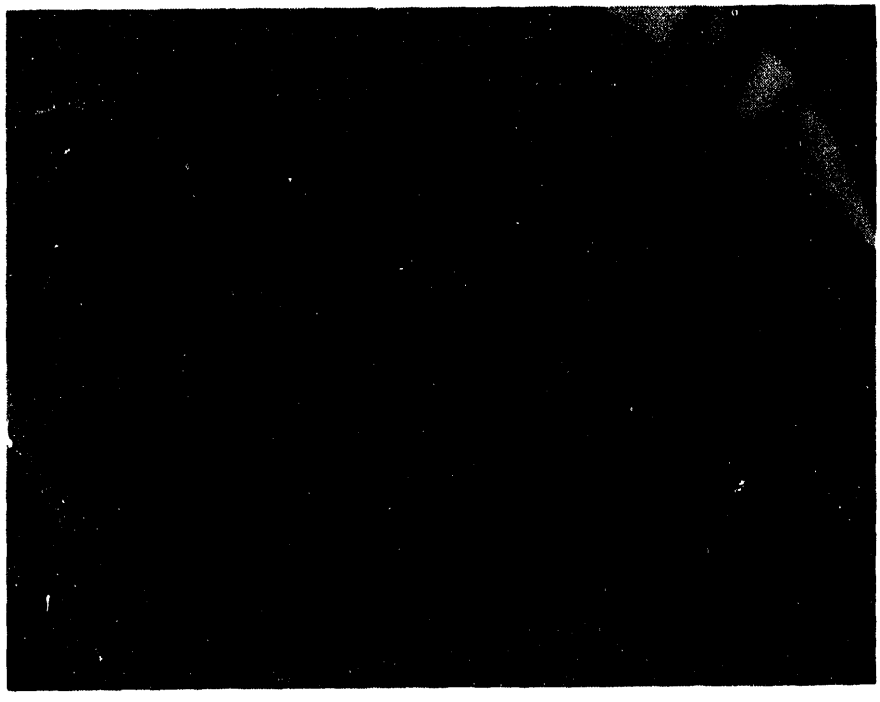

Figure B-9. Macro side view of sample M-10-1B.

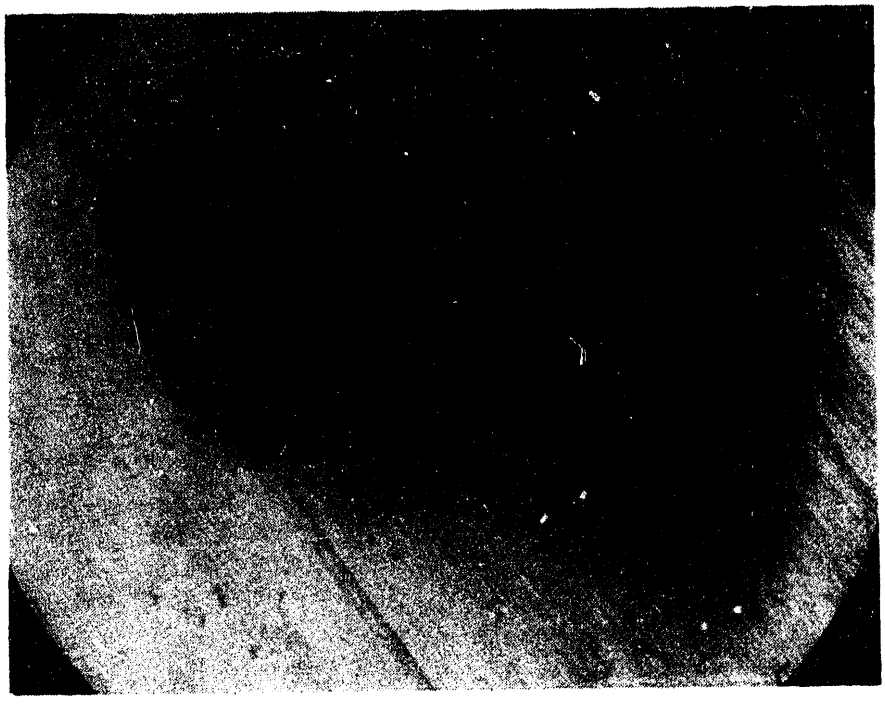

Figure B-10. View of the bottom end of the transverse section, M-10-2, showing the beginning of the melt penetration.

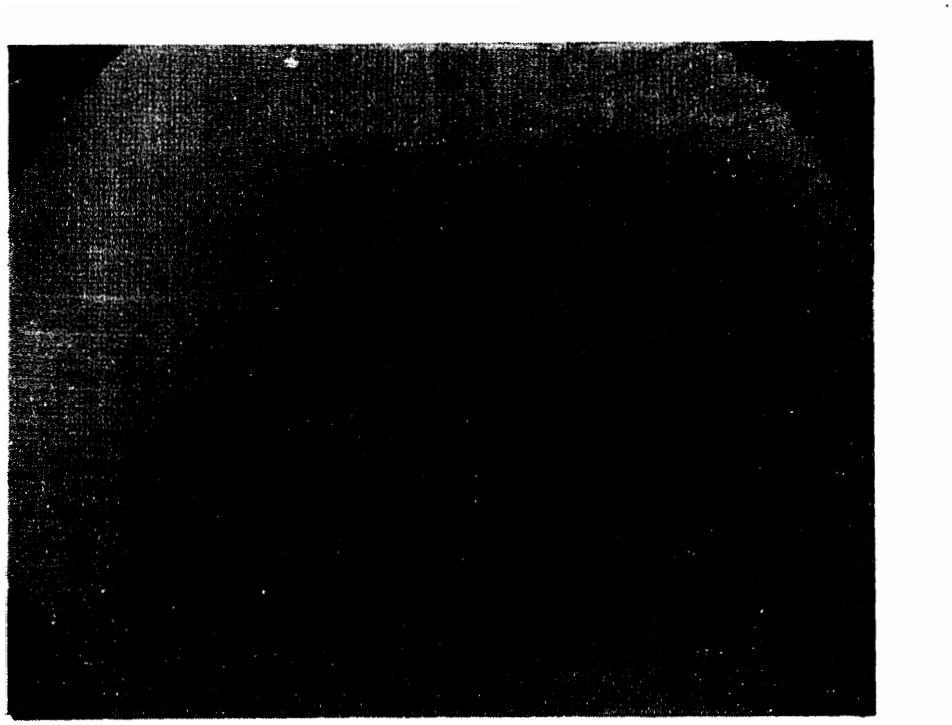

Figure B-11. Top (tip) end perspective of the transverse section, M-10-2, exhibiting extensive melt interaction.

Figure B-12. Full-length (9-1/2 in.) view of the H-9 nozzle.

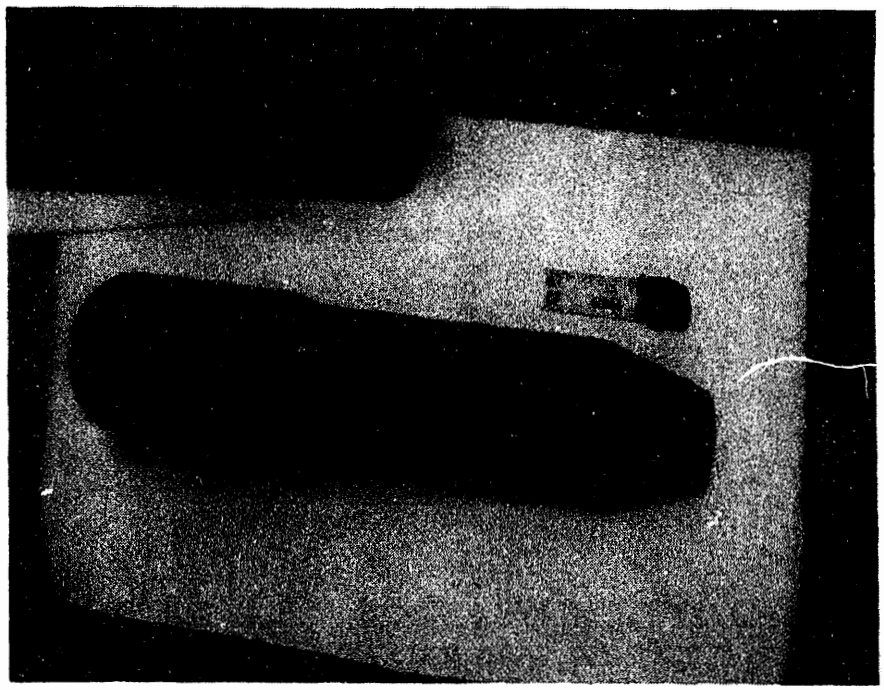

Figure B-13. A side (long) view of nozzle H-9, showing the instrument core string still intact.

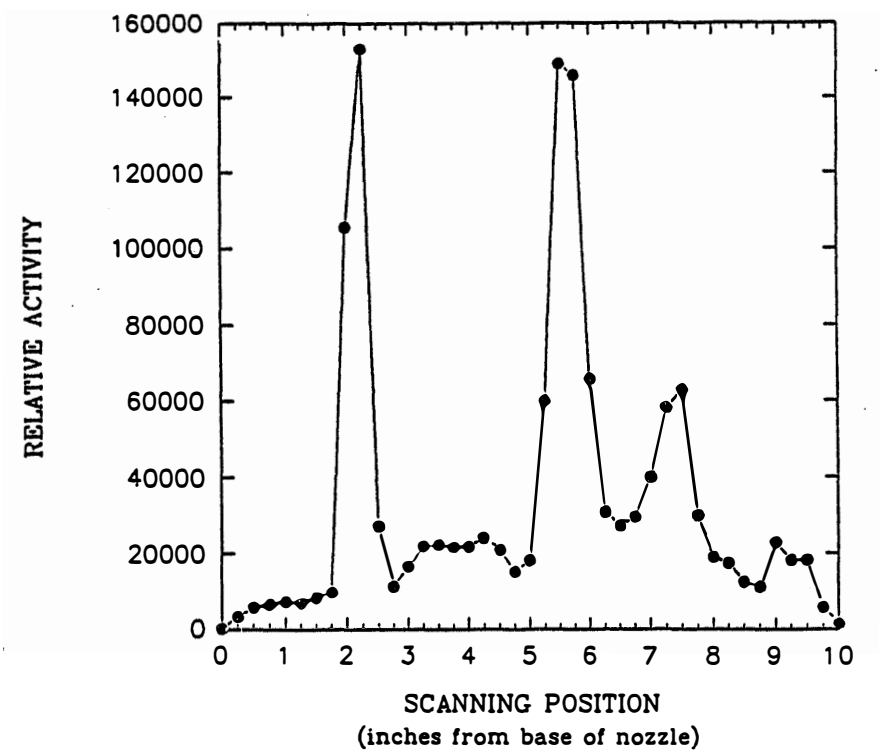

Figure B-14. The Cs-137 activity profile of nozzle H-9.

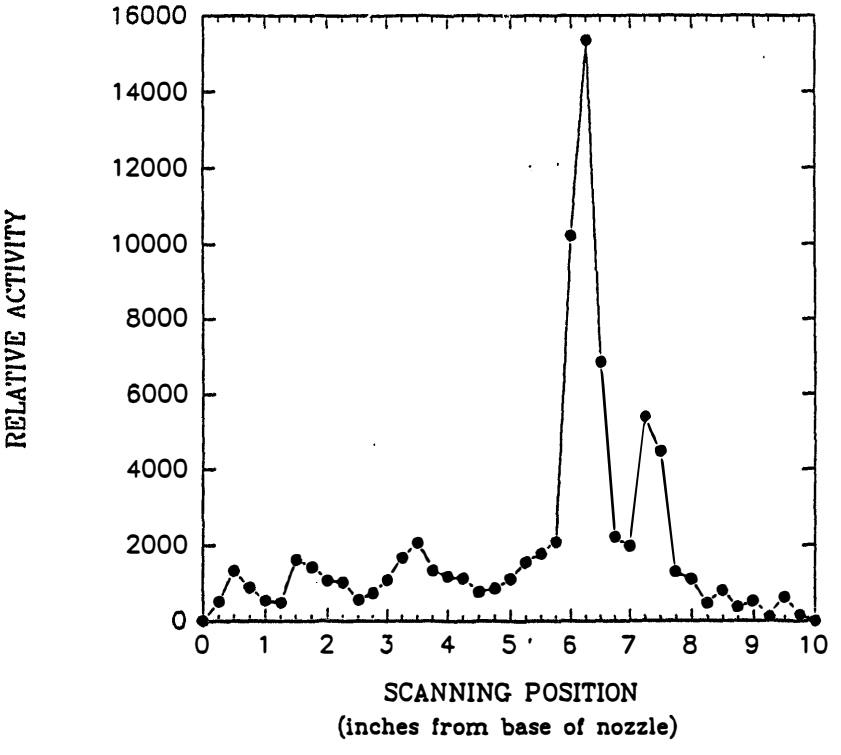

Figure B-15. The Co-60 activity profile of nozzle H-9.

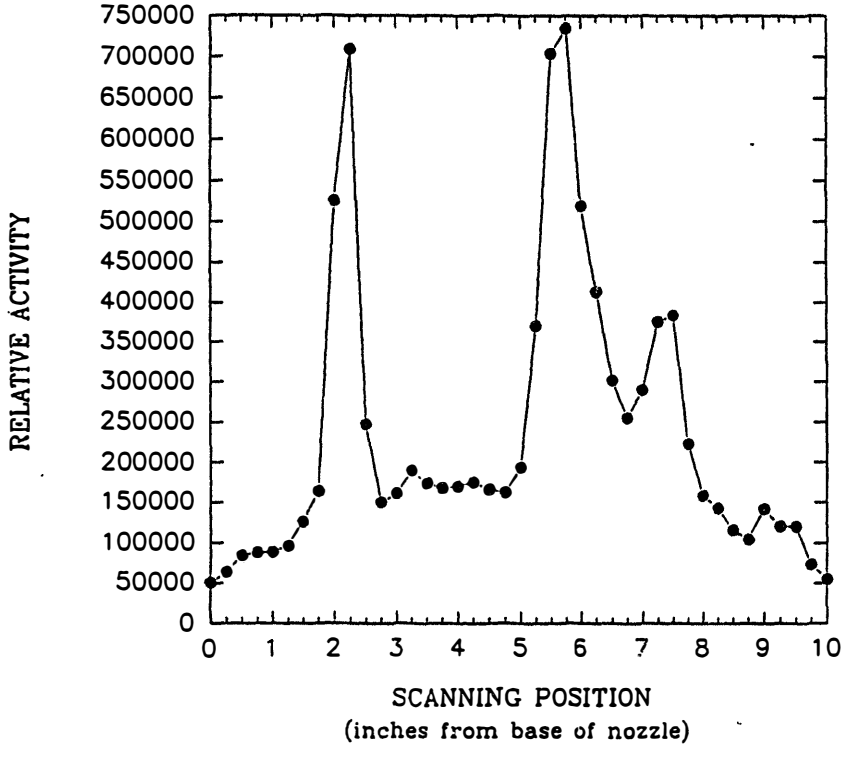

Figure B-16. The full-spectrum activity profile of nozzle H-9.

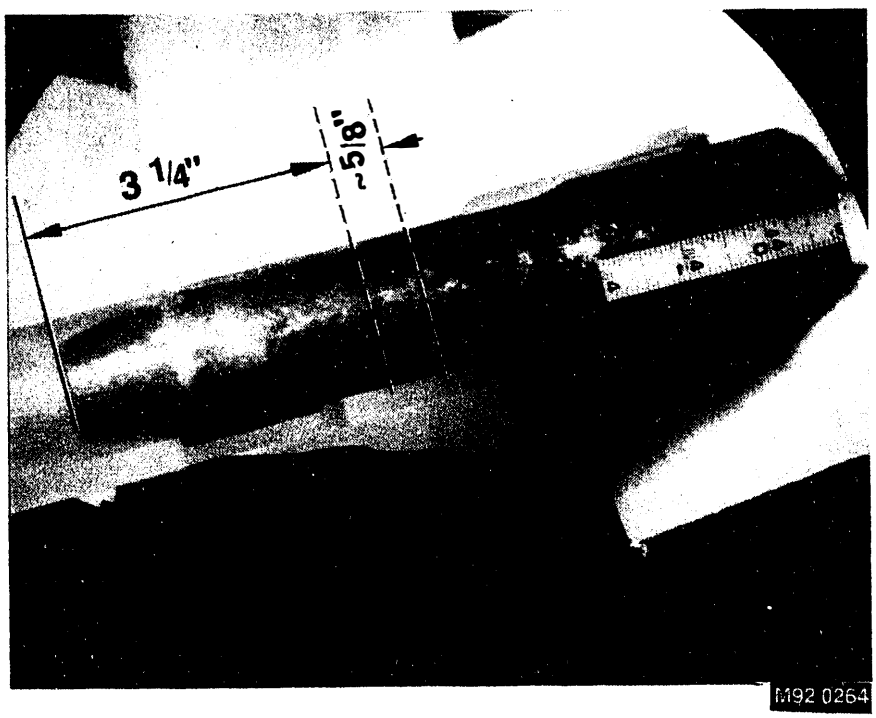

Figure B-17. Sectioning diagram of the H-9 nozzle.

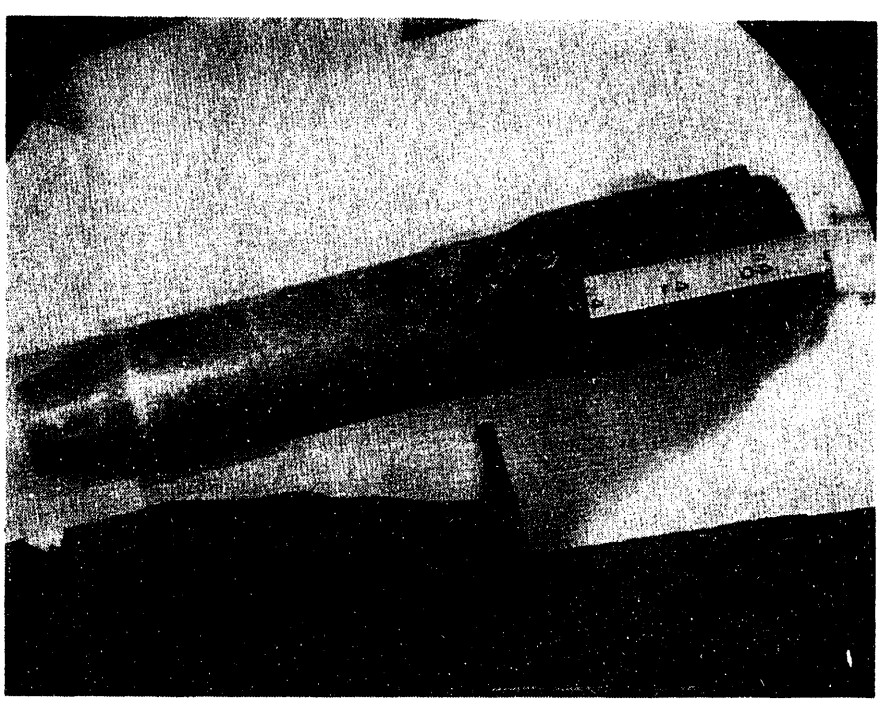

Figure B-18. Full-length (9-in.) view of nozzle L-11.

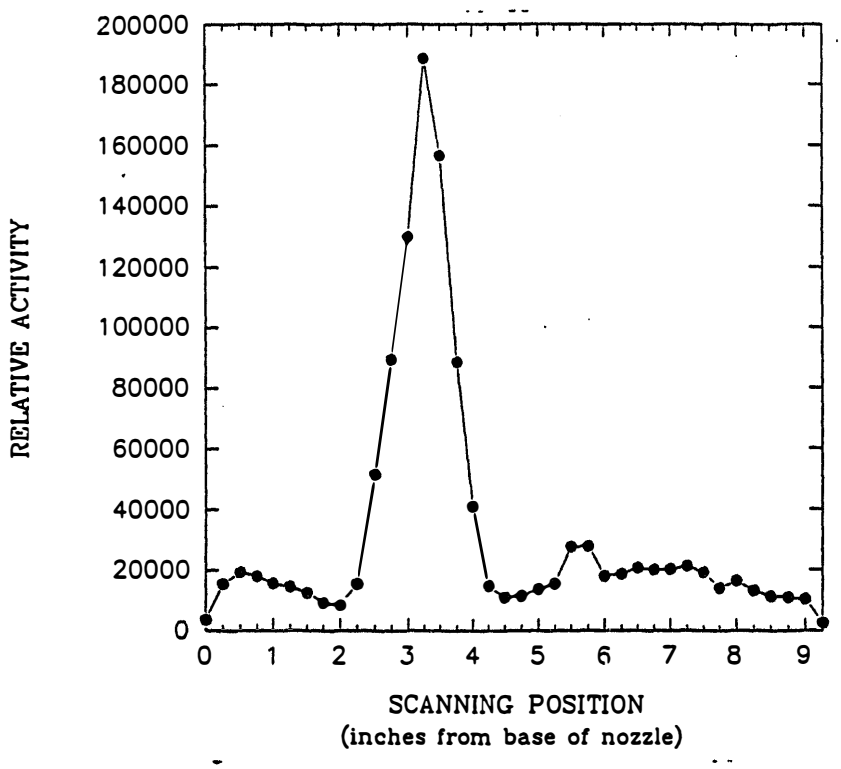

Figure B-19. The Cs-137 activity profile of nozzle L-11.

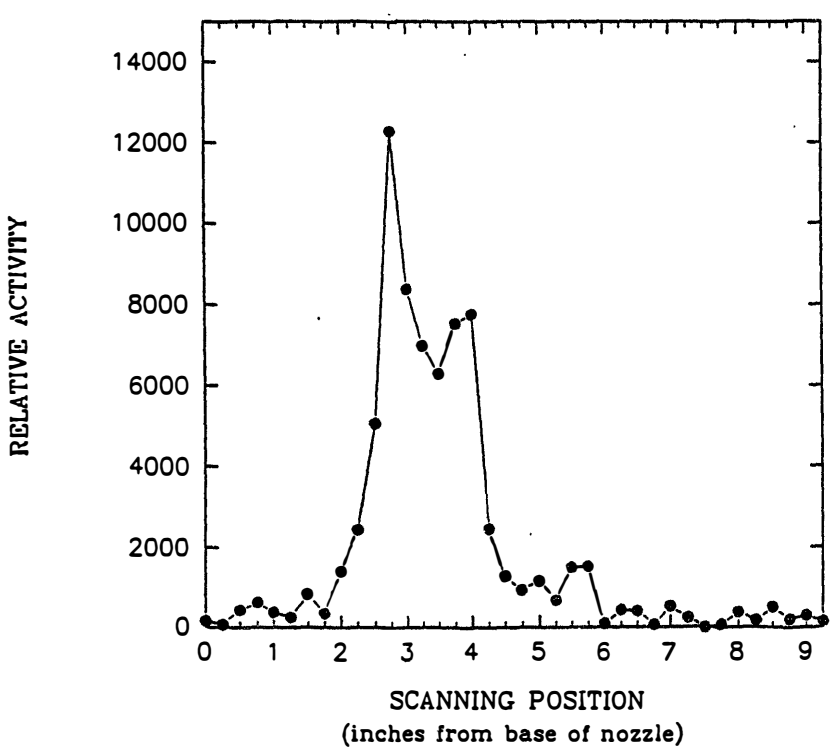

Figure B-20. The Co-60 activity profile of nozzle L-11.

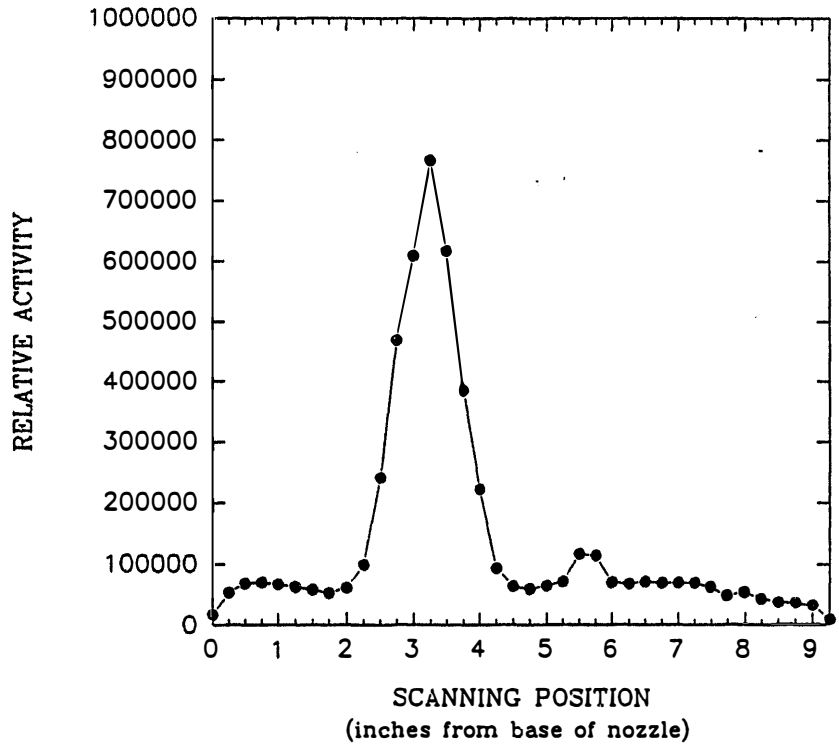

Figure B-21. The full-spectrum activity profile of nozzle L-11.

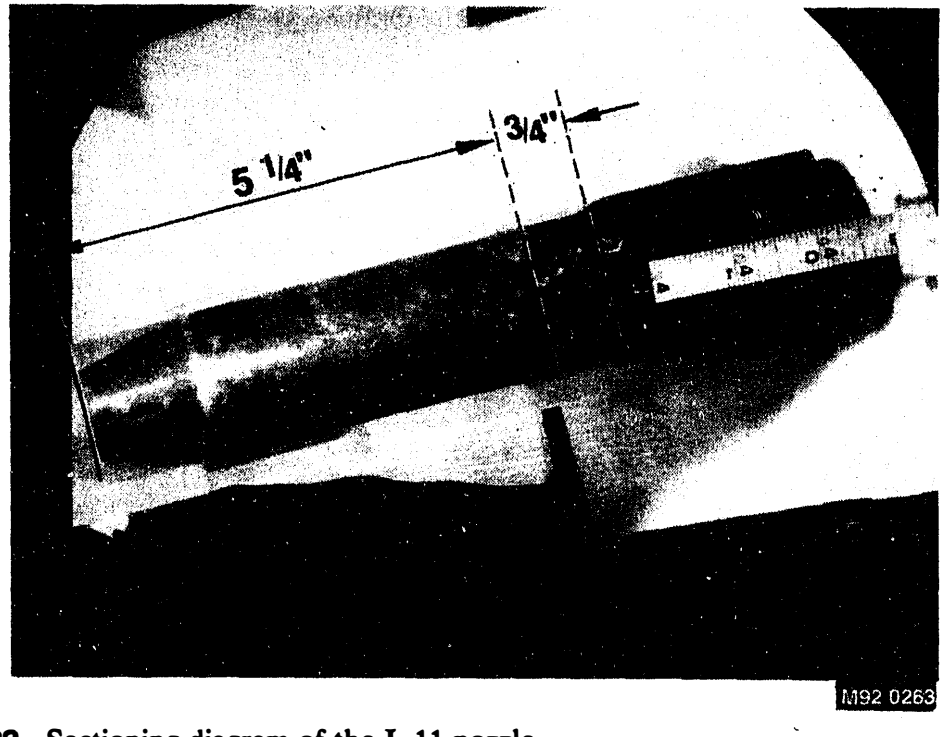

Figure B-22. Sectioning diagram of the L-11 nozzle.

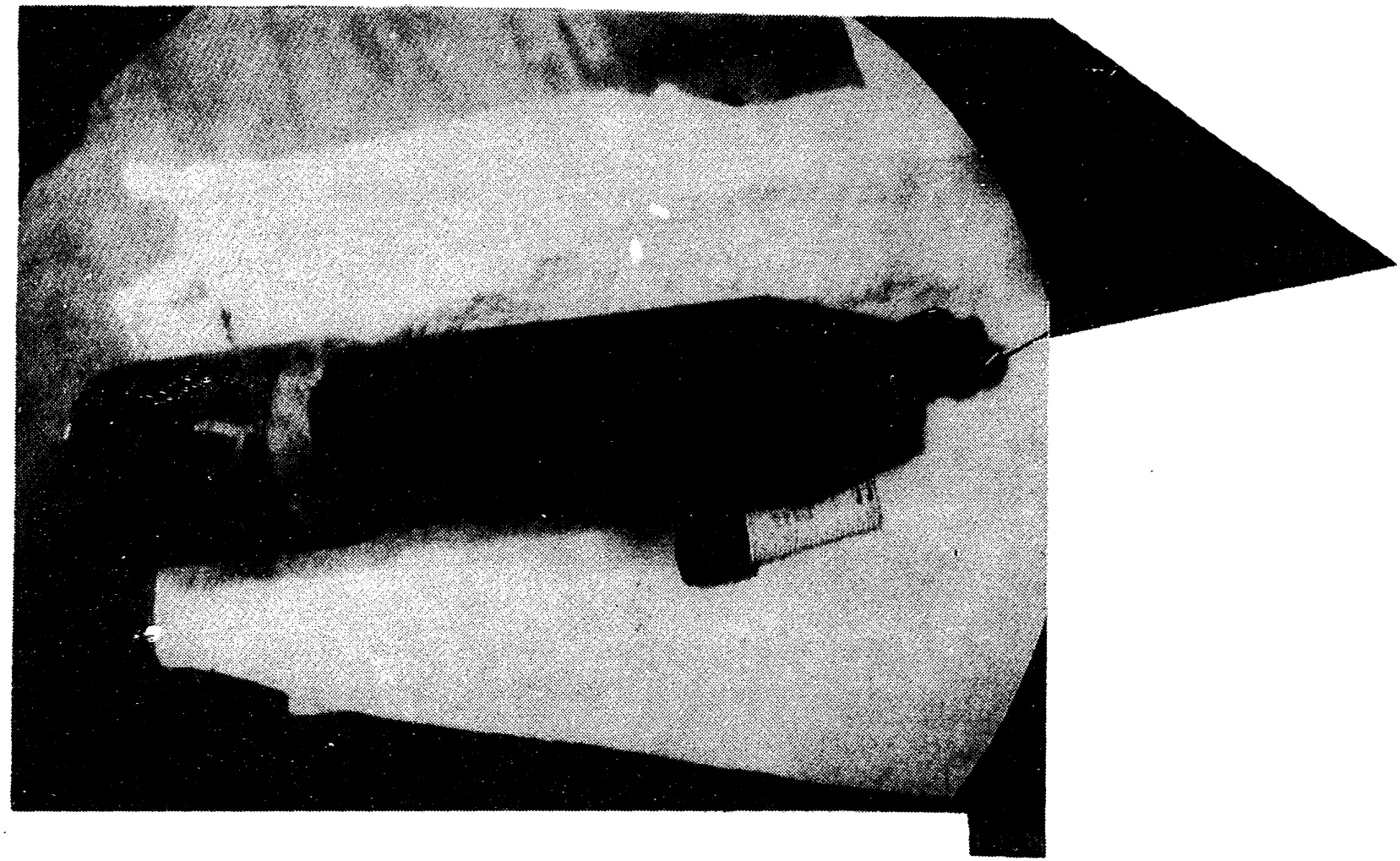

Figure B-23. Full-length view of the R-7 nozzle with the instrument core string and melt bulb still attached.

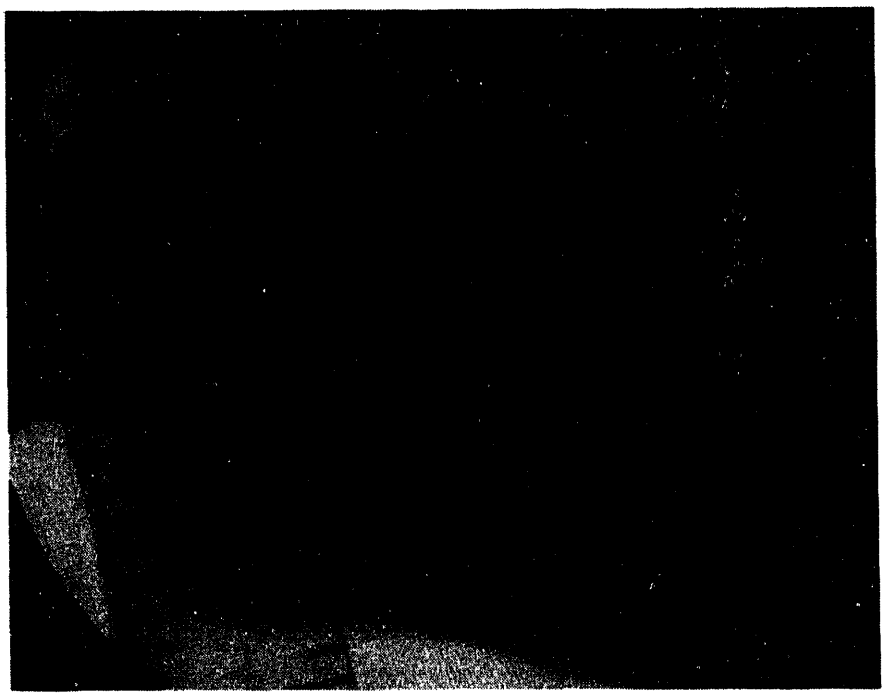

Figure B-24. A closeup perspective of the lip of R-7 with instrument string still intact.

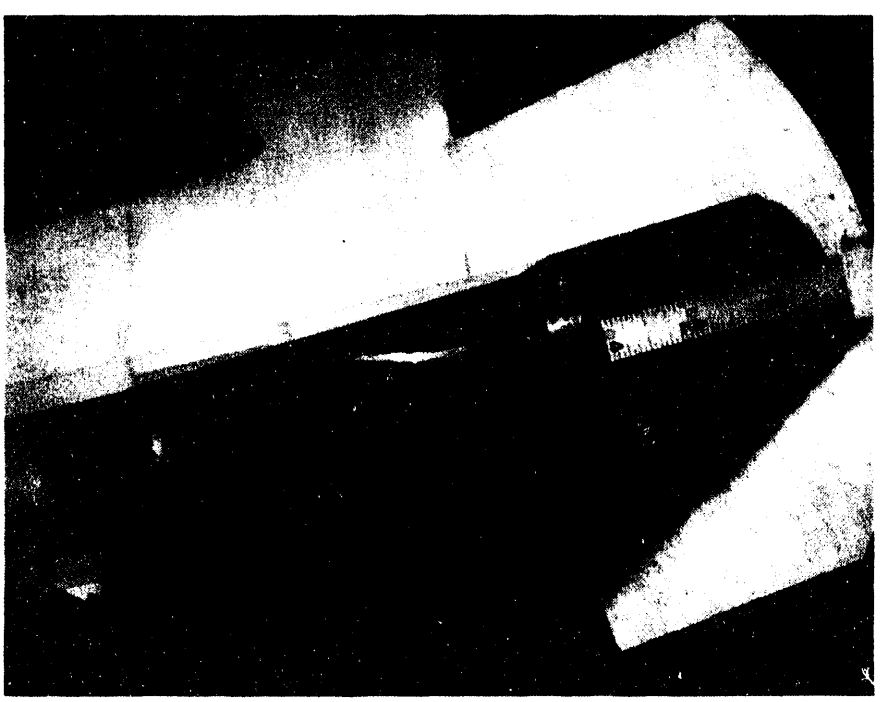

Figure B-25. Full-length (9-1/8 in.) view of the R-7 nozzle after melt bulb removal.

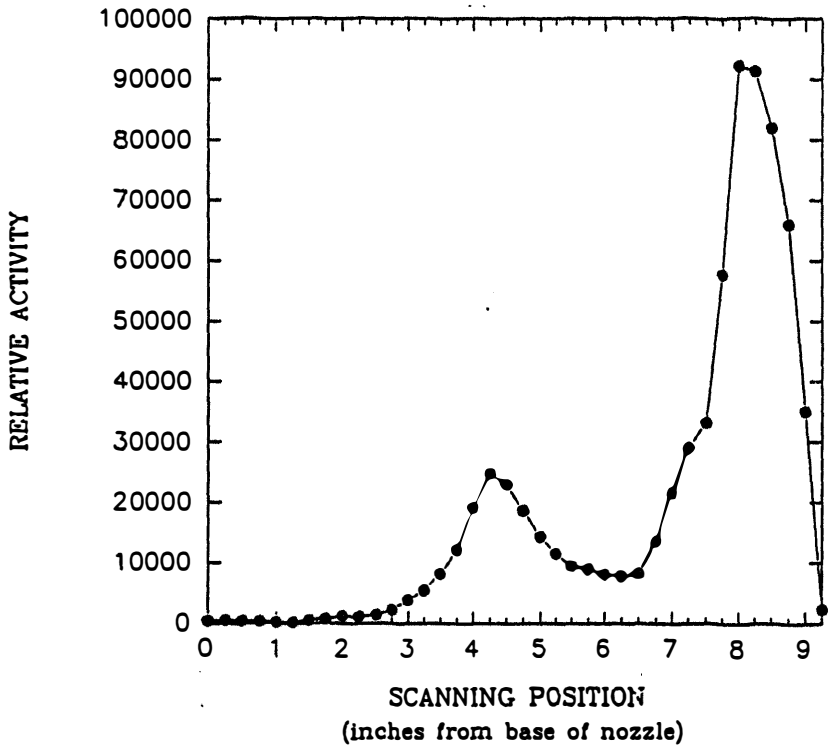

Figure B-26. The Cs-137 activity profile of nozzle R-7.

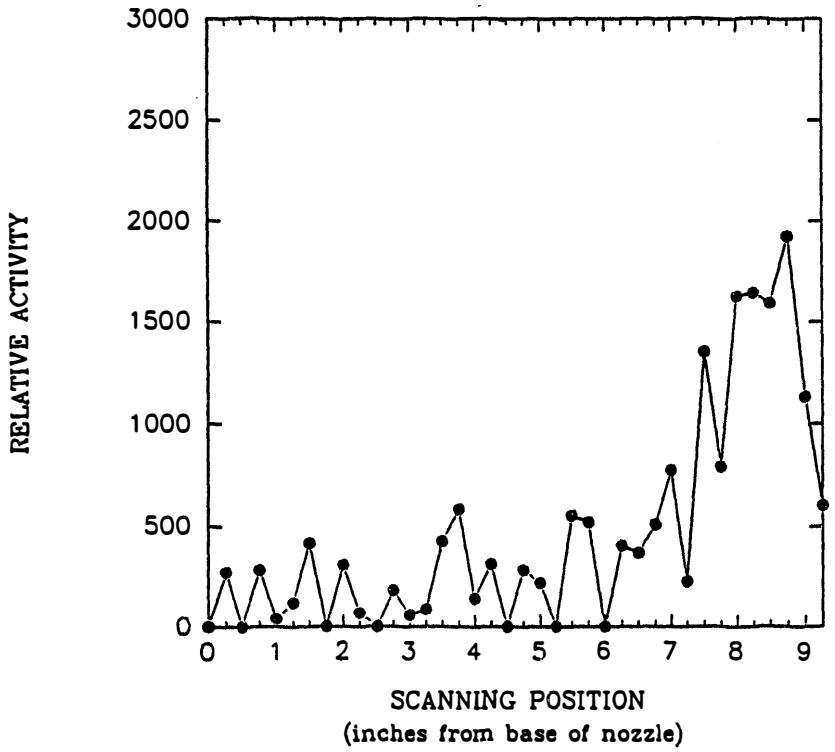

Figure B-27. The Co-60 activity profile of nozzle R-7.

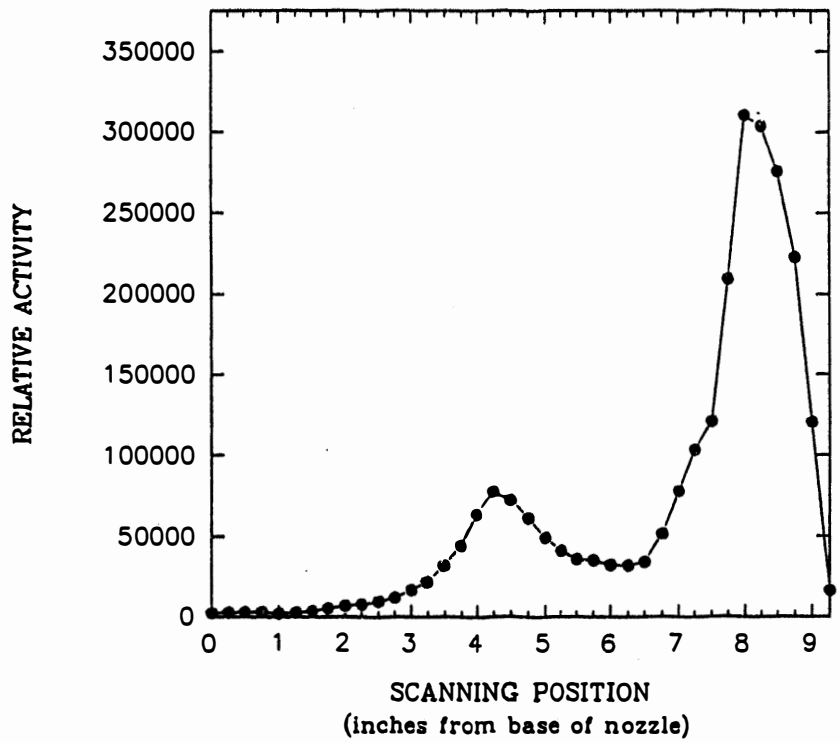

Figure B-28. The full-spectrum activity profile of nozzle R-7.

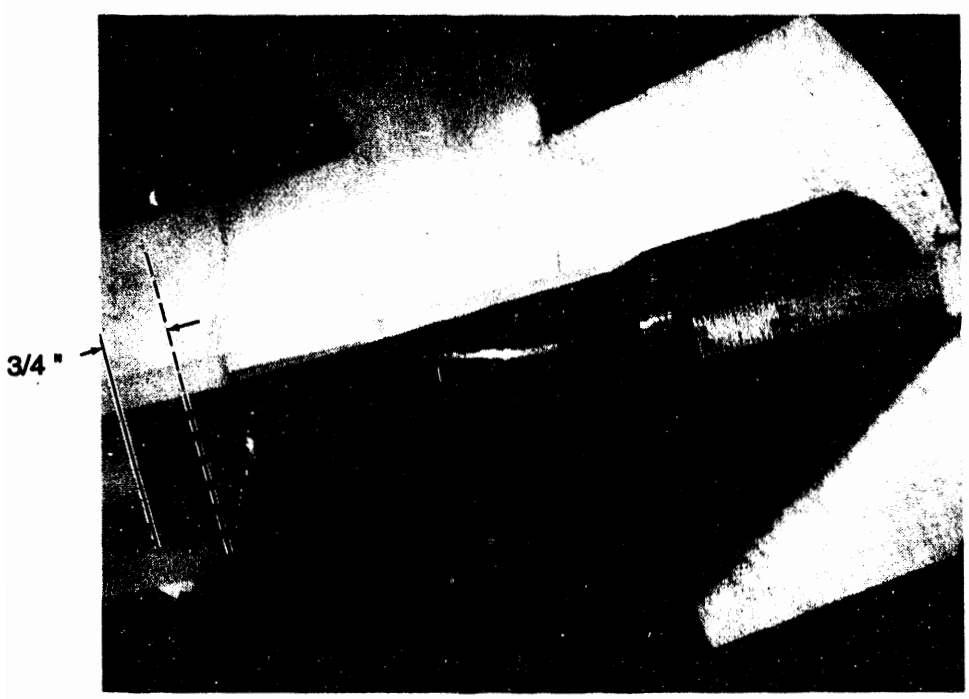

Figure B-29. Sectioning diagram of the R-7 nozzle.

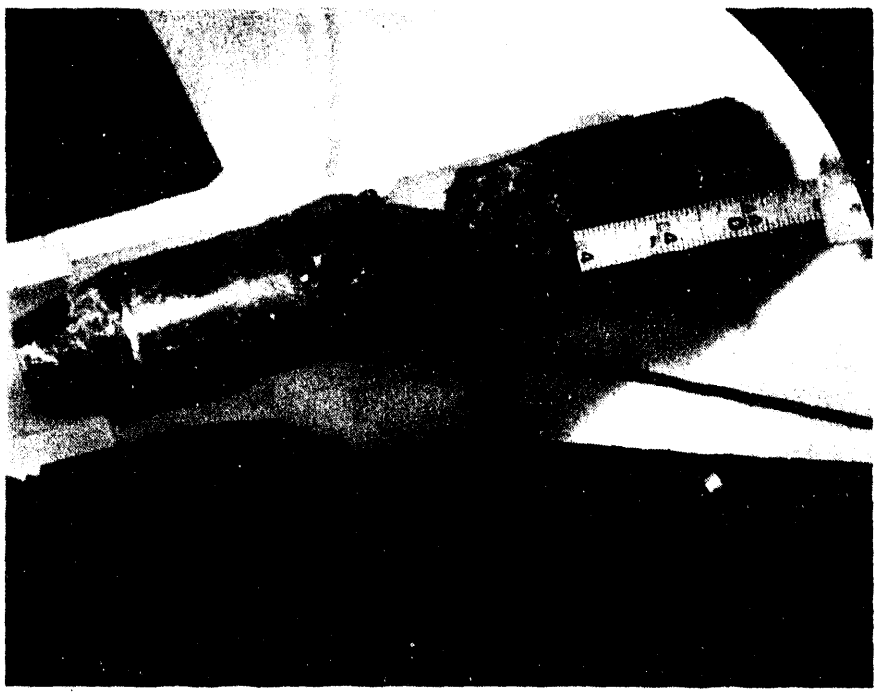

Figure B-30. Full-length (9-1/4 in.) view of K-11 nozzle at a 0-degree reference.

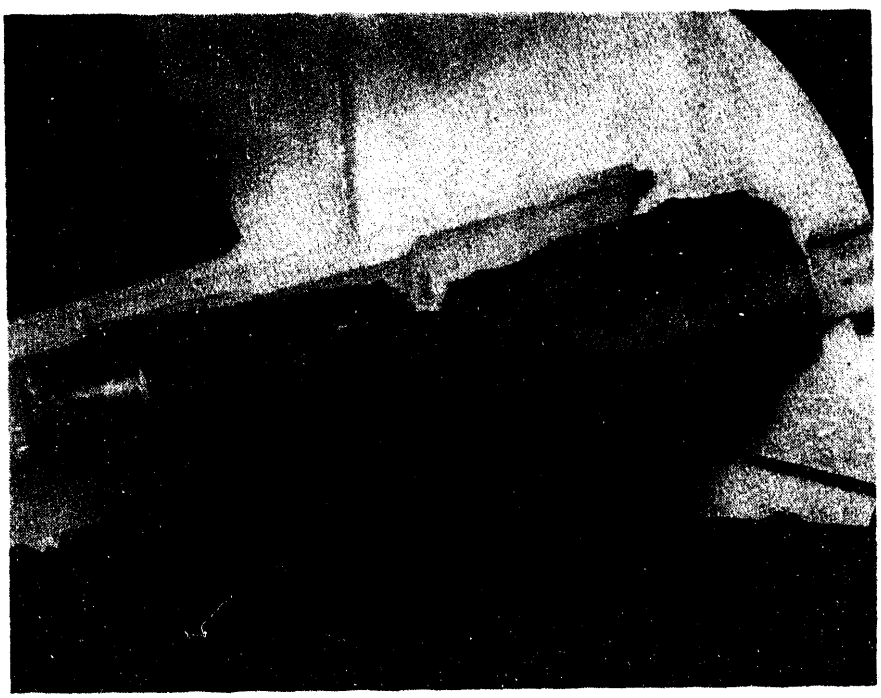

Figure B-31. K-11 nozzle with a 180-degree rotation.

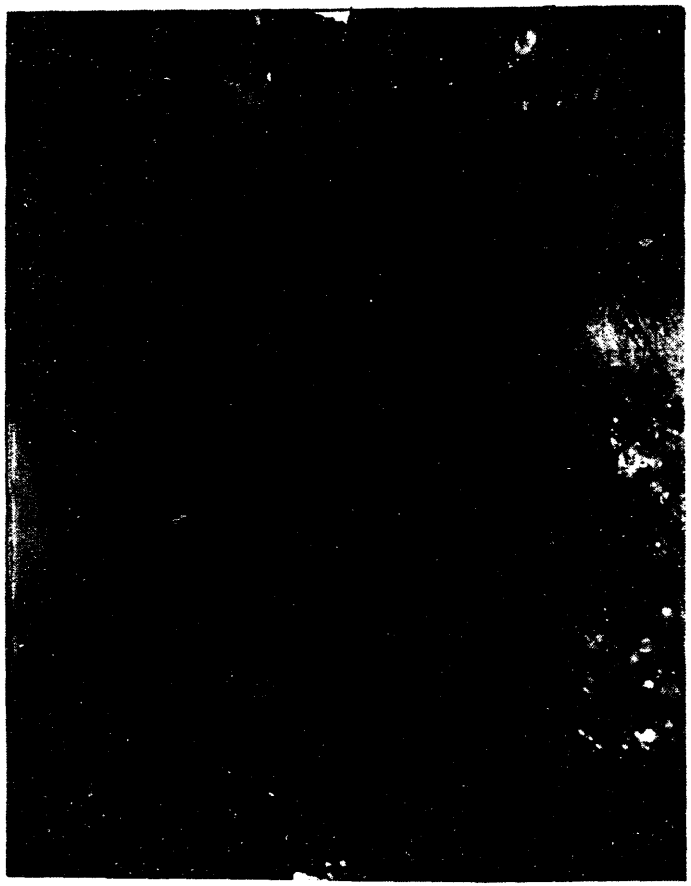

Figure B-32. Closeup perspective of the K-11 nozzle at a 0-degree reference.

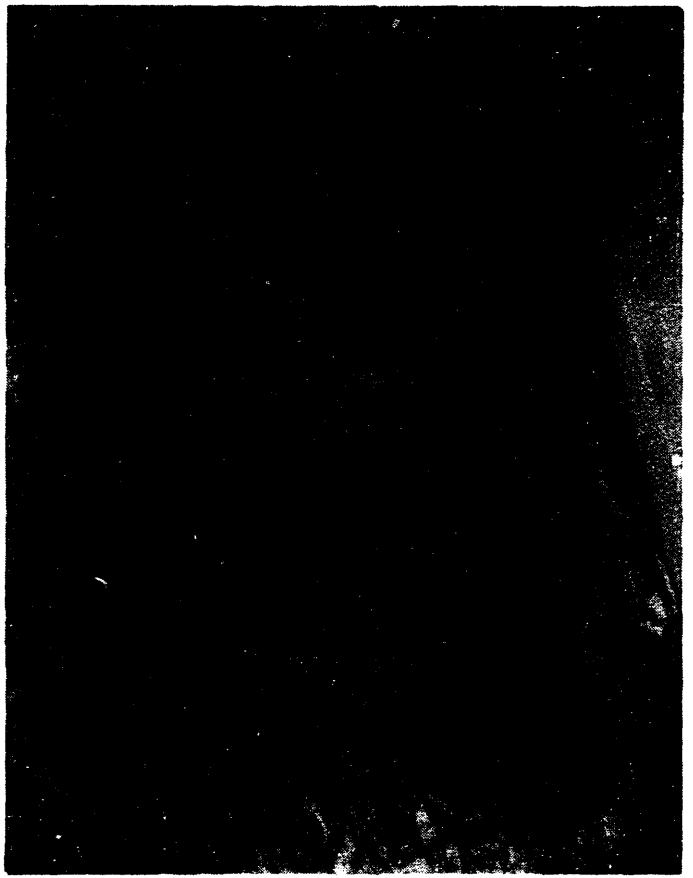

Figure B-33. Magnified view of the K-11 nozzle at a 180-degree reference.

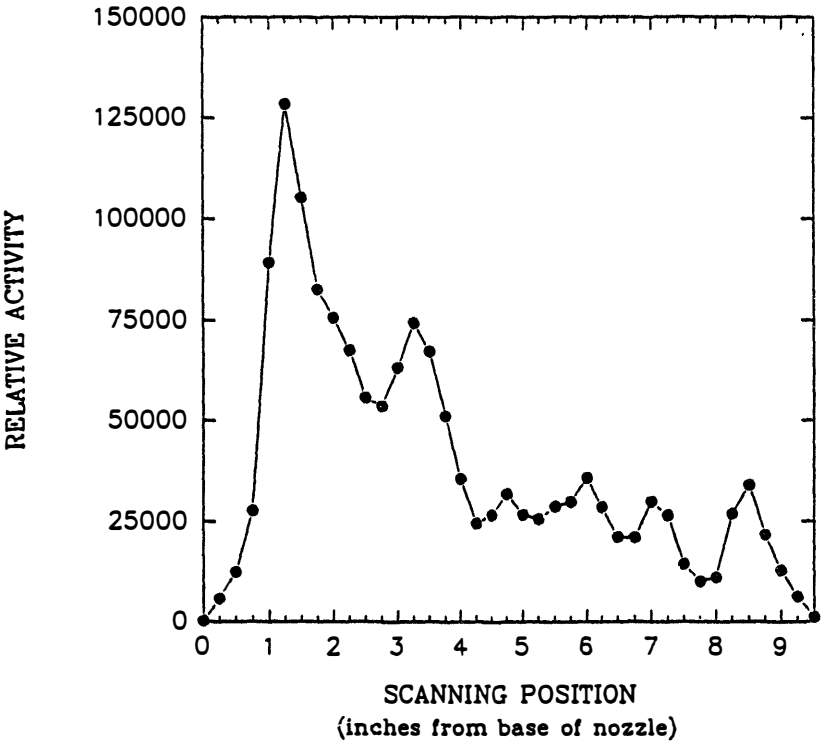

Figure B-34. The Cs-137 activity profile of nozzle K-11.

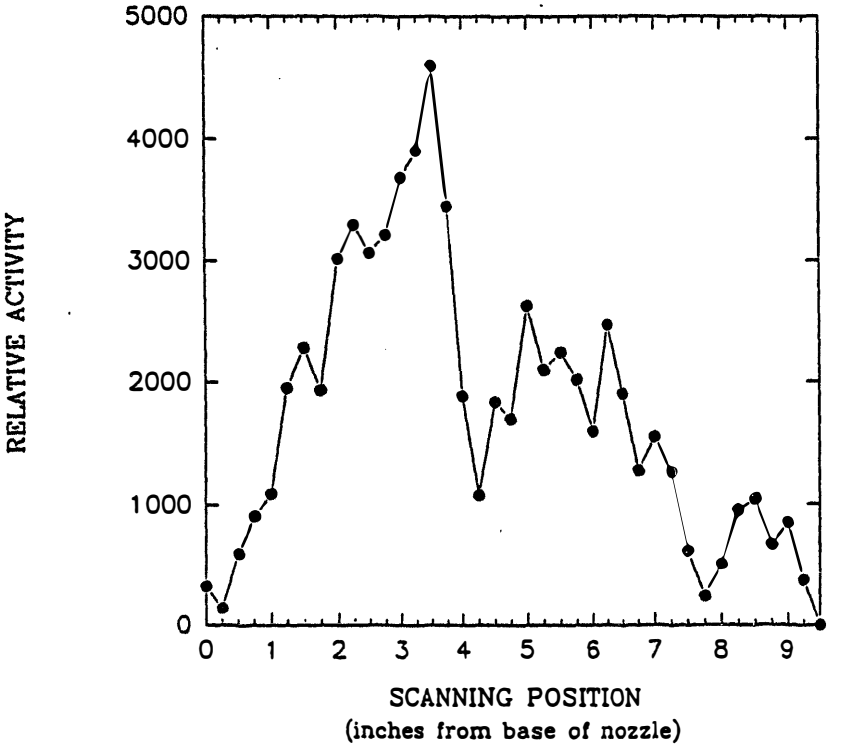

Figure B-35. The Co-60 activity profile of nozzle K-11.

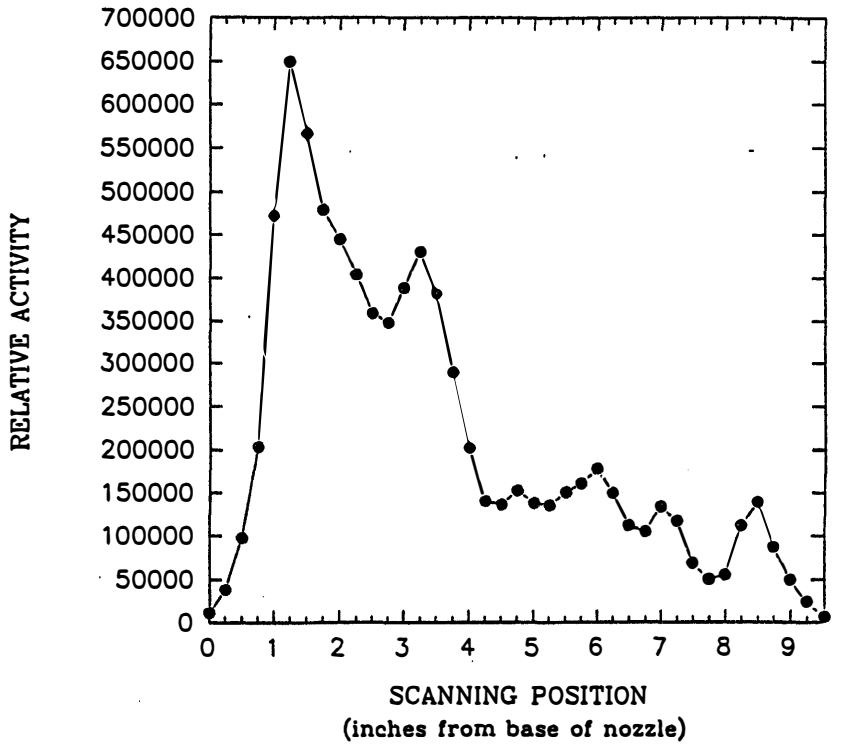

Figure B-36. The full-spectrum activity profile of nozzle K-11.

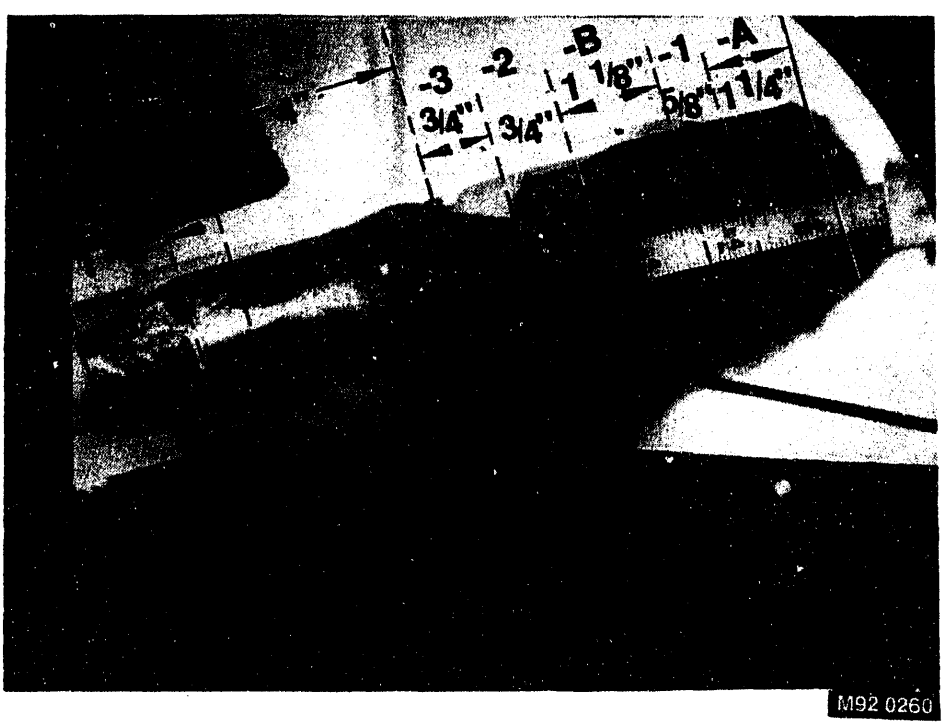

Figure B-37. Sectioning diagram of the K-11 nozzle.

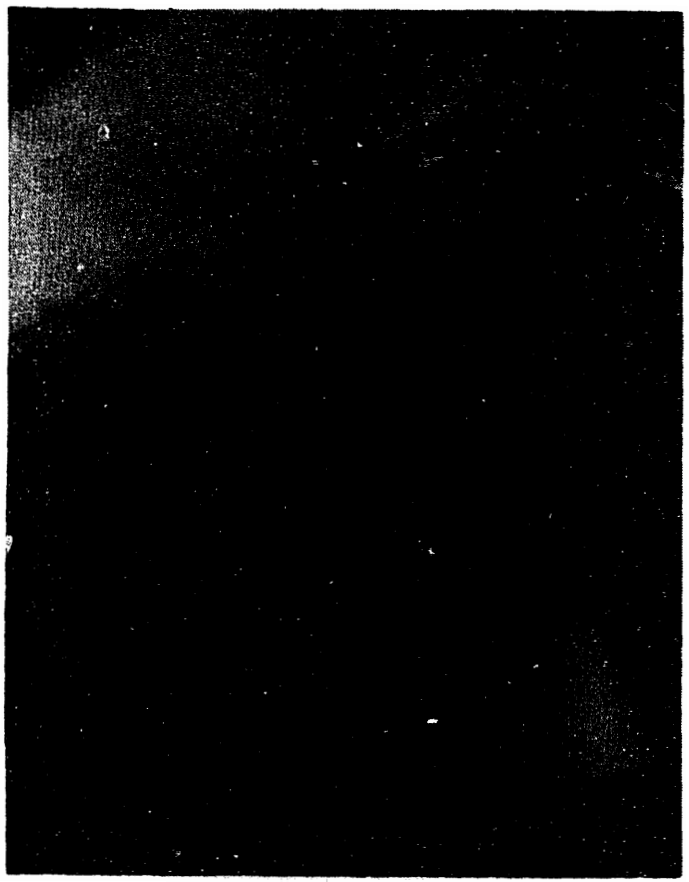

Figure B-38. Side view of sample K-11-2A.

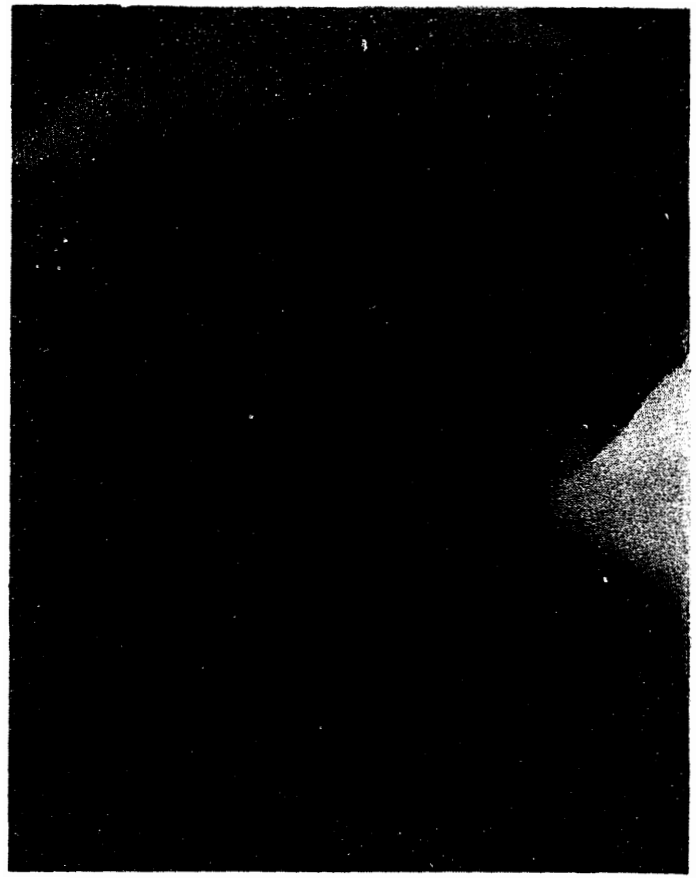

Figure B-39. Side view of sample K-11-2B.

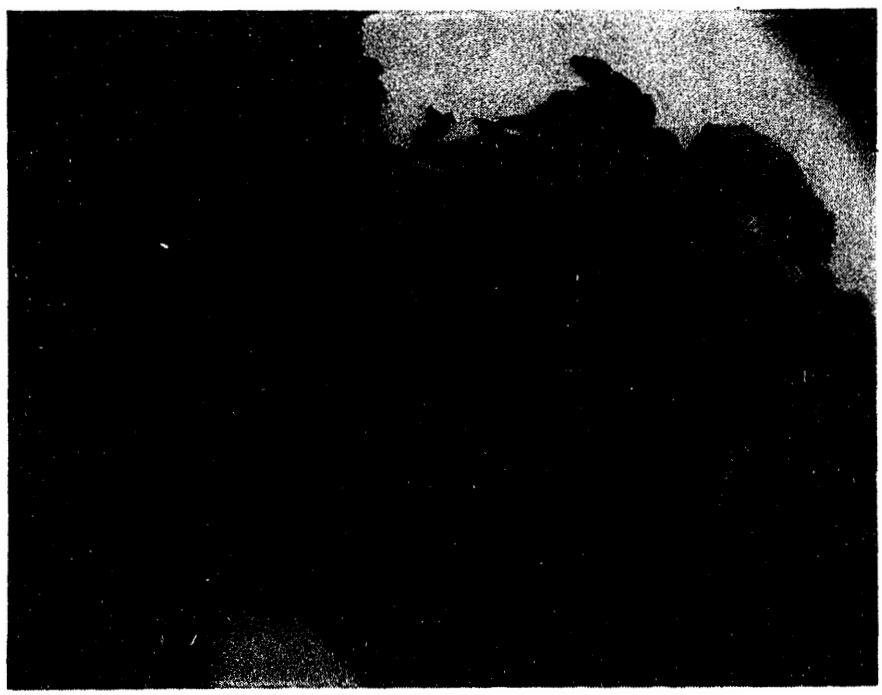

Figure B-40. Post-cutting side view of K-11-3A.

Figure B-41. Post-cutting side view of K-11-3B.

Figure B-42. Side view of the G-5 nozzle.

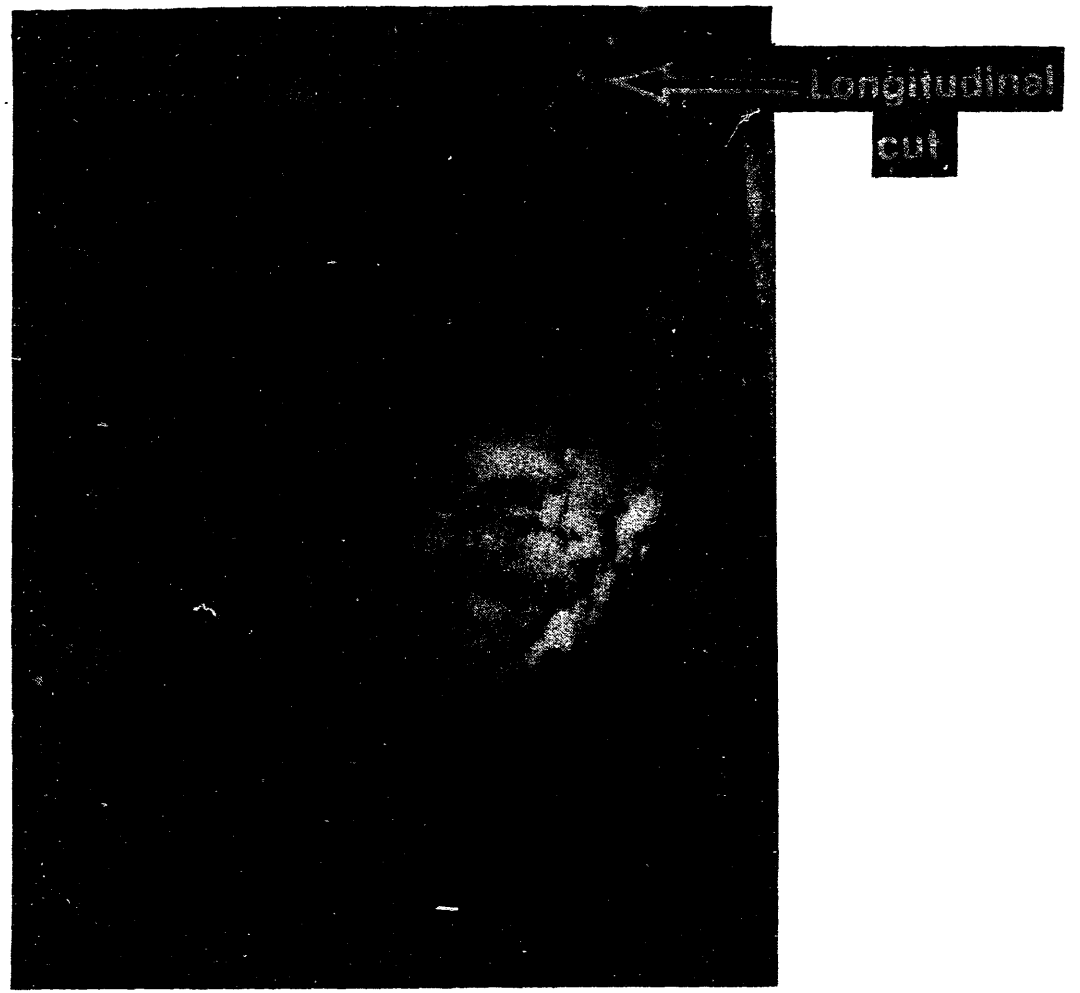

Figure B-43. Magnified view of the top of nozzle G-5 and the proposed sectioning line.

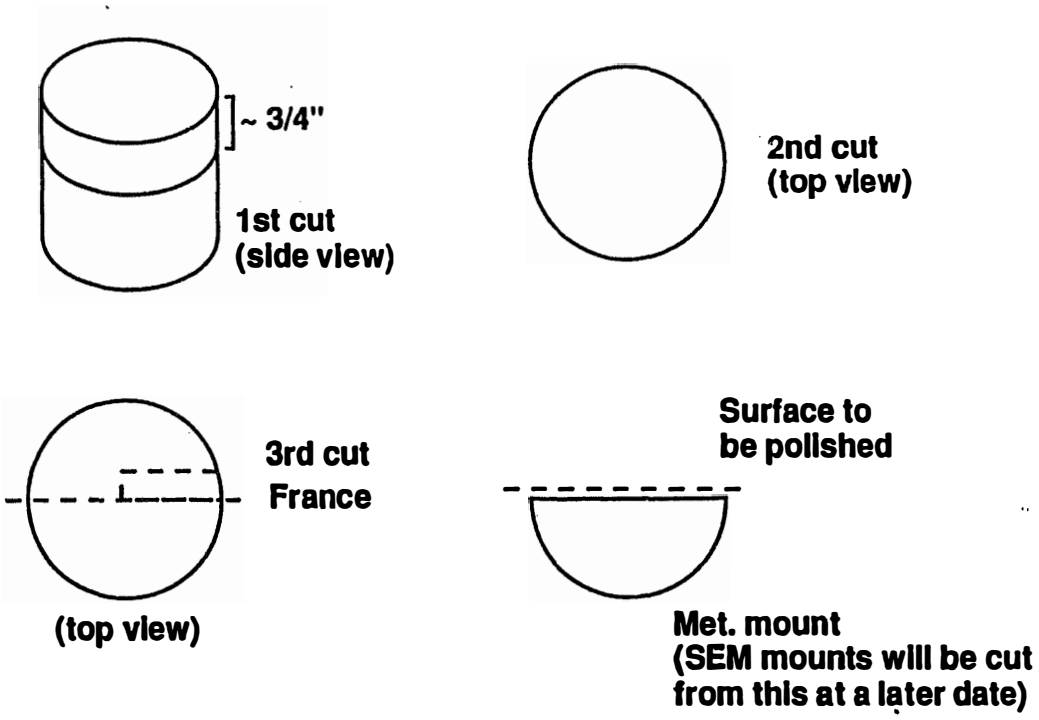

Figure B-44. Sectioning diagram of the G-5 nozzle.

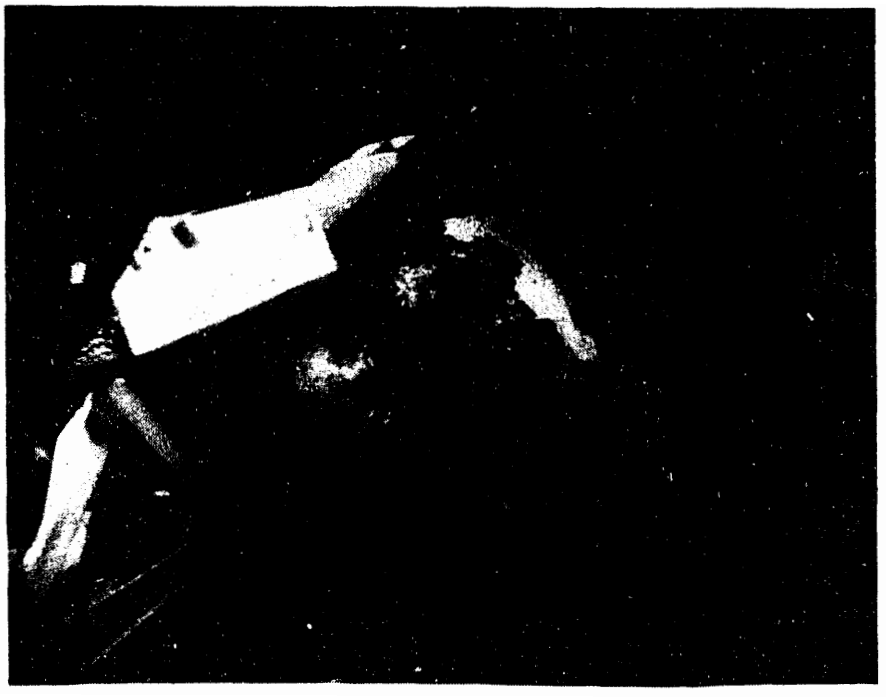

Figure B-45. Top view of nozzle E-7.

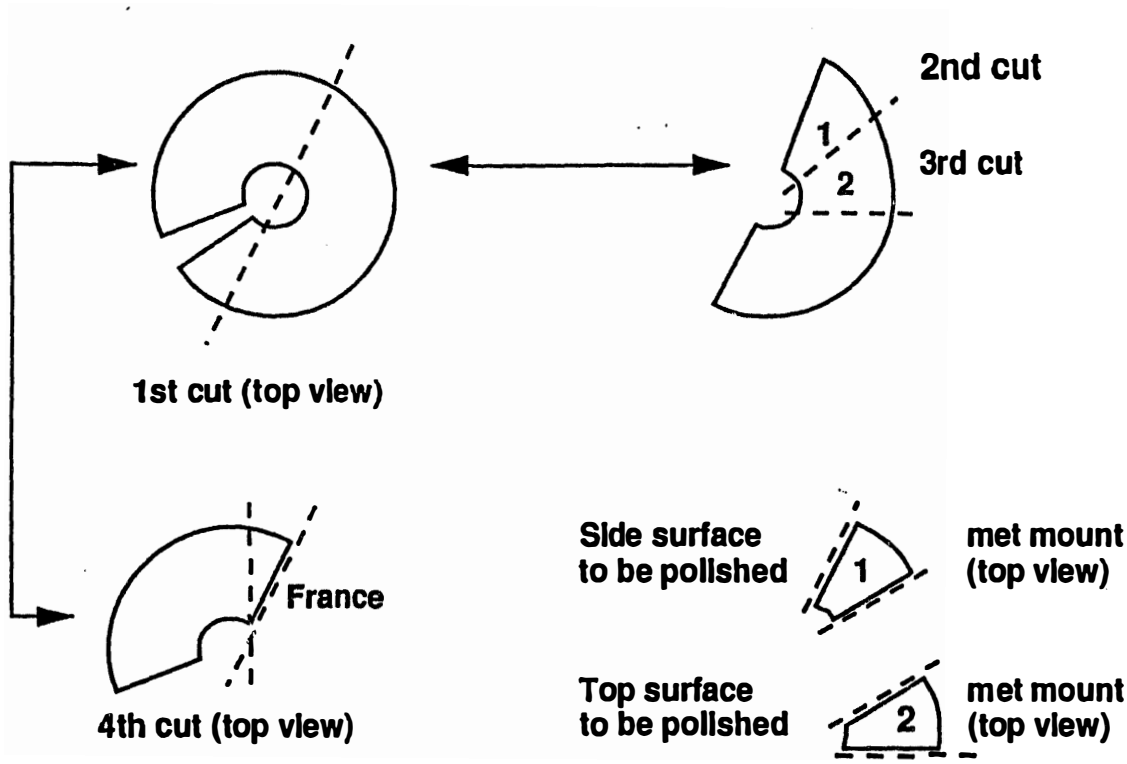

Figure B-46. Cutting diagram of the E-7 nozzle.

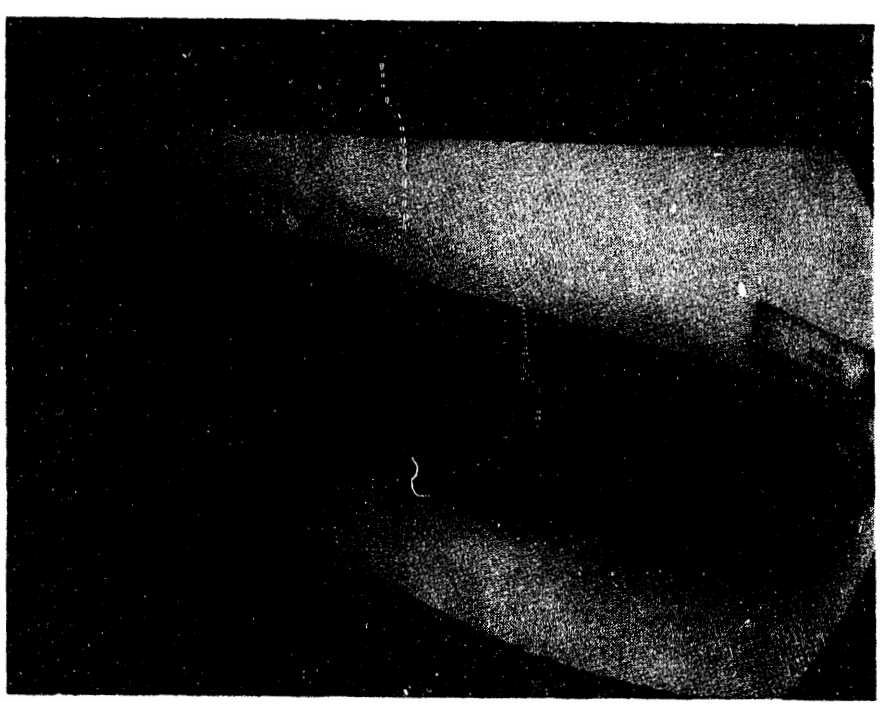

Figure B-47. Full-length view (including instrument string, 10-1/8 in.) of nozzle K-12.

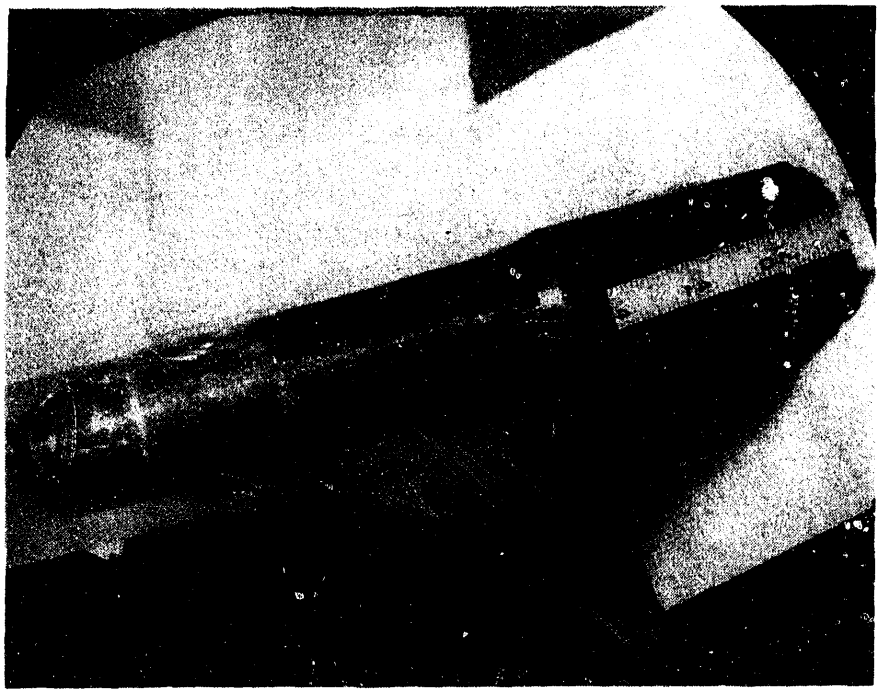

Figure B-48. Full-length view (excluding instrument string, 9-5/8 in.) of nozzle K-12.

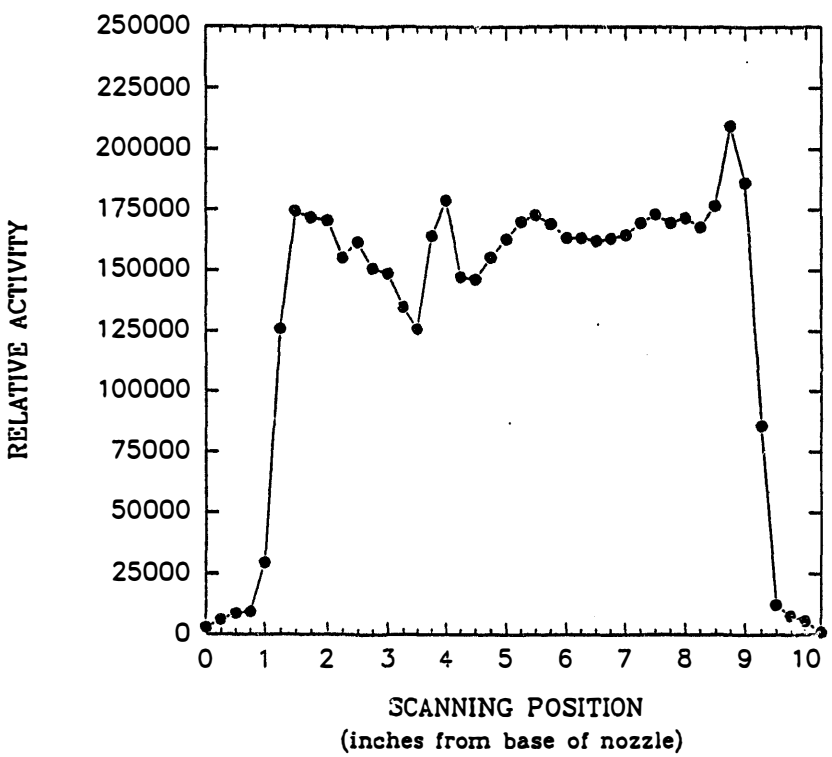

Figure B-49. The Cs-137 activity profile of nozzle K-12.

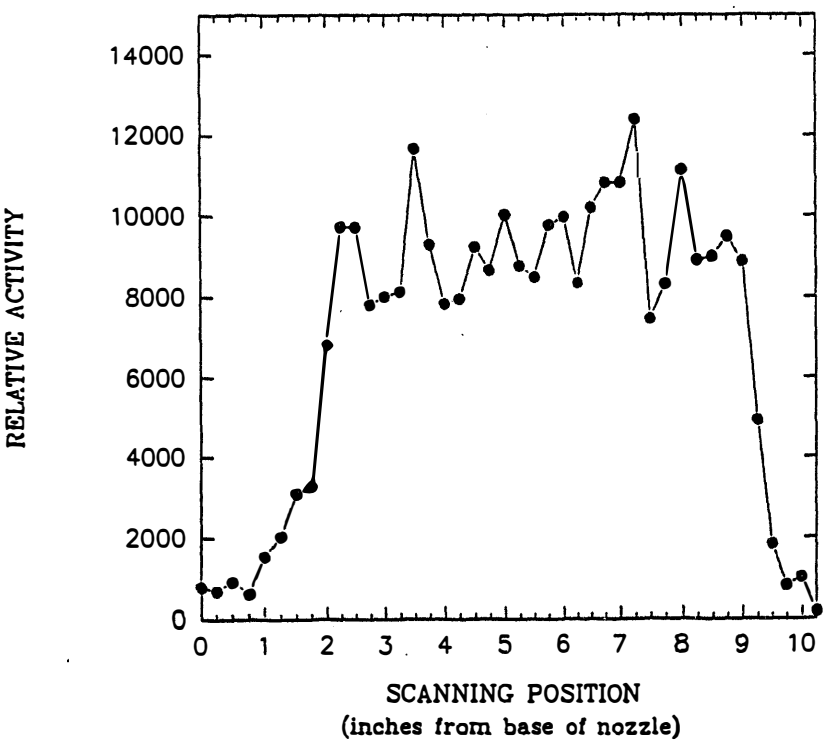

Figure B-50. The Co-60 activity profile of nozzle K-12.

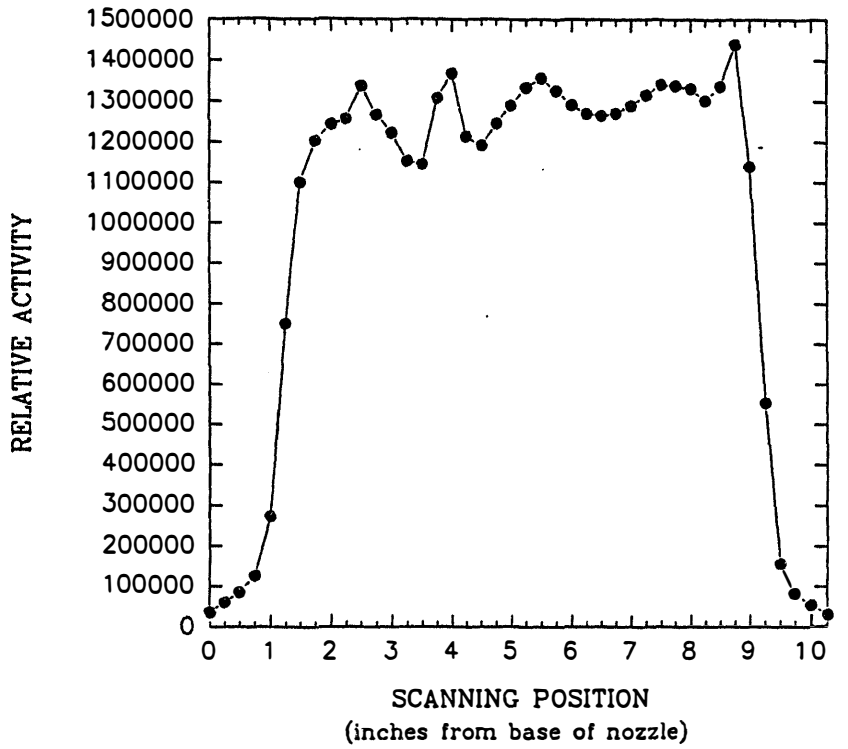

Figure B-51. A full-spectrum activity profile of nozzle K-12.

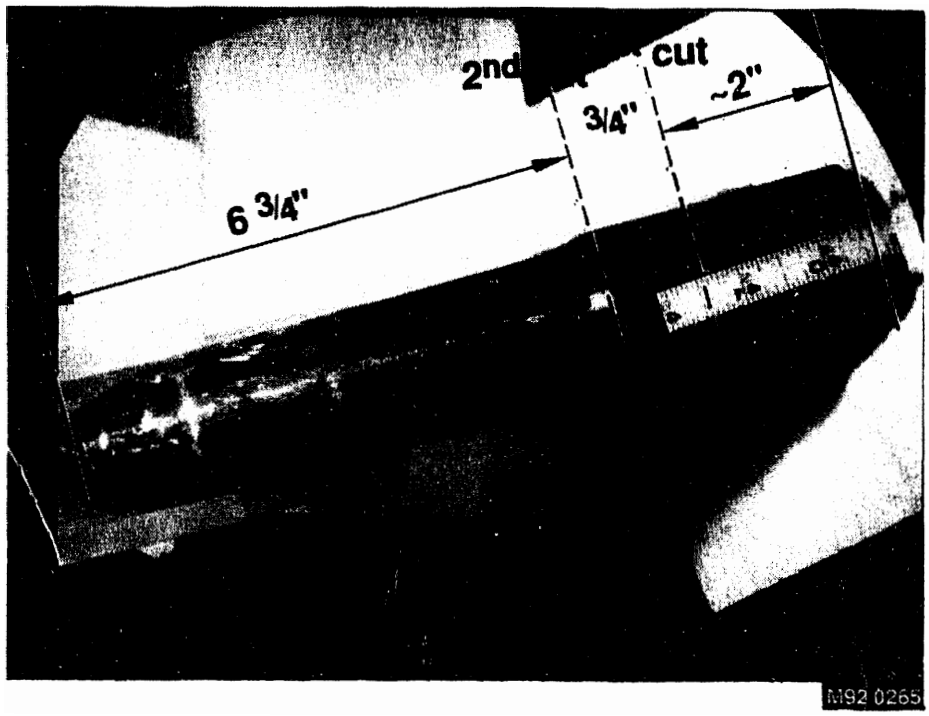

Figure B-52. Sectioning diagram of nozzle K-12.

Figure B-53. Full-length side view (~9-3/8 in.) of the K-5 guide tube.

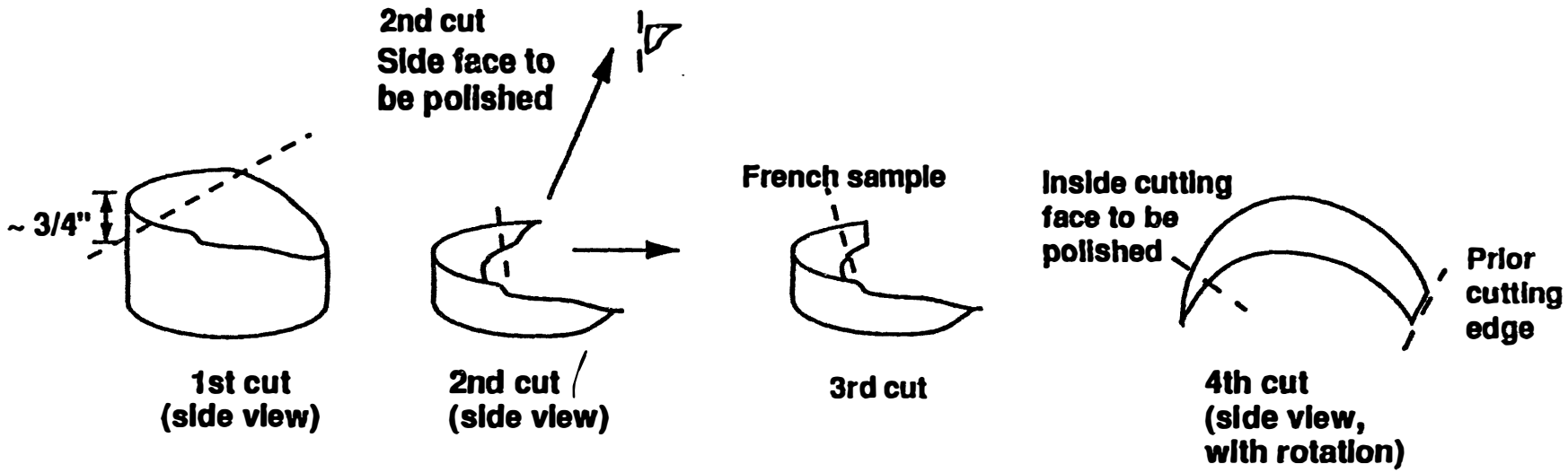

Cutting diagrams determined during meeting with:
D. Akers D. Sparks B. Schuetz

Figure B-54. Sectioning diagram of the K-5 guide tube.

Appendix C

Microstructural Examination Results

Appendix C

Microstructural Examination Results

Microstructure samples were obtained from each of the eight nozzles (E-7, G-5, H-9, K-11, K-12, L-11, M-10, and R-7) and from one guide tube (K-5). In addition, an initial examination was performed on a sample taken from the melt bulb that was attached to the instrument core string on the R-7 nozzle. Results of the microstructural examinations are described below.

The microstructural sample from the K-5 guide tube was obtained by the cutting sequence shown in Figure C-1. A second cut produced sample K-5-1, which was mounted and polished on the face exposed by the sectioning procedure (see Figure C-2). Sample K-5-1 was divided up into examination locations as shown in Figure C-3. Microstructural examinations were conducted at each of these locations or regions of interest (ROI) (91M209 through 91M214), as shown in Figures C-4 through C-9. These photomicrographs indicate that apparent molten fuel material interacted with the stainless steel of the guide tube and melted into its surface. In most cases, the clear separation between the stainless steel and the fuel material phases suggest that the mechanism for this interaction appears to be melting of the stainless steel with no apparent chemical interaction. However, Figure C-8 shows the presence of an apparent intermediate phase that may be the result of a dissolution of the stainless steel by the fuel debris. Further SEM/WDX analysis would be required to confirm the formation of this intermediate phase.

The R-7 nozzle was sectioned as shown in Figure C-10. Sample R-7-B, as shown in Figure C-11, was produced from cutting the R-7 nozzle. Figure C-12 shows the examination locations that were examined. The photomicrographs of the these ROIs (91M197 through 91M208) are shown in Figures C-13 through C-18. Examination of these photomicrographs indicates apparent interaction between the fuel debris and the instrument string material. Figure C-15 shows the interaction zone between the instrument string and the fuel material and suggests the formation of a number of intermediate phases composed of fuel material and constituents of the instrument string.

The G-5 cutting diagram, Figure C-19, shows how the G-5 nozzle was cut. As shown in Figure C-20, the cut surface was polished; ROIs were then selected, as shown in Figure C-21. Each of these ROIs (91M215 through 91M228) are shown in Figures C-22 through C-27. Evaluation of these photomicrographs indicates the presence of melt interspersed with metallic Inconel sections near the periphery of the nozzle. Further, the presence of what was determined to be silver is shown in Figure C-24. This figure suggests that silver was present on the lower head prior to the relocation of fuel debris to the lower head. Figure C-26 is a series of photographs that show the melt in the center of the nozzle from the top surface to the near the bottom of the melt region. These photomicrographs show a range of interactions from what appears to pure metallic material to a range of intermediate phases with molten material apparently interacting with the instrument string and the nozzle material.

The E-7 nozzle was sectioned as shown in Figure C-28. After samples E-7-1 (Figure C-29) and E-7-2 (Figure C-30) were mounted and polished, ROIs for sample E-7-1 were selected, as

shown in Figure C-31. Figures C-32 through C-40 show the ROIs (91M175 through 91M188) for sample E-7-1. Figures C-34 and C-35 show melt interaction between the nozzle material and the apparent fuel material. Figure C-35 indicates the presence of an intermediate phase, which suggests that some molten interaction occurred.

The selected ROIs for sample E-7-2 are shown in Figure C-41, and each of these ROIs (91M189 through 91M193) are shown in Figures C-42 through C-46. Typically, the interactions shown here are similar to those shown for sample E-7-1.

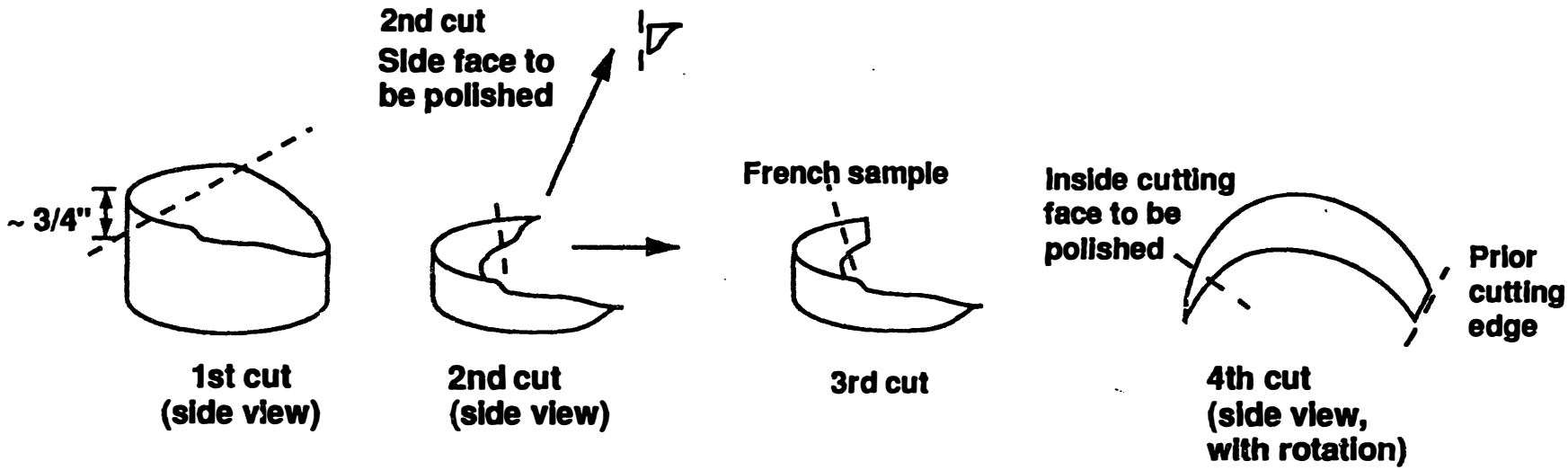

Figure C-1. Metallographic section of the K-5 guide tube.

Figure C-2. Guide tube sample K-5-1 shown mounted and polished in the mount for metallography.

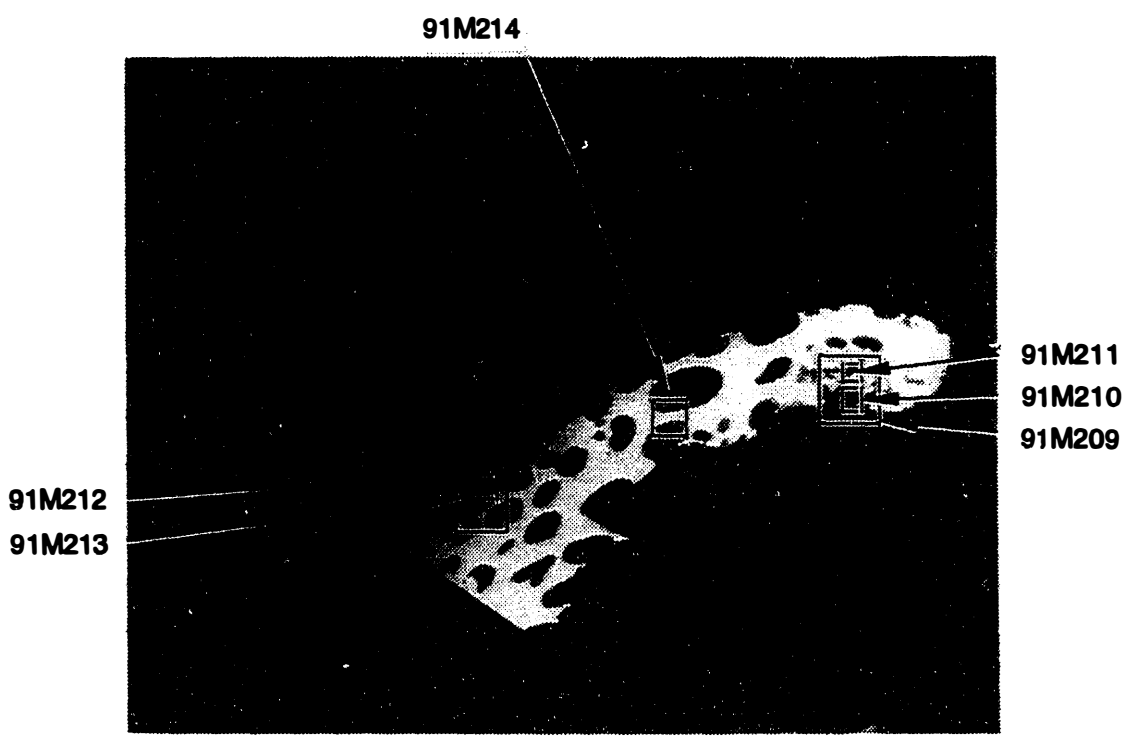

Figure C-3. Metallographic examination map showing ROIs of sample K-5-1 from the K-5 guide tube.

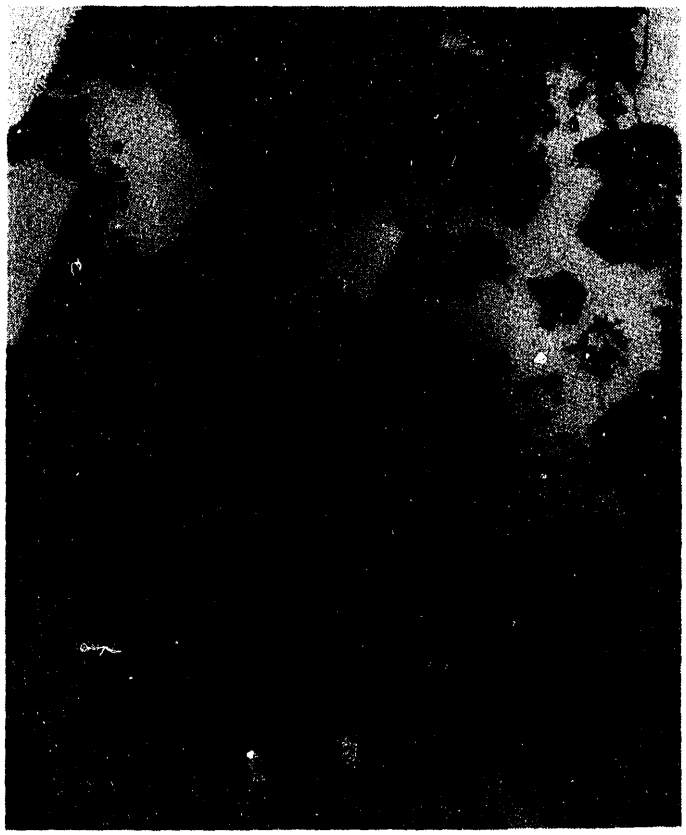

Figure C-4. ROI 91M209 at 50x magnification.

Figure C-5. ROI 91M210, showing 200x view of an isolated particle.

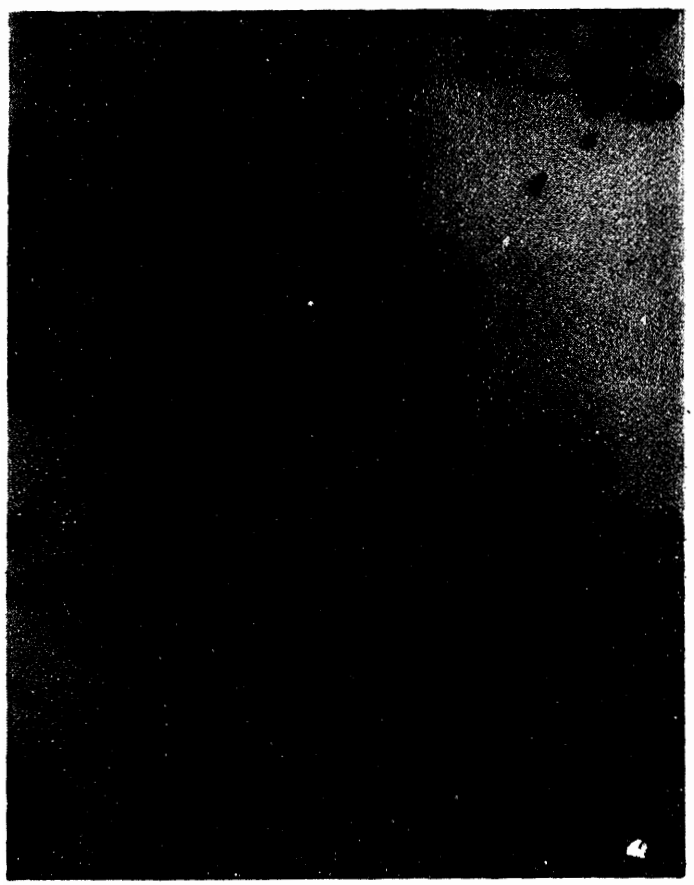

Figure C-6. ROI 91M211, showing a 200x view of a mottled structure.

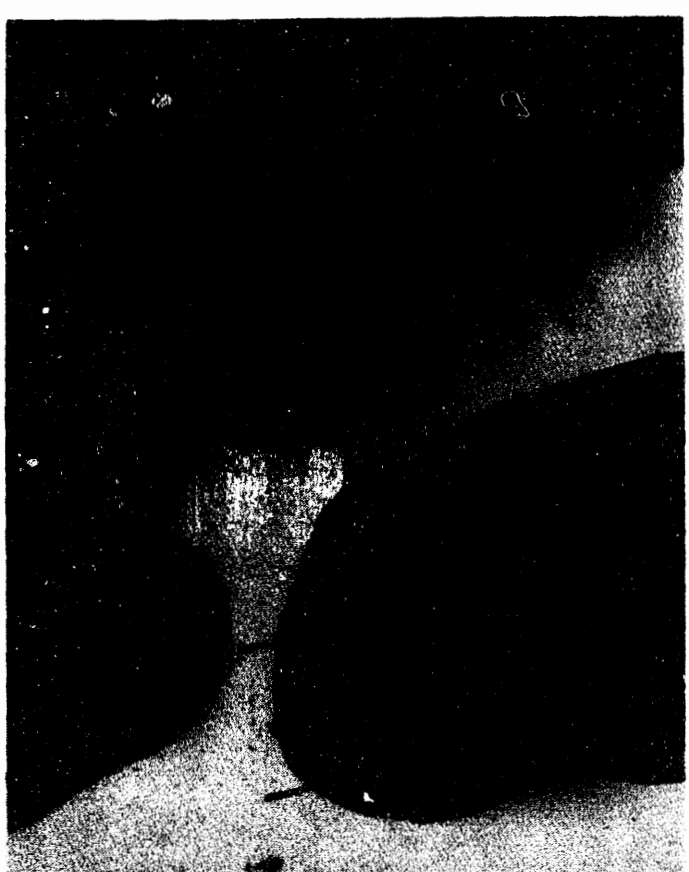

Figure C-7. ROI 91M212, showing porous K-5 material with attached melt.

Figure C-8. ROI 91M213, displaying higher magnification view of fuel grains.

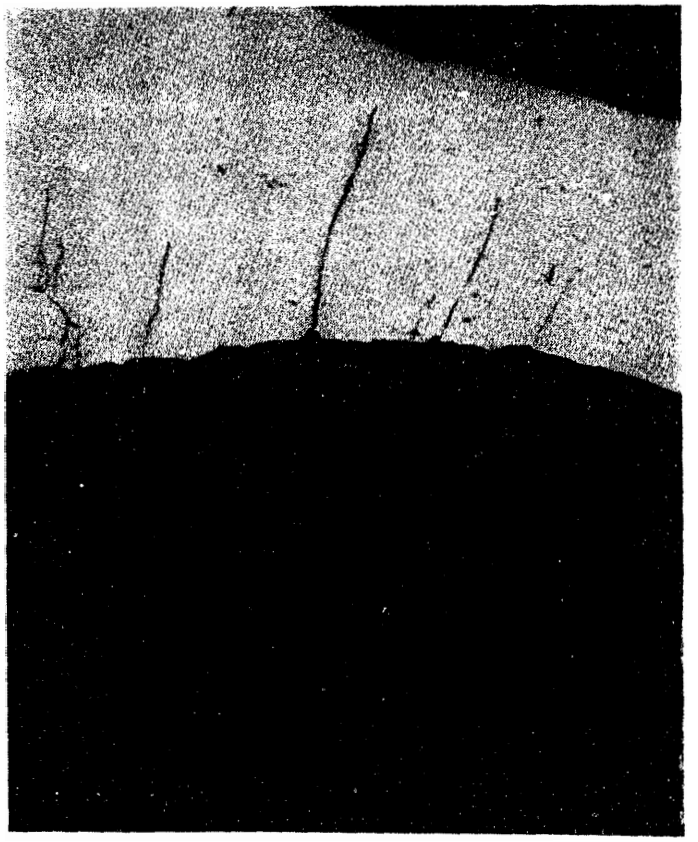

Figure C-9. ROI 91M214, showing evidence of cracking of the guide tube material.

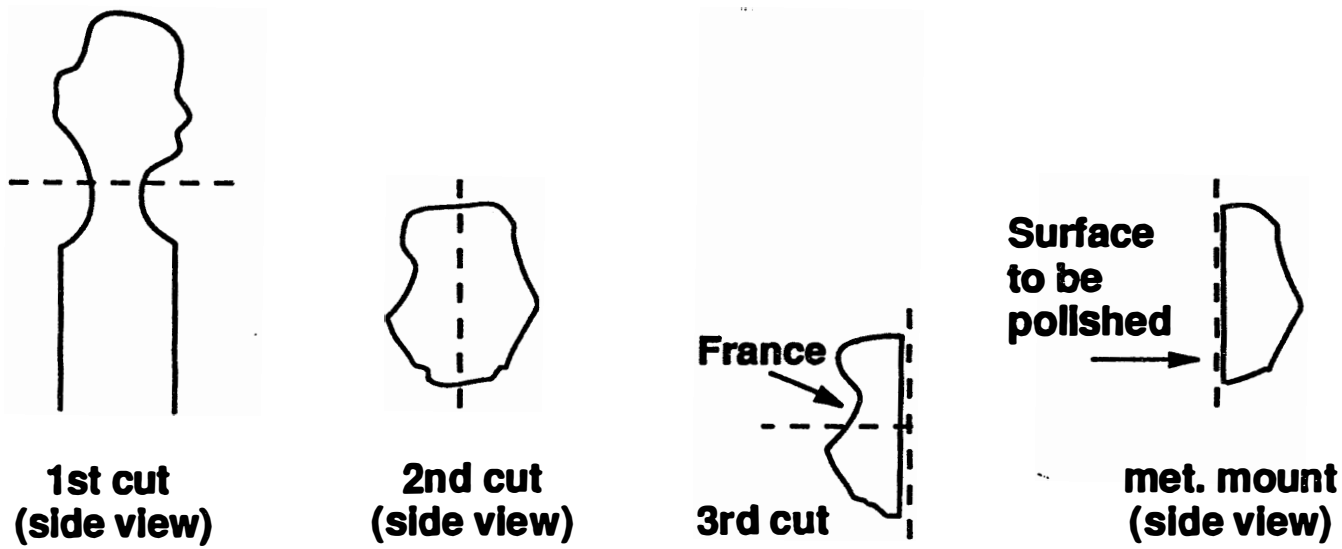

Figure C-10. Sectioning diagram of the R-7 nozzle with attached melt bulb.

Figure C-11. Metallographic sample of R-7 nozzle melt bulb shown mounted and polished.

Figure C-12. Metallographic examination map showing ROIs of sample R-7-B.

Figure C-13. ROI 91M197, showing apparent molten fuel.

Figure C-14. Fuel adjacent to instrument leads at ROI 91M198.

Figure C-15. ROI 91M199, showing 100x view of fuel and instrument leads.

Figure C-16. ROI 91M208, showing material resembling braze metal.

Figure C-17a. ROI 91M203 (view #1 of a five-photo composite) (starting from edge of sample).

Figure C-17b. ROI 91M204 (view #2 of a five-photo composite).

Figure C-17c. ROI 91M205 (view #3 of a five-photo composite).

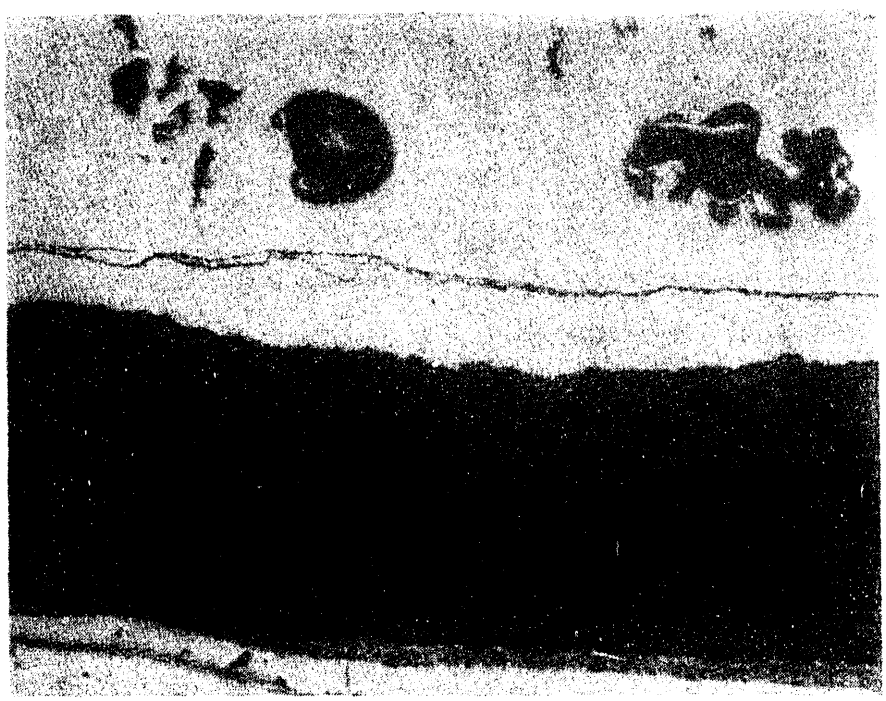

Figure C-17d. ROI 91M206 (view #4 of a five-photo composite).

Figure C-17e. ROI 91M207 (view #5 of a five-photo composite).

Figure C-18a. ROI 91M202 at 100x (view #1 of a three-photo composite).

Figure C-18b. ROI 91M201 at 100x (view #2 of a three-photo composite).

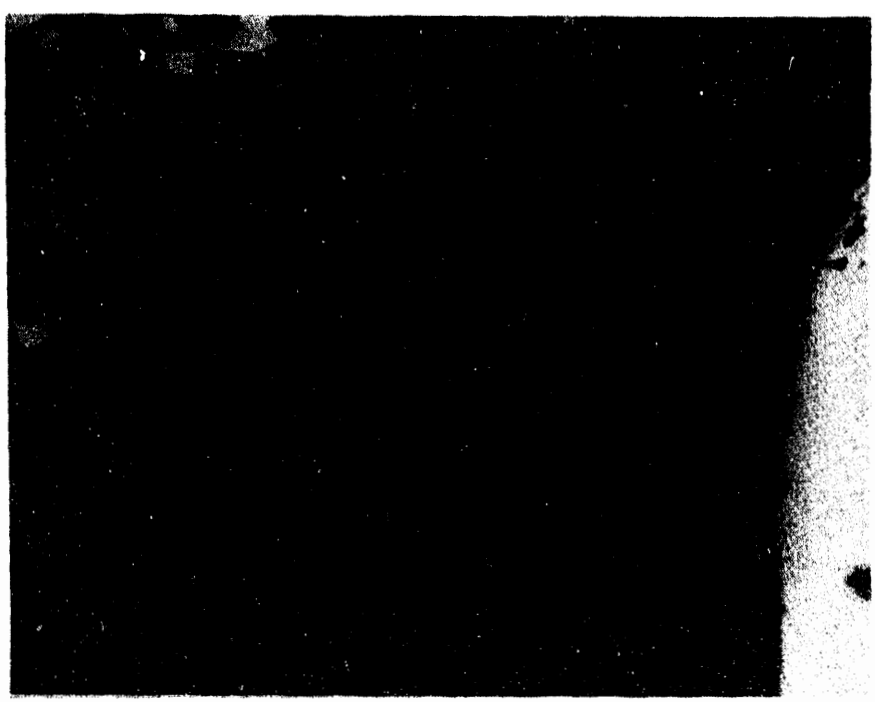

Figure C-18c. ROI 91M200 at 100x (view #3 of a three-photo composite).

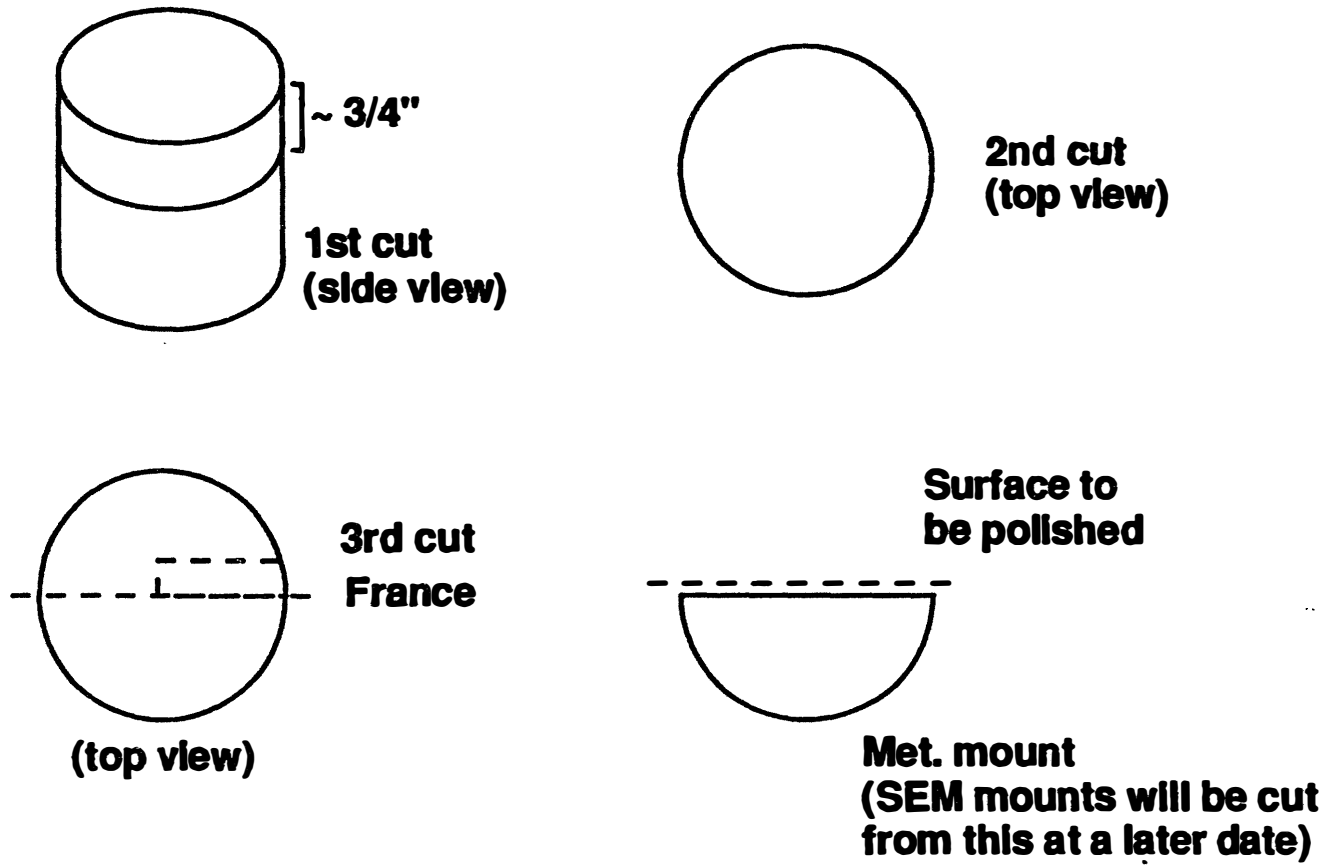

Figure C-19. Cutting diagram for the G-5 nozzle.

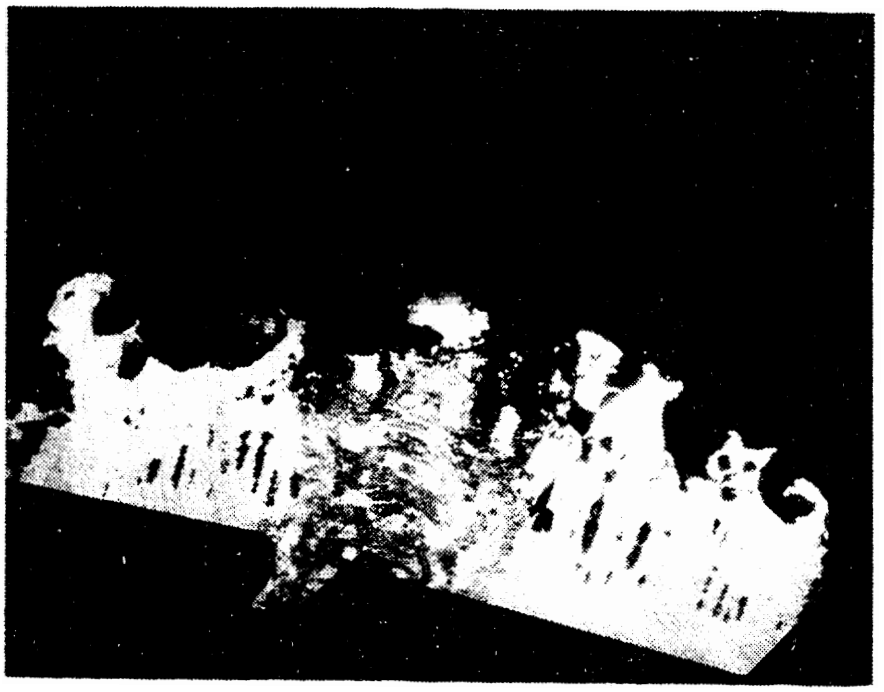

Figure C-20. The G-5 metallography sample mounted and polished for examination of the longitudinal face.

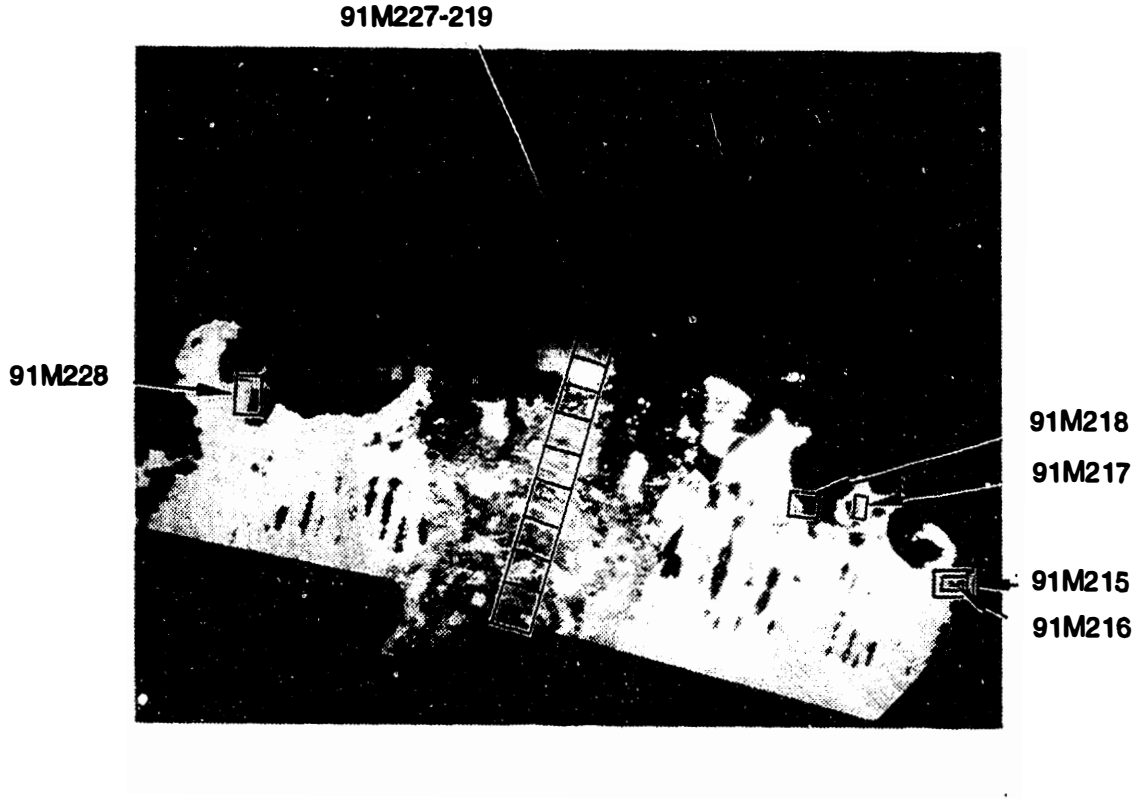

Figure C-21. Metallographic examination map showing ROIs of the G-5 nozzle.

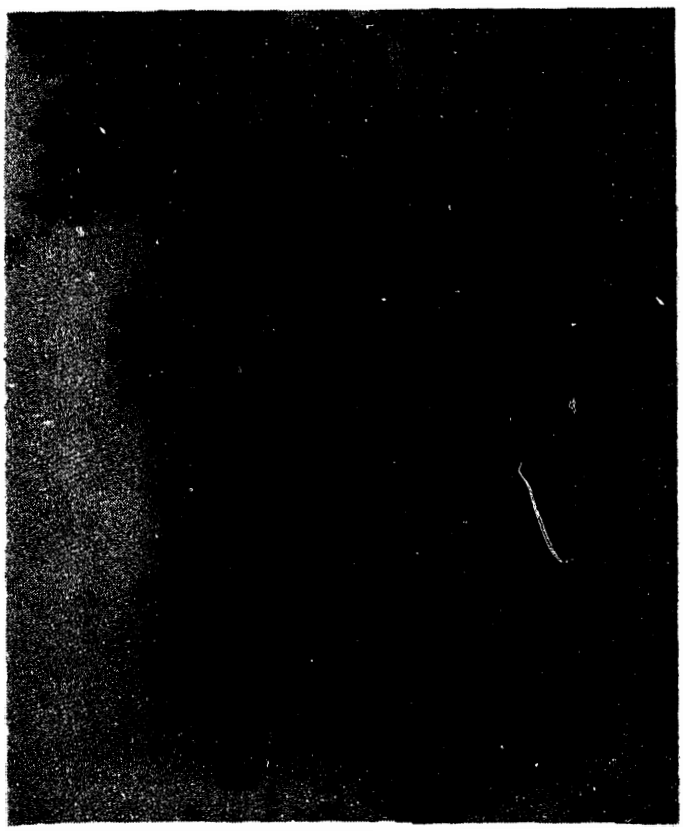

Figure C-22. 50x view of the melt at ROI 91M215.

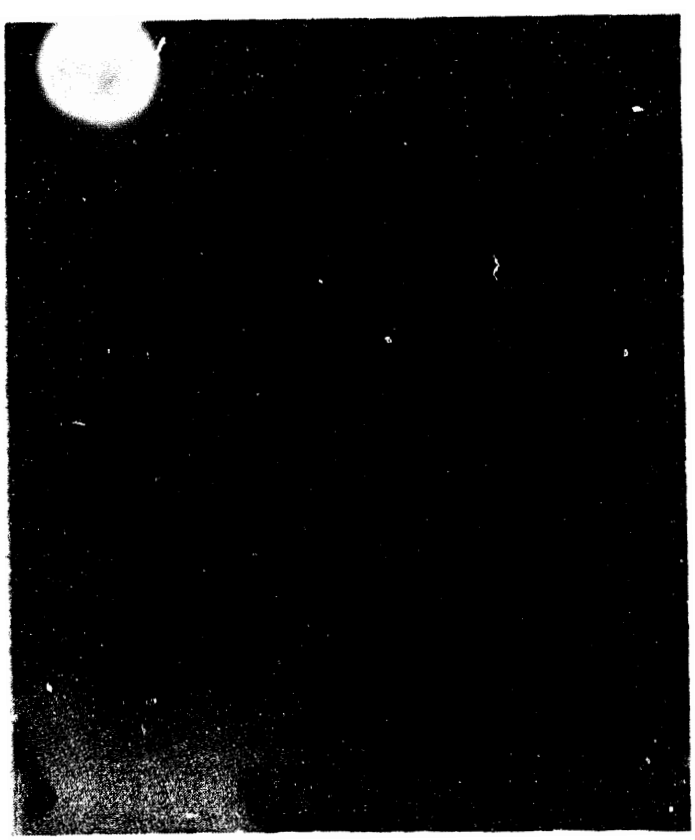

Figure C-23. Higher magnification (200x) view of ROI 91M215.

Figure C-24. ROI 91M217, showing debris inside hole (200x).

Figure C-25. 100x view displaying silver drops at ROI 91M218.

Figure C-26a. ROI 91M227 (view #1 of a nine-photo composite) (proceeding from the top to the bottom).

Figure C-26b. ROI 91M226 (view #2 of a nine-photo composite).

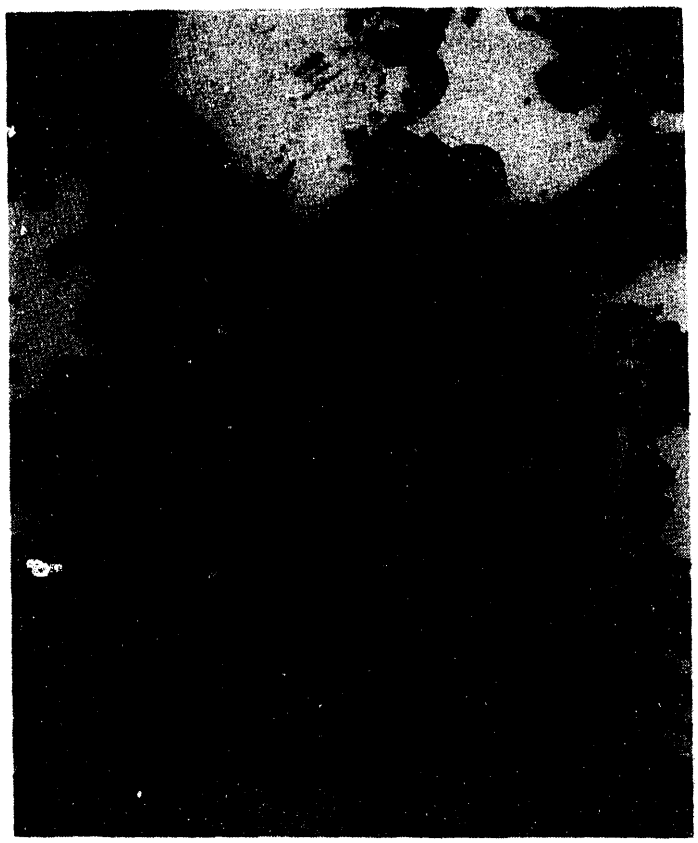

Figure C-26c. ROI 91M225 (view #3 of a nine-photo composite).

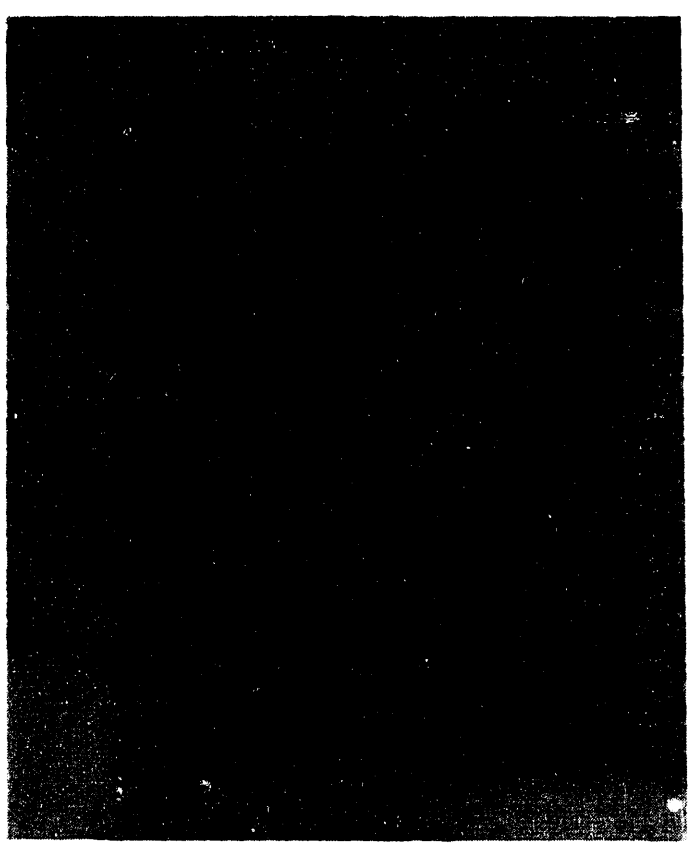

Figure C-26d. ROI 91M224 (view #4 of a nine-photo composite).

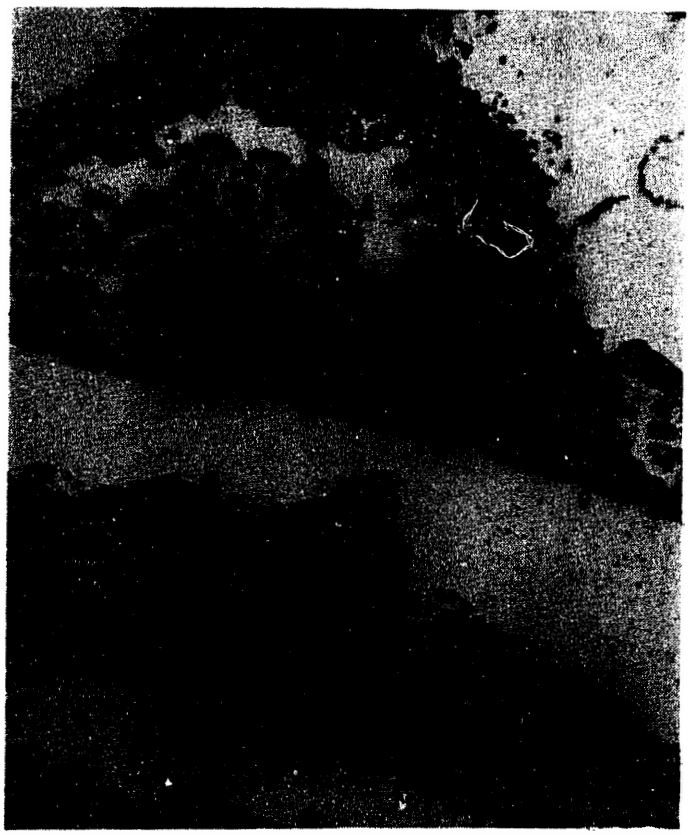

Figure C-26e. ROI 91M223 (view #5 of a nine-photo composite).

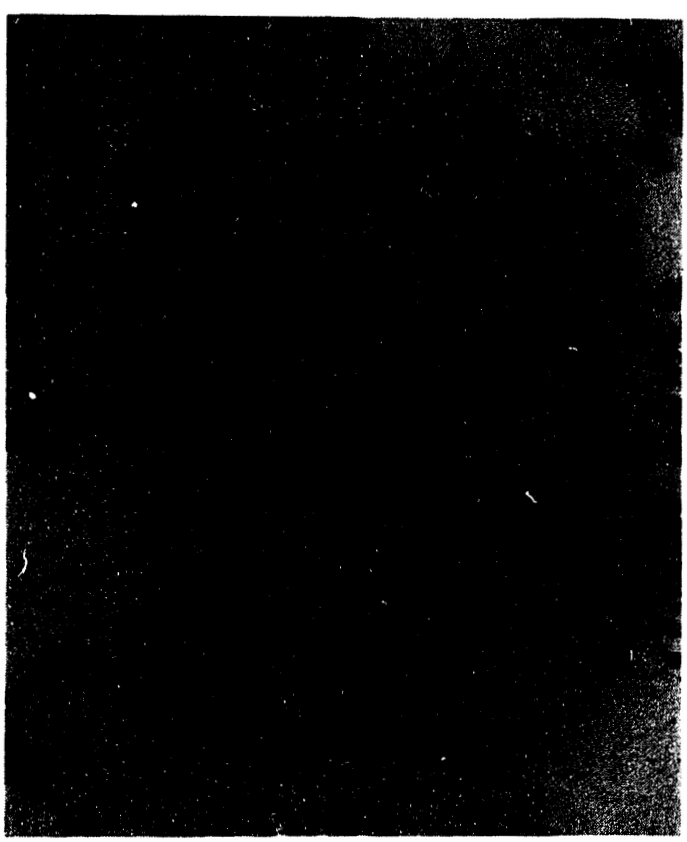

Figure C-26f. ROI 91M222 (view #6 of a nine-photo composite).

Figure C-26g. ROI 91M221 (view #7 of a nine-photo composite).

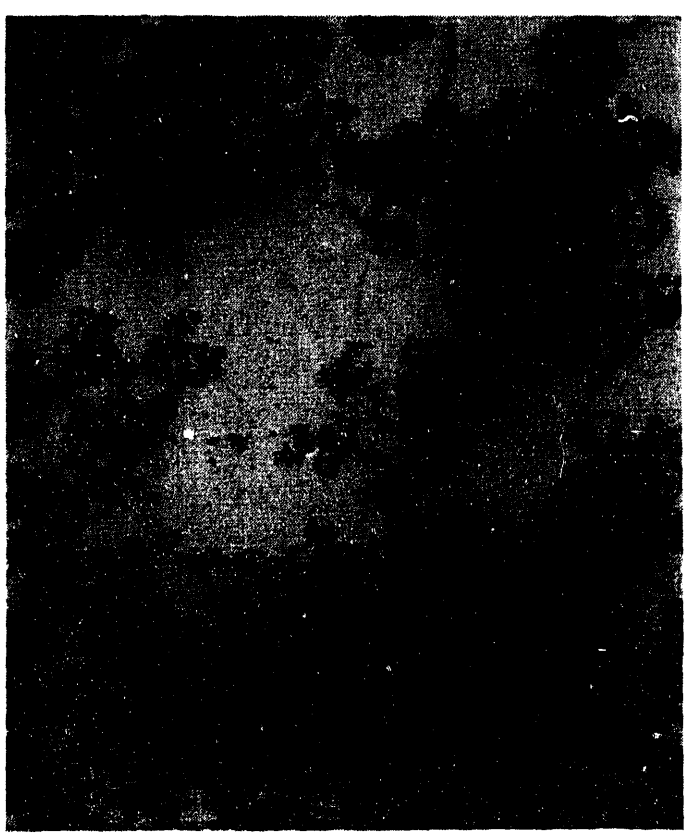

Figure C-26h. ROI 91M220 (view #8 of a nine-photo composite).

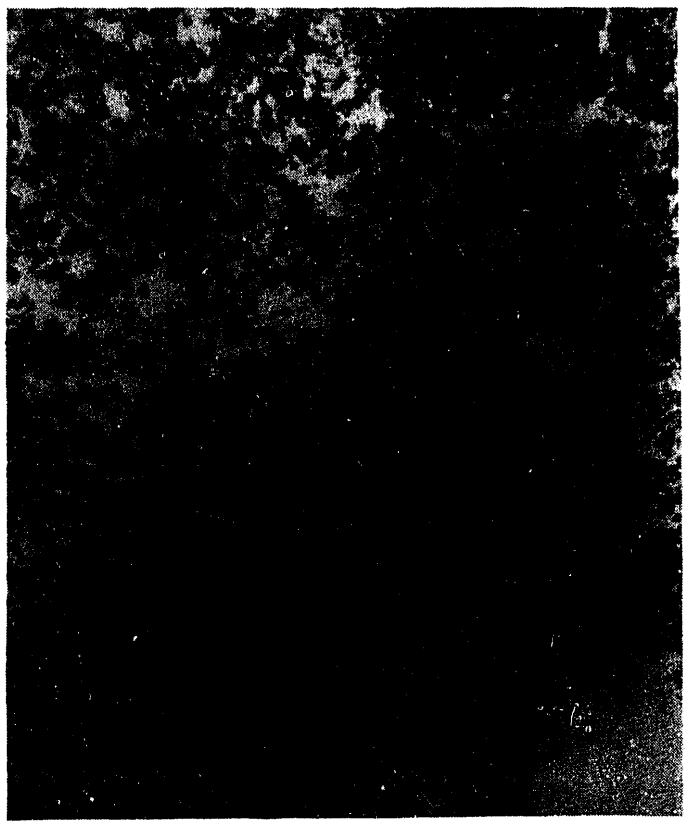

Figure C-26i. ROI 91M219 (view #9 of a nine-photo composite).

Figure C-27. ROI 91M228, exhibiting material cracking.

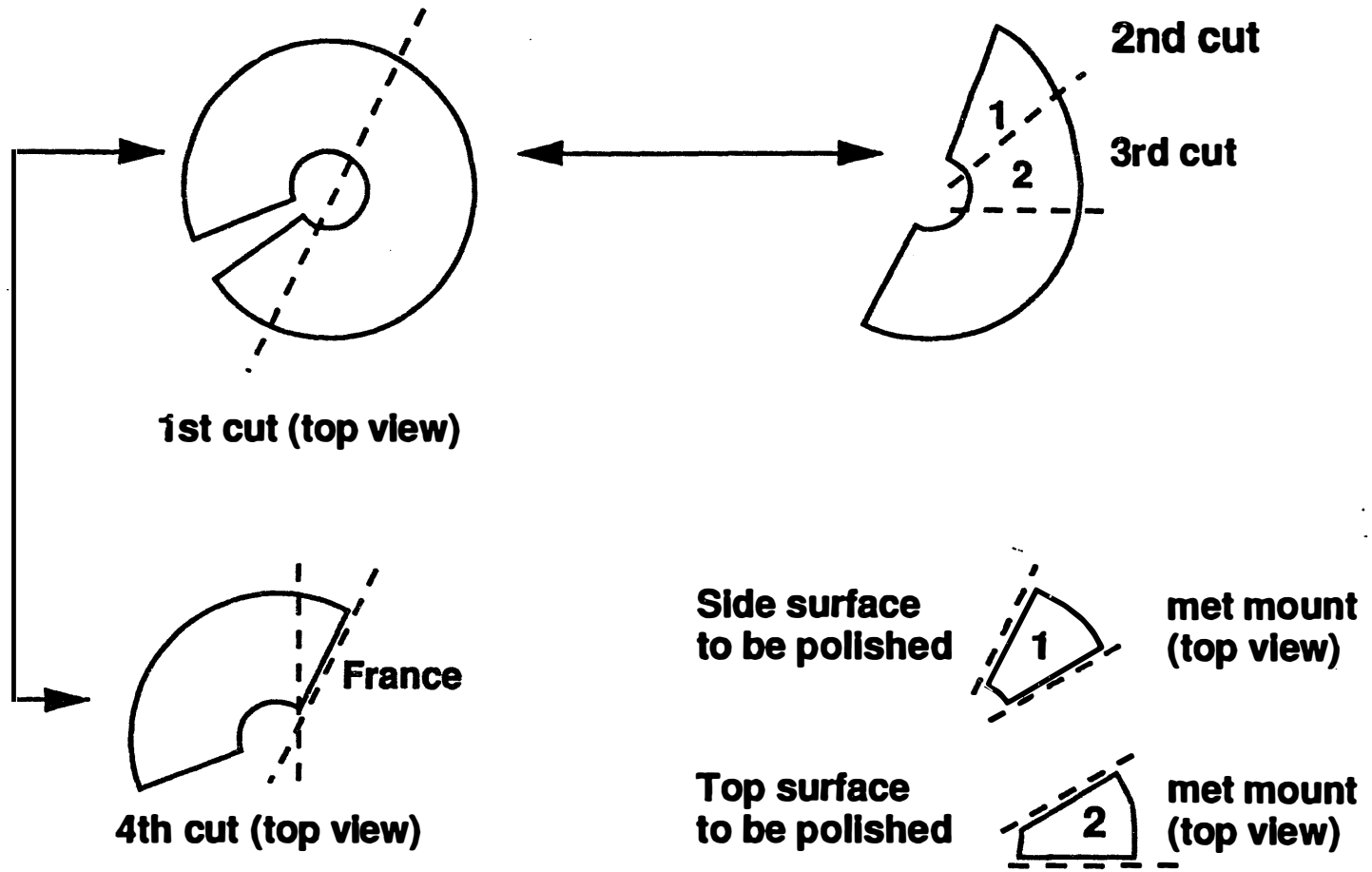

Figure C-28. Sectioning procedure for the E-7 nozzle.

Figure C-29. Metallographic sample E-7-1, showing the side face.

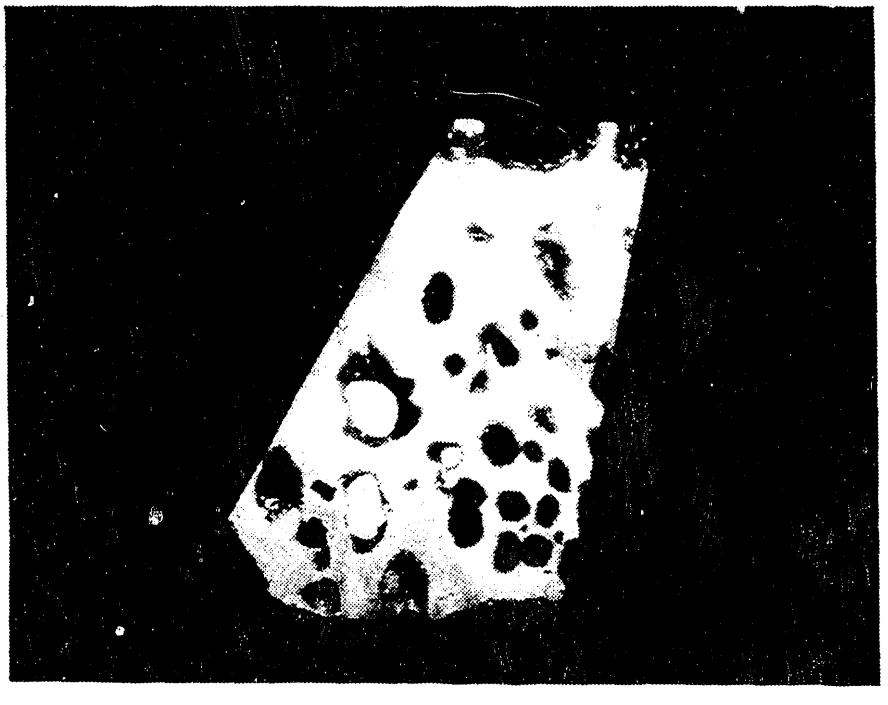

Figure C-30. Metallographic sample E-7-2, featuring the top surface.

Figure C-31. Metallographic examination map showing ROIs of sample E-7-1.

Figure C-32. ROIs 91M175 and 91M176, showing possible cracking (two-photo composite).

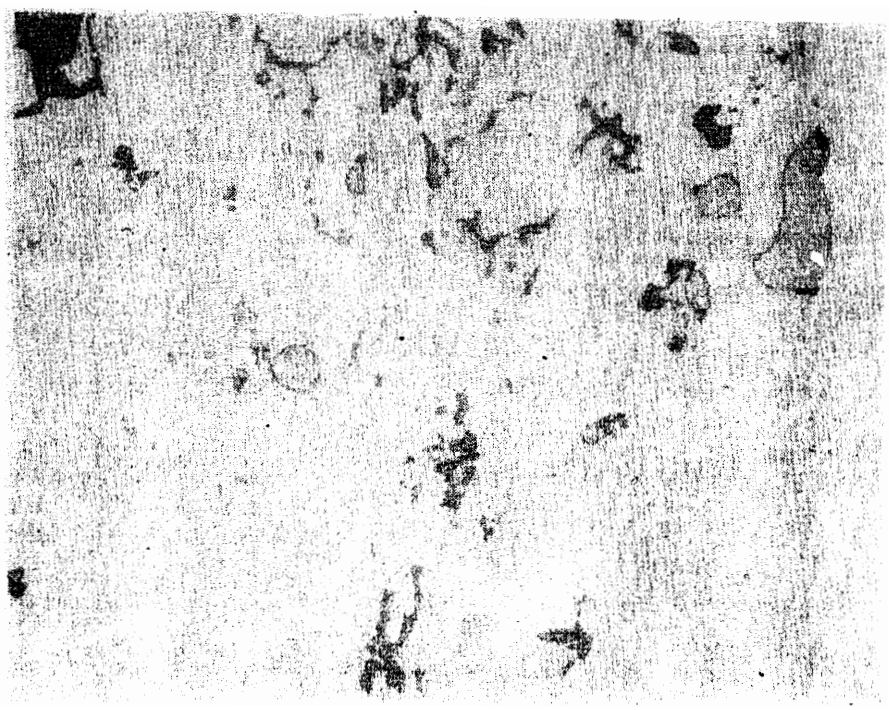

Figure C-33. ROI 91M177, showing higher magnification (200x) view of possible cracking.

Figure C-34. ROIs 91M178 and 91M179, exhibiting fuel melt interaction (two-photo composite).

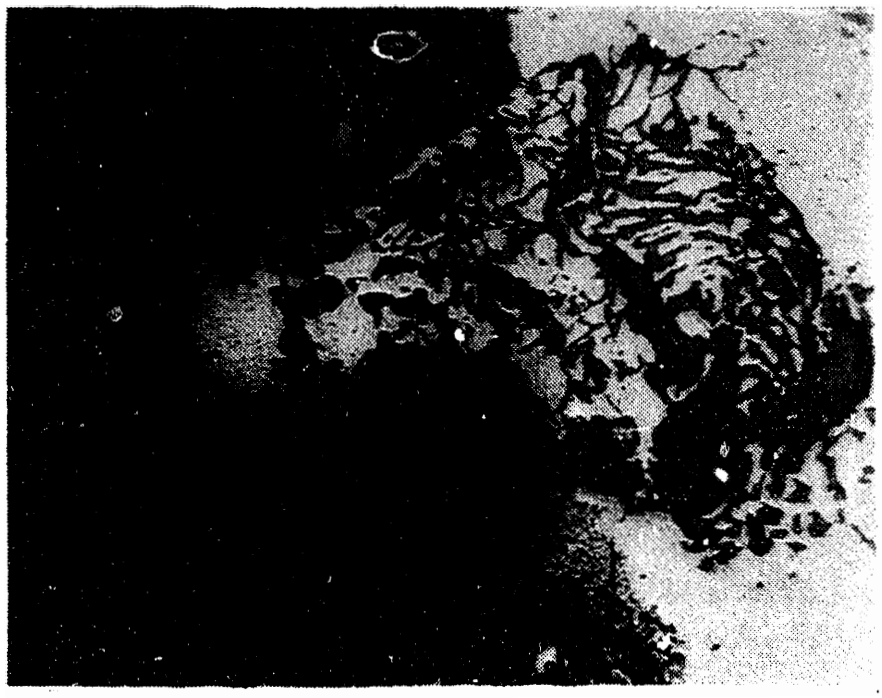

Figure C-35. ROI 91M182, showing indication of fluid melt interaction.

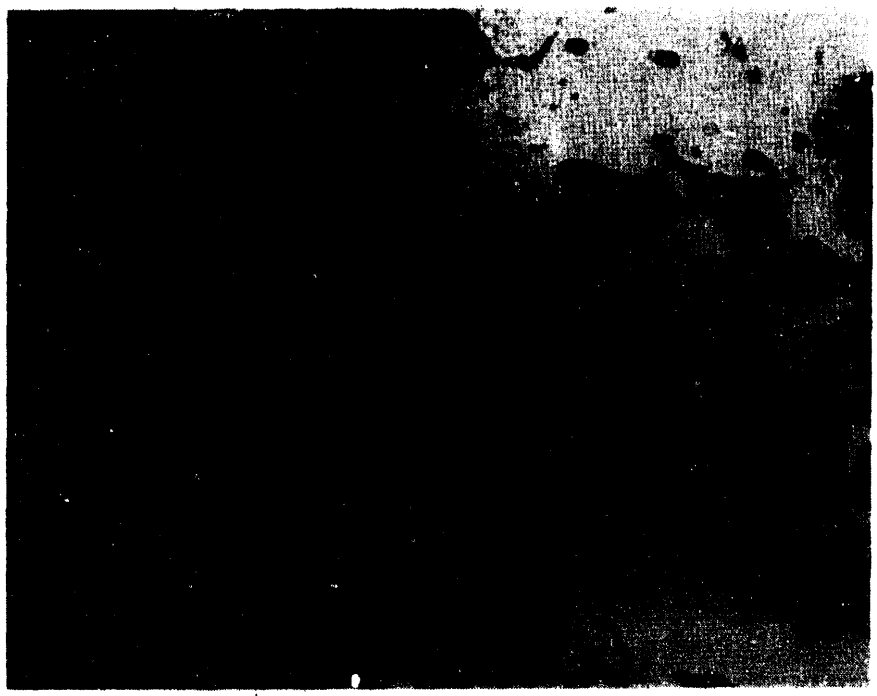

Figure C-36a. ROI 91M180, exhibiting interspersed fuel (view #1 of a two-photo composite).

Figure C-36b. ROI 91M181, exhibiting interspersed fuel (view #2 of a two-photo composite).

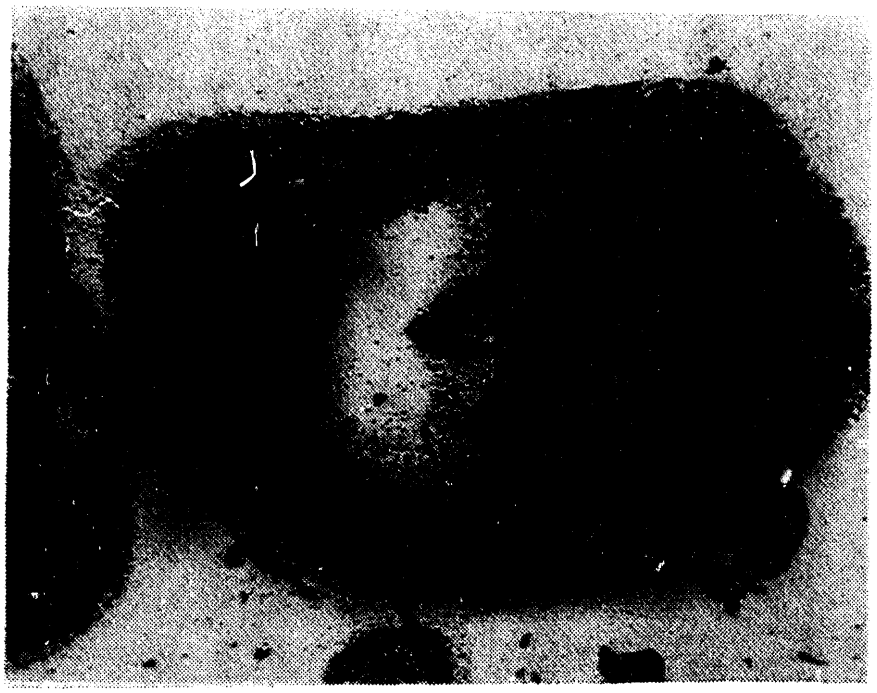

Figure C-37. ROI 91M183, showing macro view of spheroid material in hole.

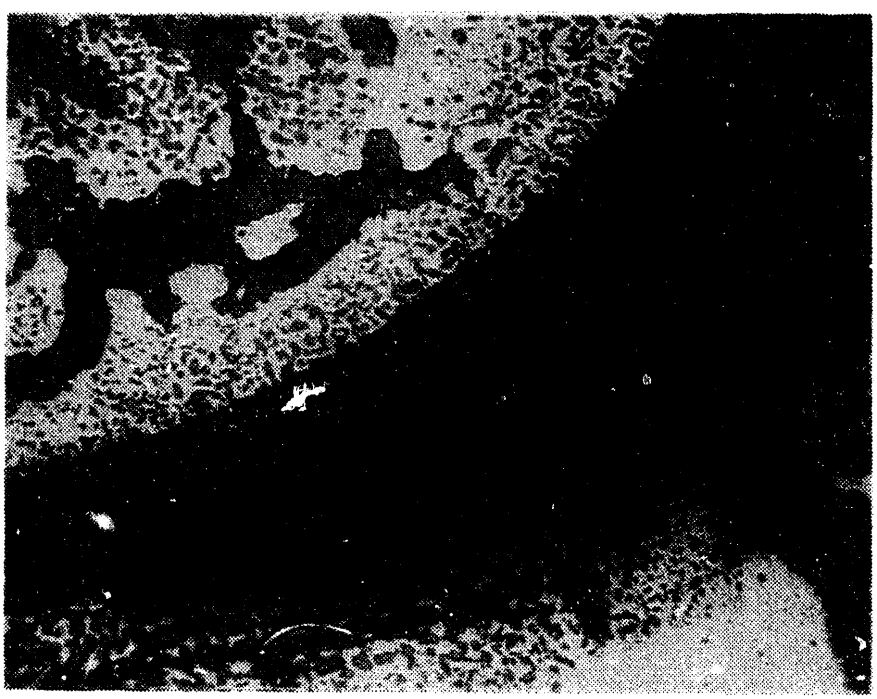

Figure C-38. ROI 91M184, showing higher magnification (200x) of hole.

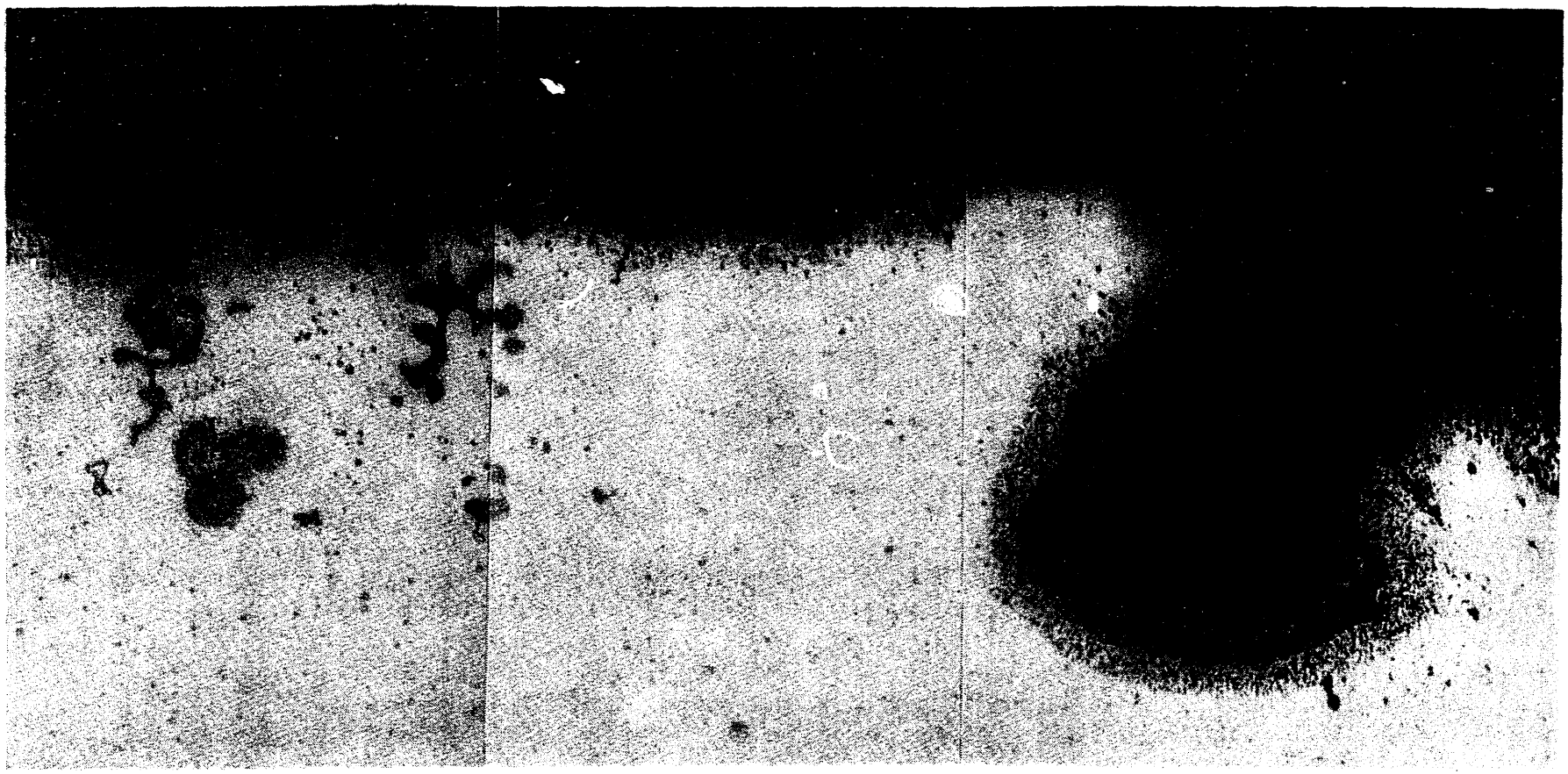

Figure C-39. ROIs 91M187, 91M186, and 91M185, respectively, displaying phase transition views (three-photo composite).

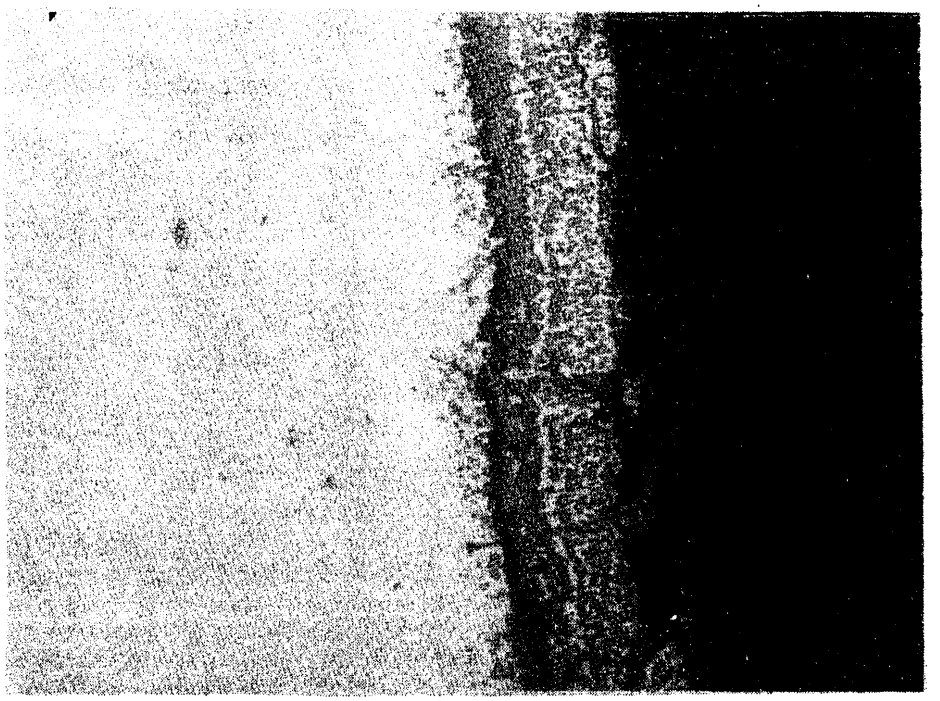

Figure C-40. ROI 91M188, showing 200x magnification of surface oxide layer.

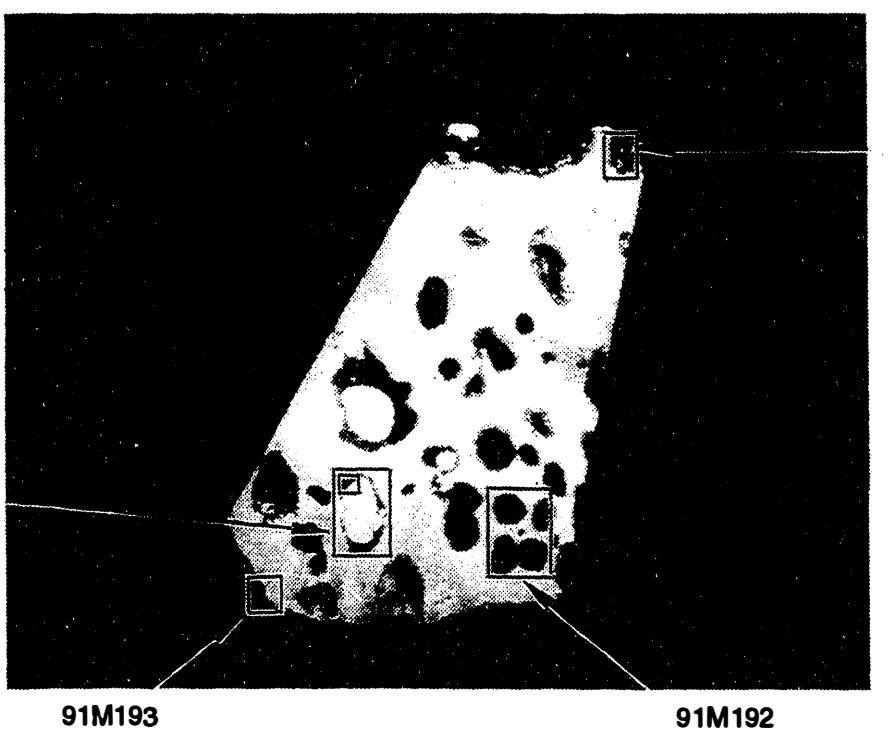

Figure C-41. Metallographic examination map showing ROIs of sample E-7-2.

Figure C-42. ROI 91M189, showing pore material at 50x.

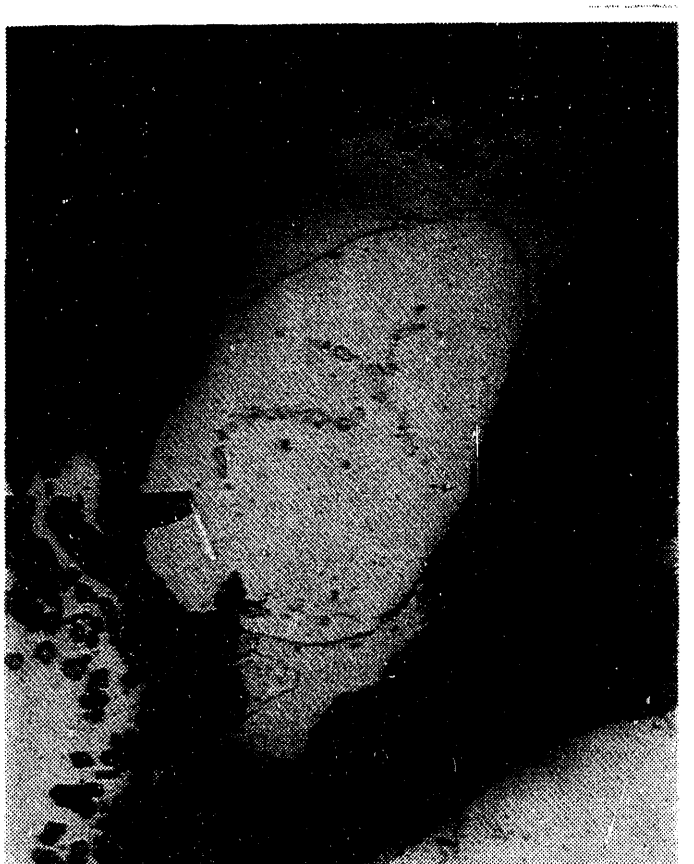

Figure C-43. ROI 91M190, showing higher magnification of top-left corner of Figure C-42.

Figure C-44. ROI 91M191 at 100x showing phase interface.

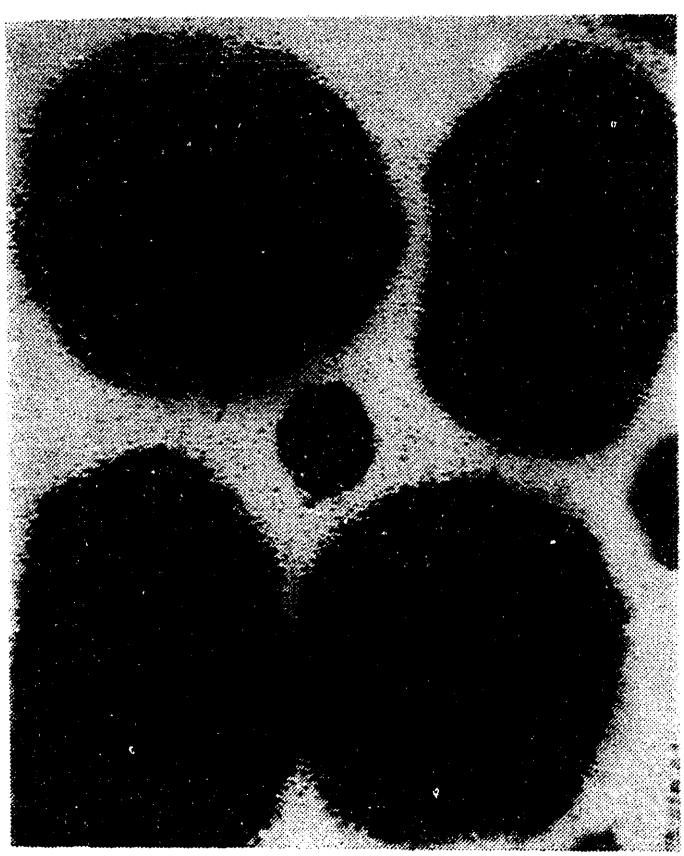

Figure C-45. ROI 91M192, displaying macro view of typical sample porosity.

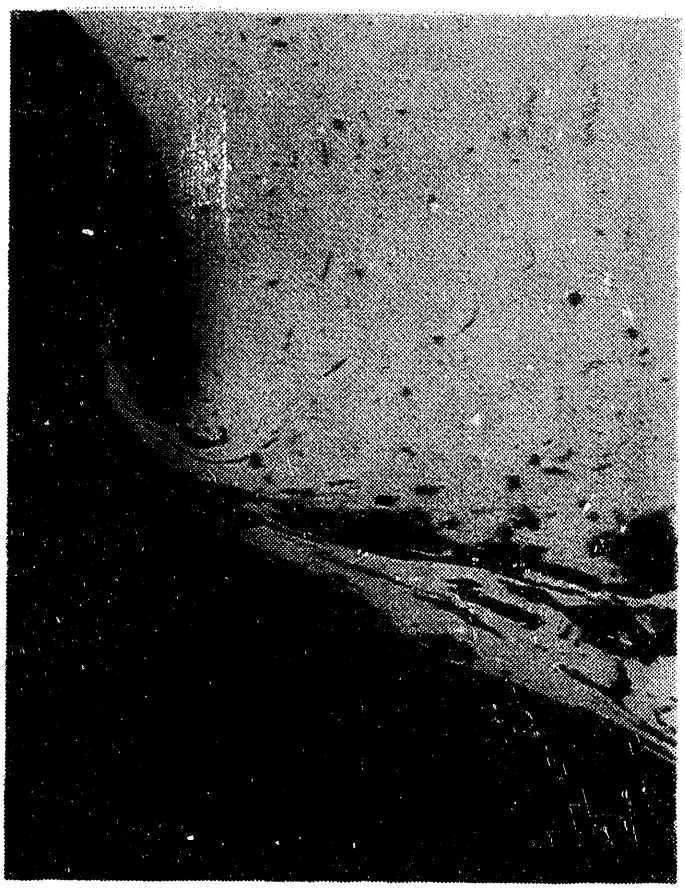

Figure C-46. ROI 91M193 at 200x, showing distinctive interface.

Appendix D

SEM and WDX Examination Results

Appendix D

SEM and WDX Examination Results

Samples of surface debris were removed from several nozzles (i.e., M-10, E-7, R-7, and G-5) and were examined using SEM and WDX techniques. Only representative results from the R-7 and E-7 samples are shown. Figure D-1 shows a cross section of the bulb removed from R-7, and Figure D-2 shows a backscattered electron (BSE) image of the same surface. As indicated in the BSE image, there are two primary phases present: a uranium phase (the light colored region), which is adjacent to the instrument string (the darker material). Figure D-3 is an expanded view of the interface between the fuel and the structural material, and D-4 is the BSE image of the interface. Examination of the U dot map (Figure D-5) indicates that the high Z (atomic number) phase on the right is primarily a $(U,Zr)O_2$ matrix. In contrast, Figure D-6 shows that Zr is evenly distributed throughout the matrix in both phases and suggests that the U and Zr did not relocate as $(U,Zr)O_2$ or that some phase separation has occurred. Figures D-7 through D-9 show the dot maps for Cr, Mn, and Fe, respectively. These dot maps suggest that the Cr was concentrated in the Zr phase and that iron oxides were present in both the Zr and U phases.

In contrast to the apparent composition discussed in the previous paragraph, a second location of R-7 is shown in Figure D-10. This is a magnified view of the bottom edge of Figure D-1 and shows the area around an instrument string. Figure D-11 shows the BSE image and indicates the presence of fuel material around the outer edge of the instrument string. Figures D-12 through D-16 indicate that this phase is composed of U, Fe, Cr, Mn, and Ni. However, as shown in Figure D-17, there is little or no apparent Zr present. These dot maps suggest that uranium phases are being formed with elements other than Zr and that, consequently, some low temperature eutectics are being formed.

Figure D-18 shows a BSE compositional image of a pore in sample E-7, as shown in Figures C-29 and C-30 in Appendix C. The BSE image indicates the presence of high Z material at the interface of the pore. Figures D-19 through D-20 show expanded views of the high Z material. Figure D-22 shows a Fe dot map, which indicates that these particles are Fe that has penetrated into the surface of E-7. In addition, Figure D-23 shows the presence of some Cd. The presence of Cd suggests that this material did not reach high temperatures or the highly volatile Cd would have been released from the melt. The dot map shown in Figure D-24 indicates that, in addition to the standard constituents of inconel, Zr was also present and had penetrated into the surface of sample E-7. Figure D-25 is a Cr dot map of sample E-7.

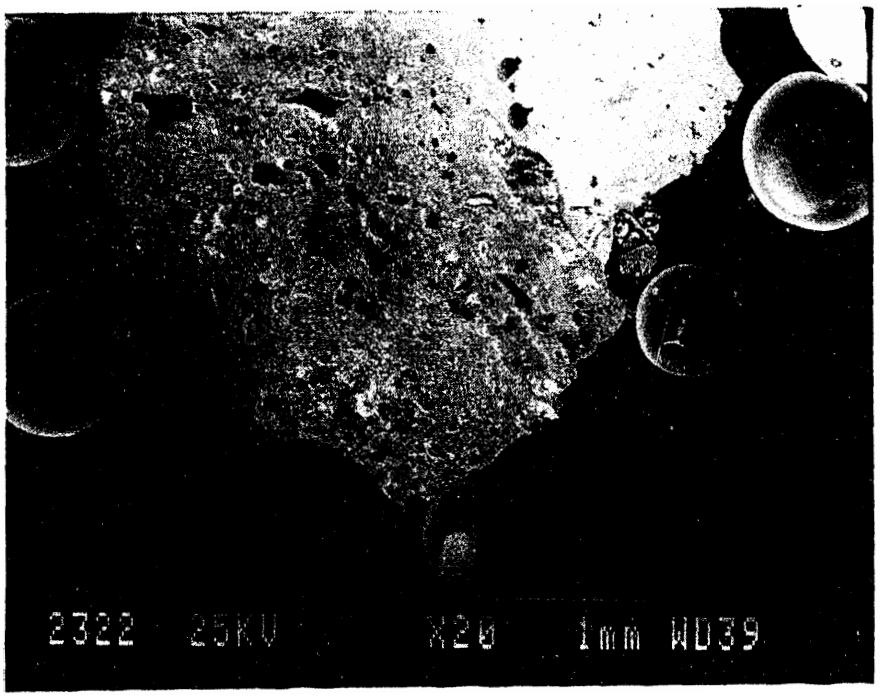

Figure D-1. R-7 Nozzle cross section at 1,000 micron.

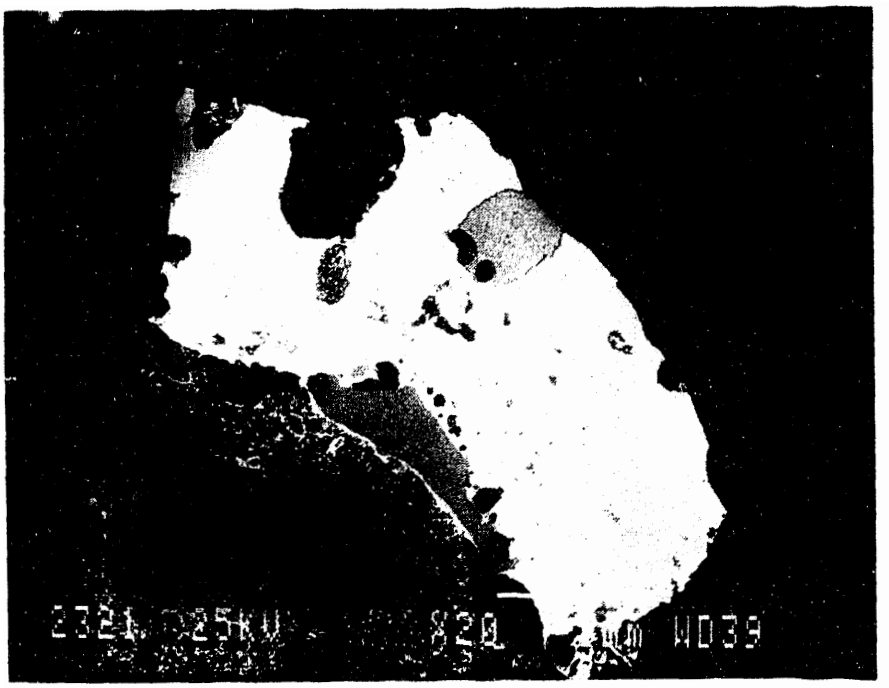

Figure D-2. BSE photograph of R-7.

Figure D-3. R-7 Uranium and structural material interface (100x).

Figure D-4. Compositional photo of U and structural material interface (100x).

Figure D-5. R-7 dot map of U.

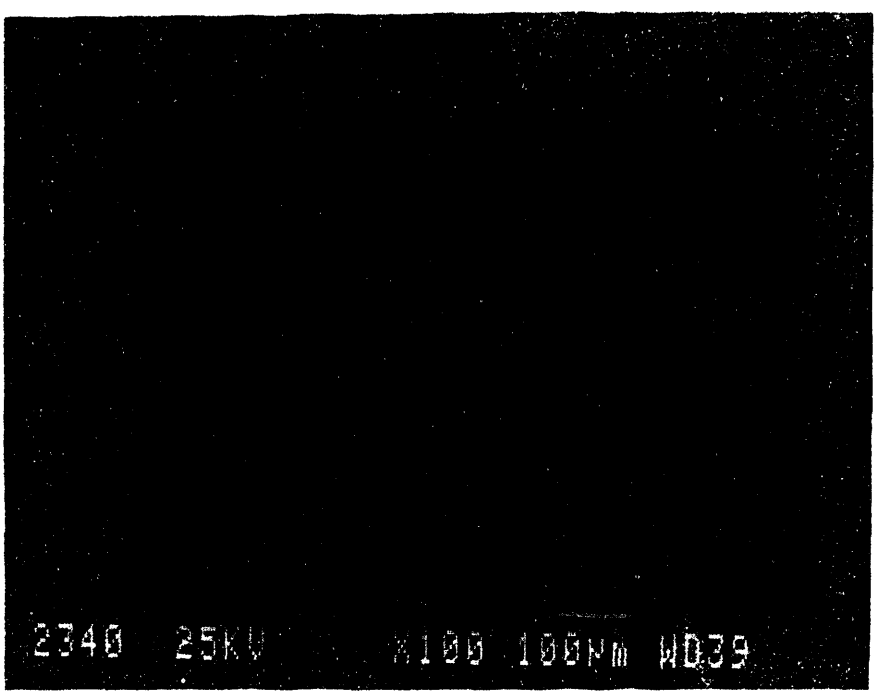

Figure D-6. R-7 dot map of Zr.

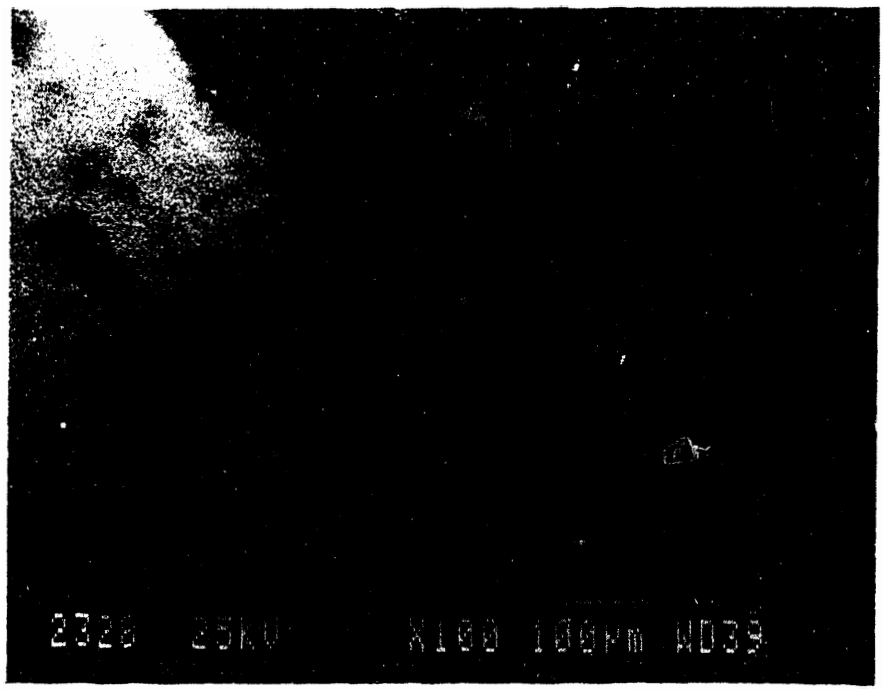

Figure D-7. R-7 dot map of Cr.

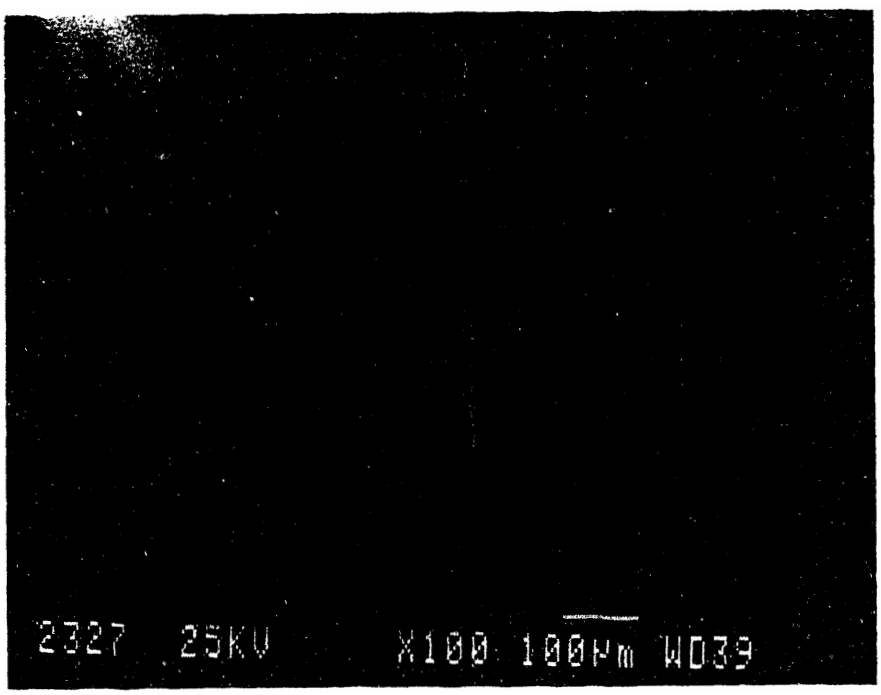

Figure D-8. R-7 dot map of Mn.

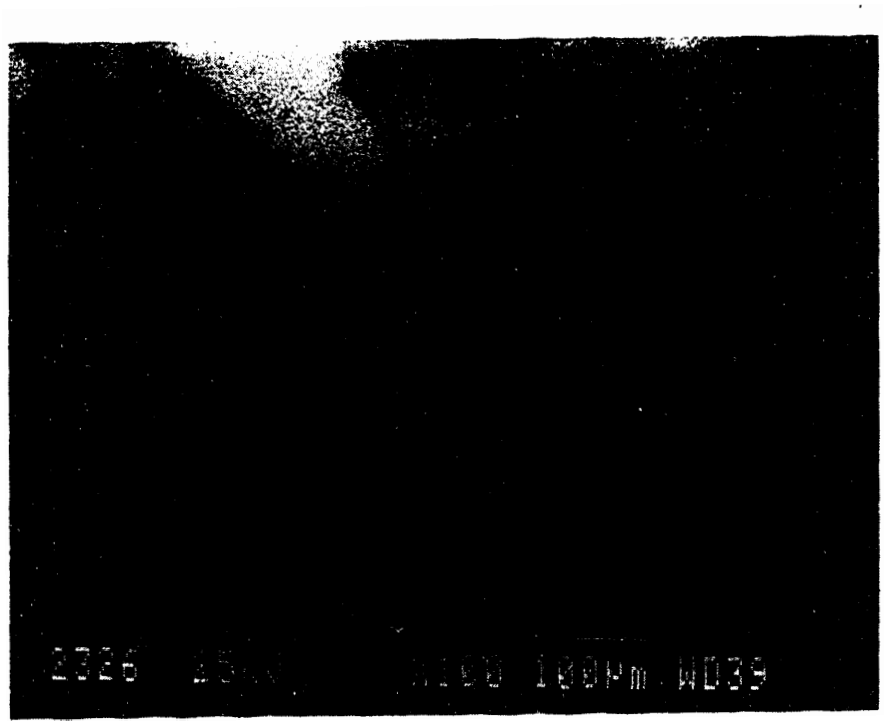

Figure D-9. R-7 dot map of Fe.

Figure D-10. R-7 instrument string interface.

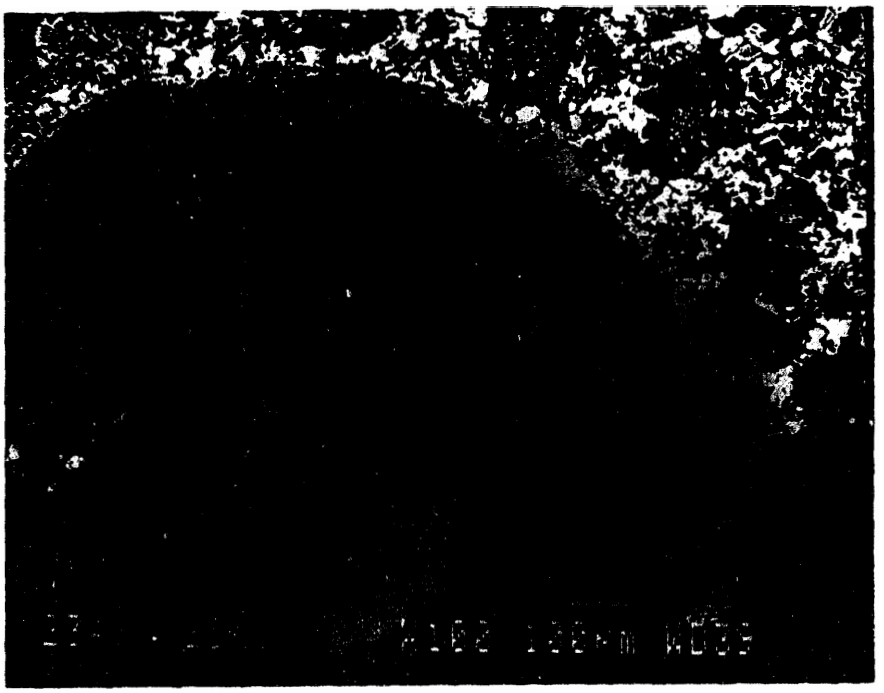

Figure D-11. R-7 instrument string compositional photomicrograph.

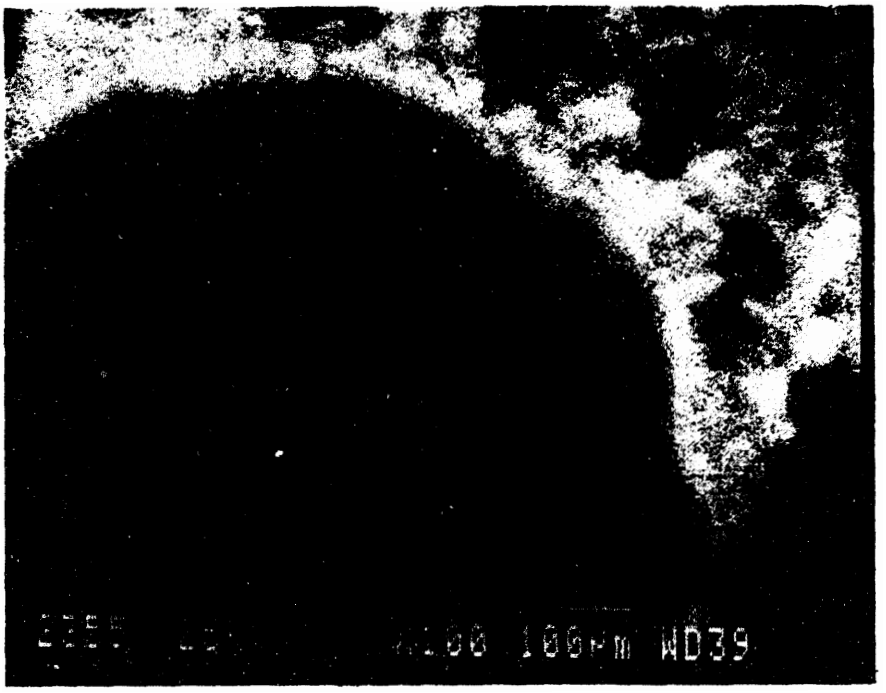

Figure D-12. R-7 instrument string dot map of U.

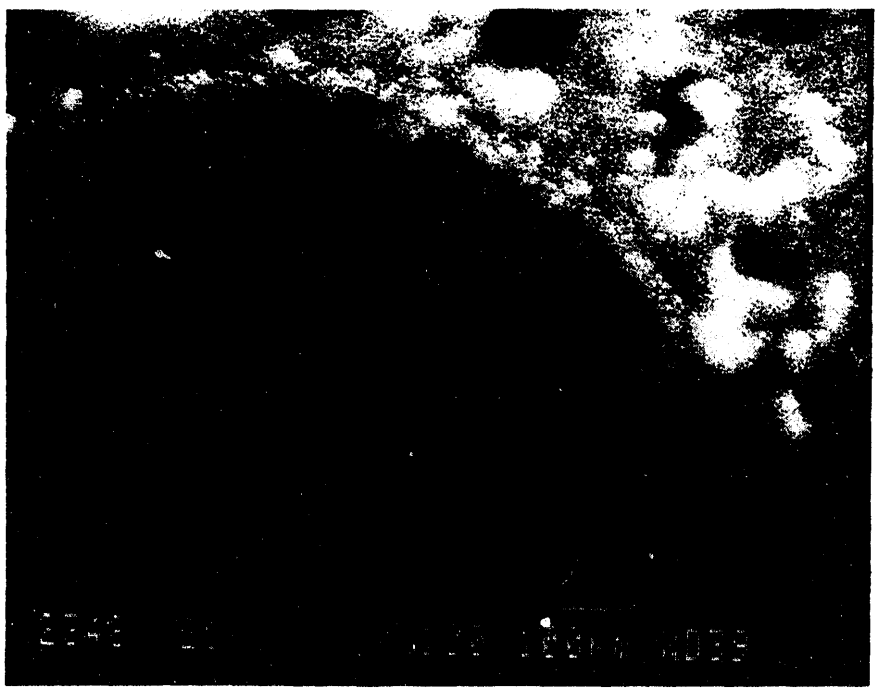

Figure D-13. R-7 instrument string dot map of Fe.

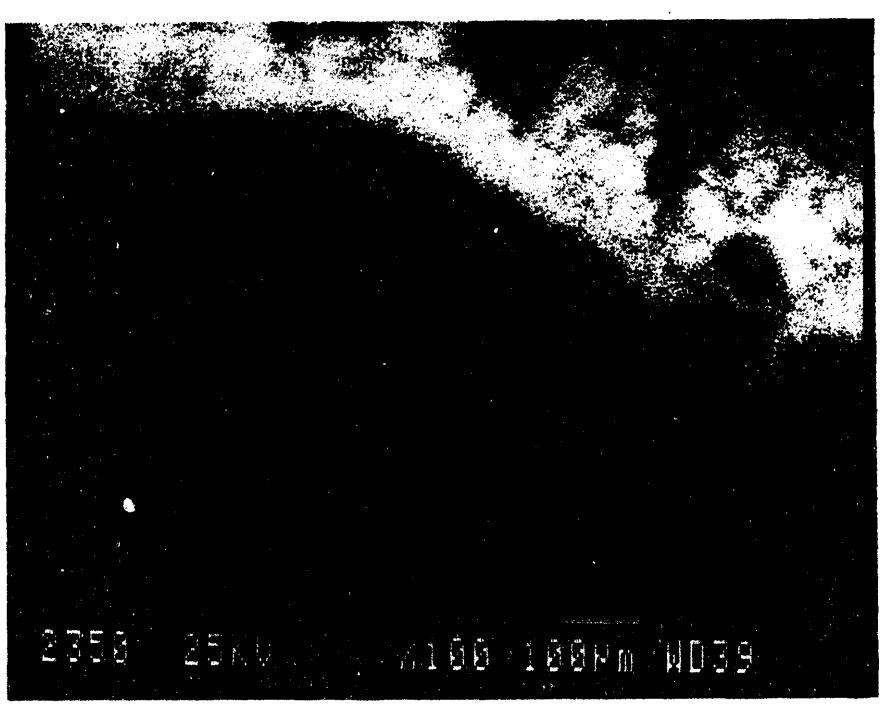

Figure D-14. R-7 instrument string dot map of Cr.

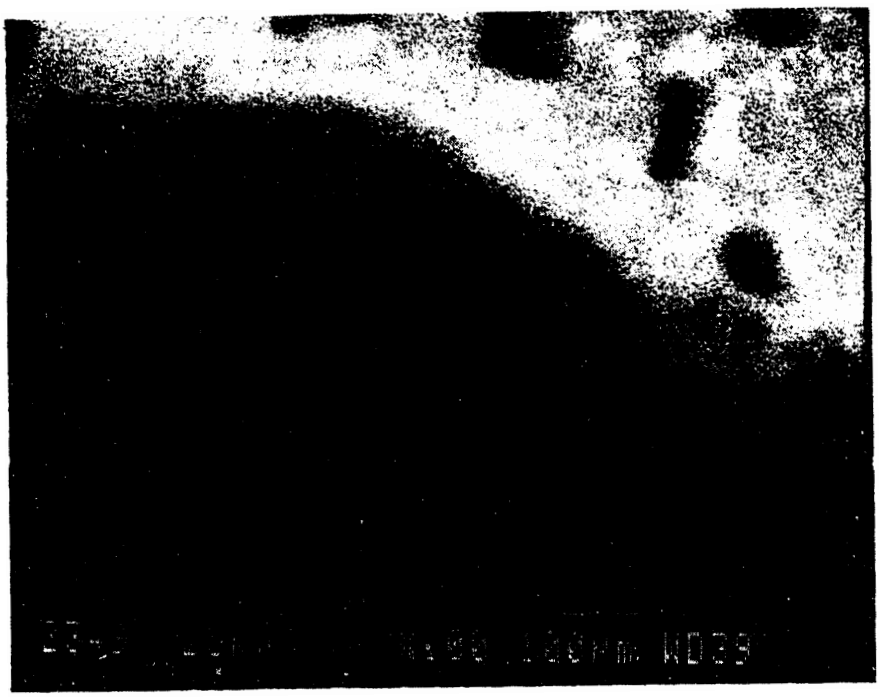

Figure D-15. R-7 instrument string dot map of Mn.

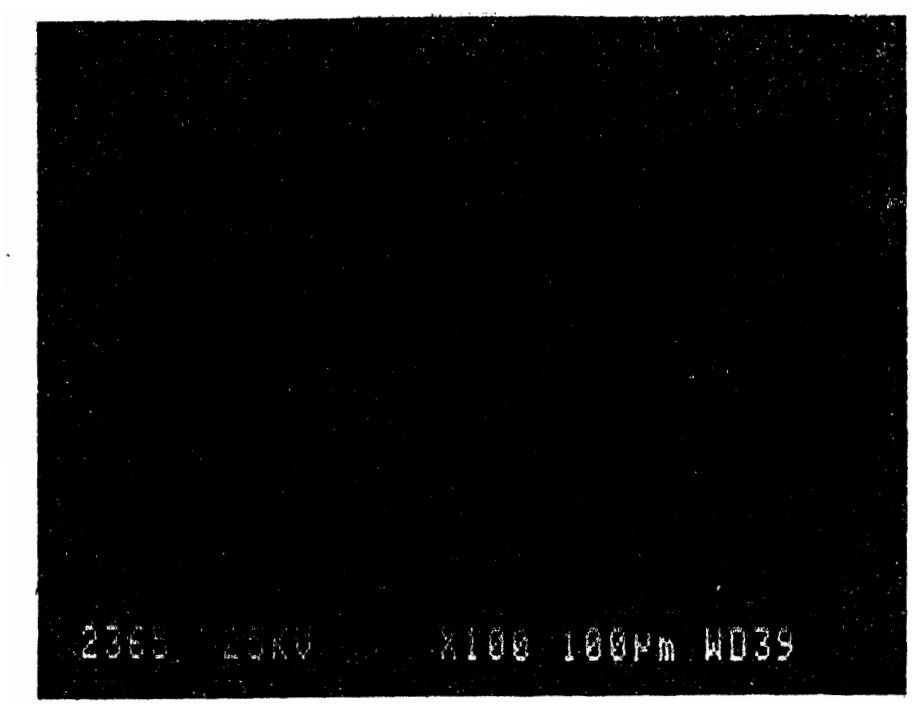

Figure D-16. R-7 instrument string dot map of Ni.

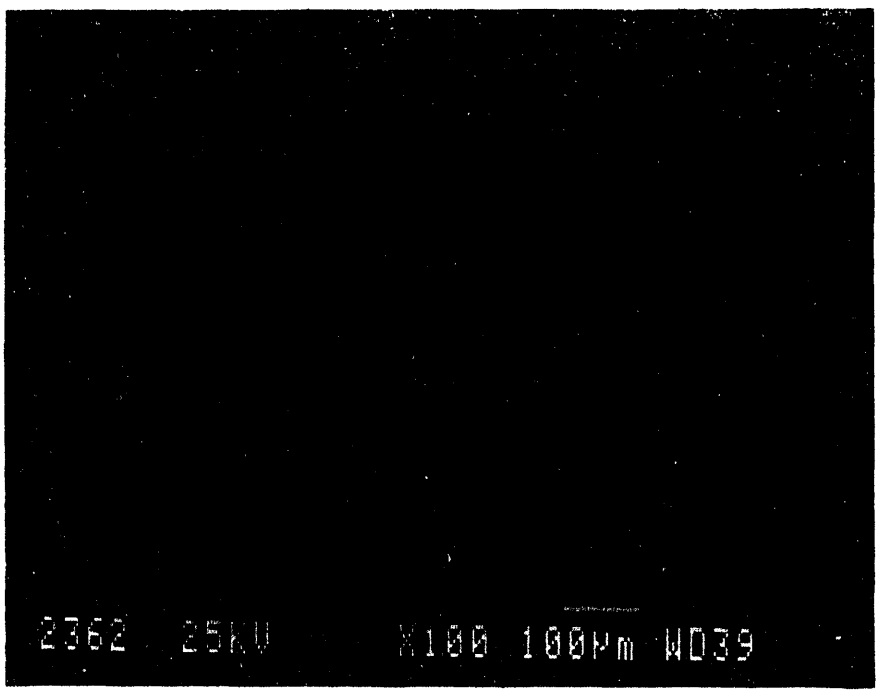

Figure D-17. R-7 instrument string dot map of Zr.

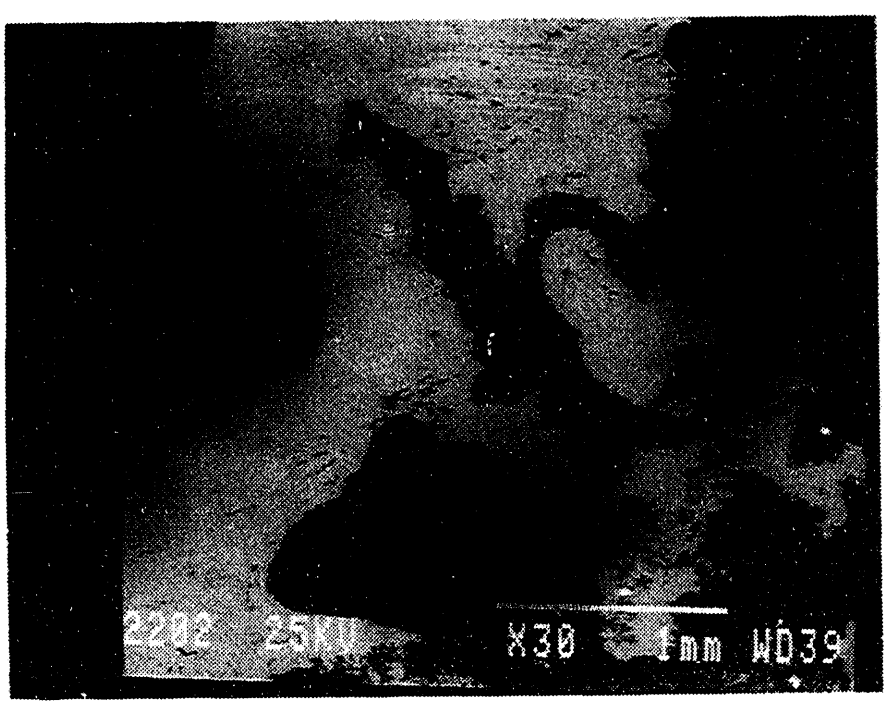

Figure D-18. E-7 cross section compositional (30x).

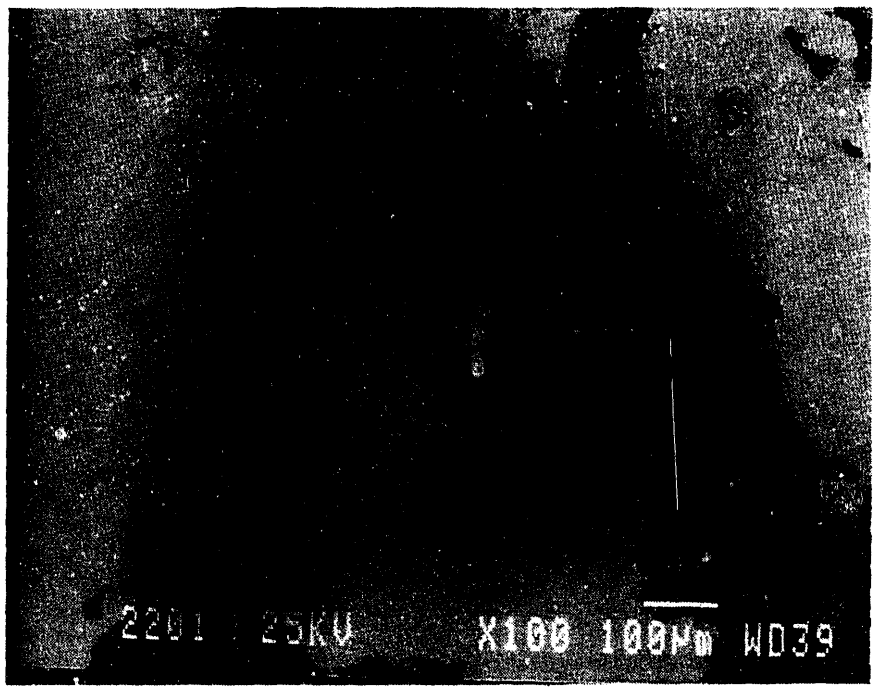

Figure D-19. E-7 cross section compositional (100x).

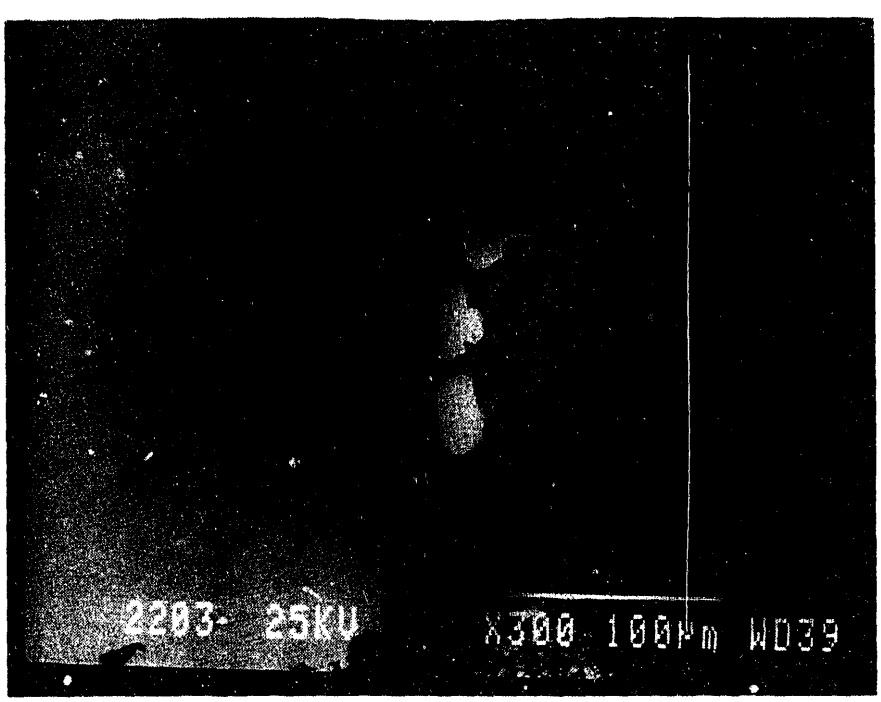

Figure D-20. E-7 cross section compositional (300x).

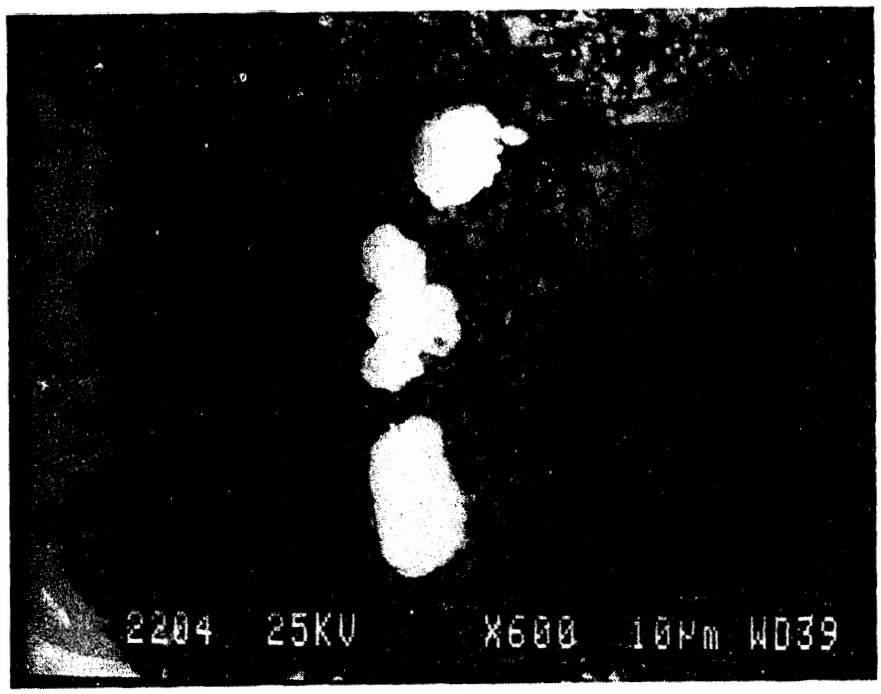

Figure D-21. E-7 cross section compositional (600x).

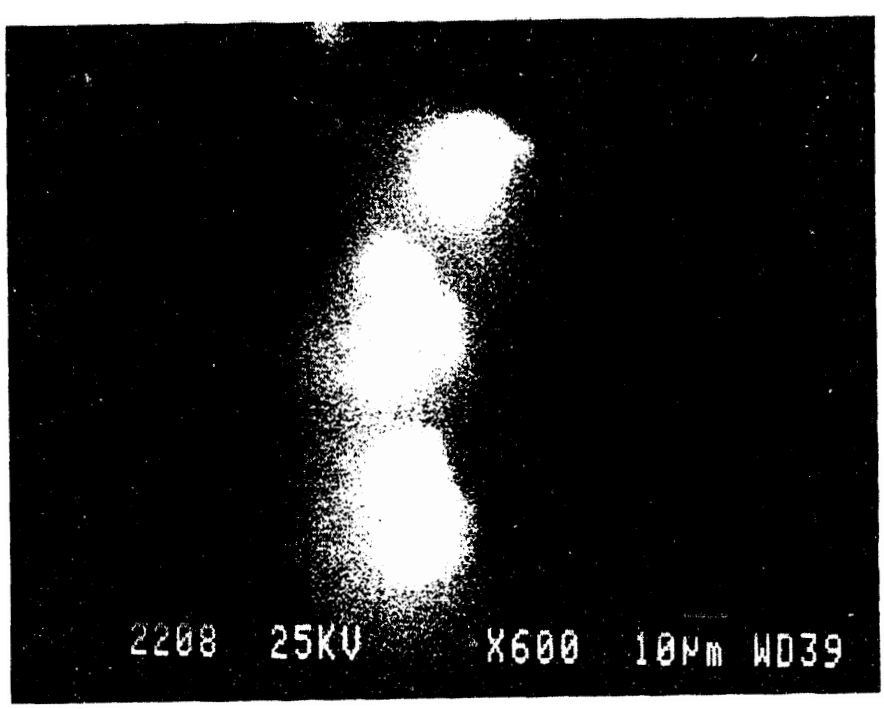

Figure D-22. E-7 dot map of Ag.

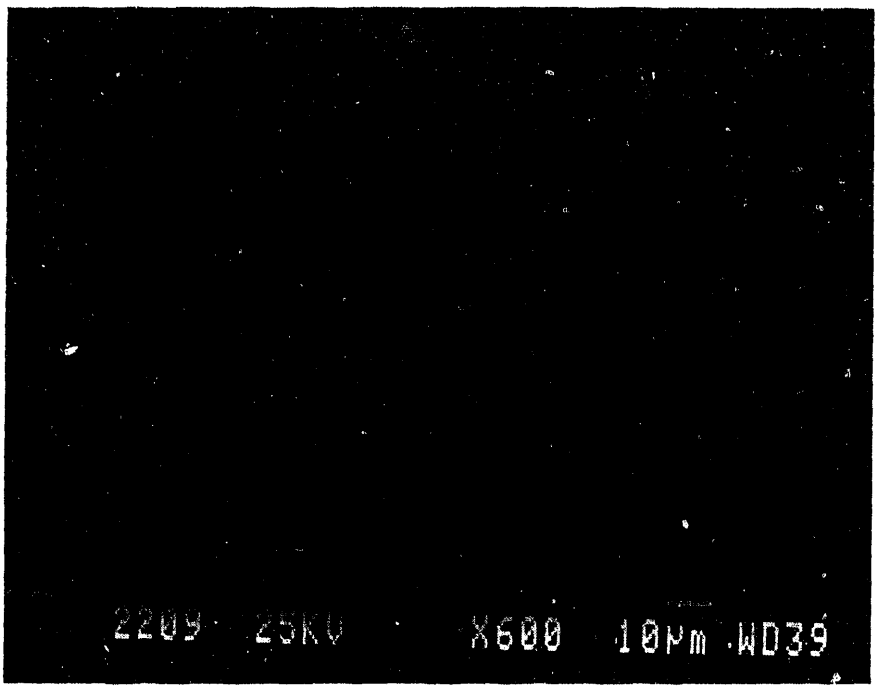

Figure D-23. E-7 dot map of Cd.

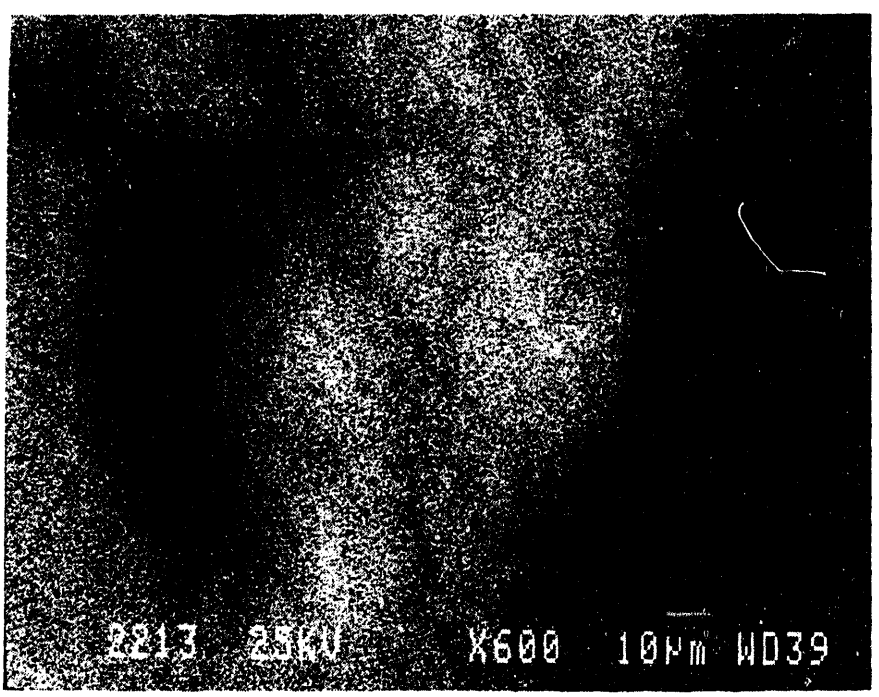

Figure D-24. E-7 dot map of Zr.

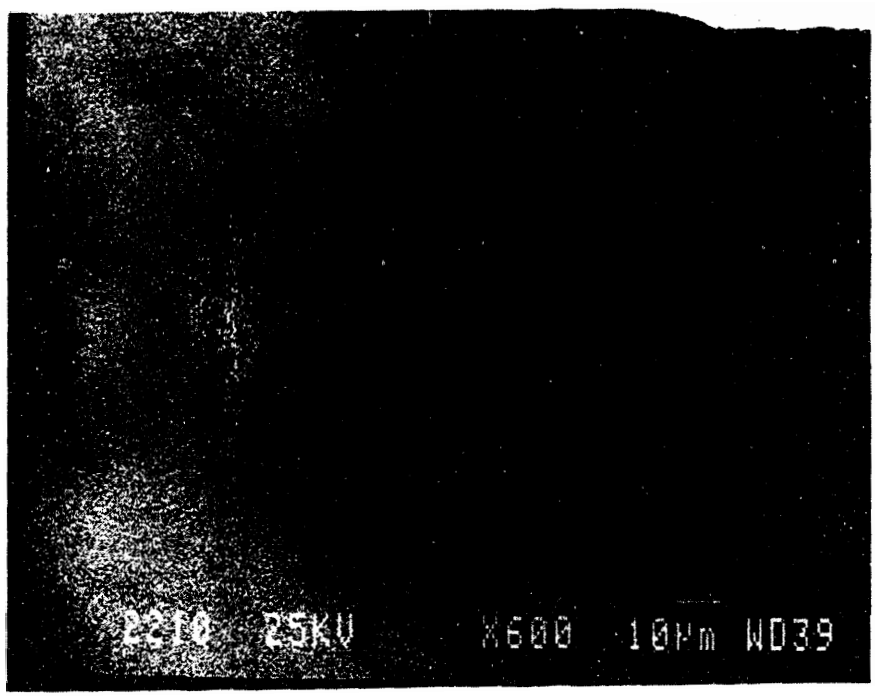

Figure D-25. E-7 dot map of Cr.

NRC FORM 335 (2-89) NRCM 1102, 3201, 3202

U.S. NUCLEAR REGULATORY COMMISSION

BIBLIOGRAPHIC DATA SHEET

(See instructions on the reverse)

1. REPORT NUMBER (Assigned by NRC. Add Vol., Supp., Rev., and Addendum Numbers, if any.)
NUREG/CR-6198
TMI V(94)EG01
EGG-2735

2. TITLE AND SUBTITLE
TMI-2 Instrument Nozzle Examinations Performed at the INEL

3. DATE REPORT PUBLISHED
MONTH: March
YEAR: 1994

4. FIN OR GRANT NUMBER
L1004

5. AUTHOR(S)
D. W. Akers, B. K. Schuetz

6. TYPE OF REPORT
Technical

7. PERIOD COVERED (Inclusive Dates)

8. PERFORMING ORGANIZATION – NAME AND ADDRESS (If NRC, provide Division, Office or Region, U.S. Nuclear Regulatory Commission, and mailing address; if contractor, provide name and mailing address.)

EG&G Idaho, Inc.
Idaho Falls, ID 83415

9. SPONSORING ORGANIZATION – NAME AND ADDRESS (If NRC, type "Same as above"; if contractor, provide NRC Division, Office or Region, U.S. Nuclear Regulatory Commission, and mailing address.)
Division of Engineering
Office of Nuclear Regulatory Research
U.S. Nuclear Regulatory Commission
Washington, D.C. 20555-0001

10. SUPPLEMENTARY NOTES

11. ABSTRACT (200 words or less)

As part of the Three Mile Island Unit 2 (TMI-2) Vessel Investigation Project, under the auspices of the Organization for Economic Cooperation and Development, examinations were performed at the Idaho National Engineering Laboratory on eight nozzles and one guide tube from the TMI-2 reactor vessel. This document describes the examination methodology, summarizes the examination results, and presents interpretations of the results as they relate to the damage to the reactor vessel and to the development of a core relocation scenario. Not all examinations originally proposed as part of this program were completed due to facility problems at the INEL. Consequently, only the results of completed aspects of the examination program are presented.

12. KEY WORDS/DESCRIPTORS (List words or phrases that will assist researchers in locating the report.)
TMI-2, Nuclear Material, Core Materials Behavior, Reactor Material Interactions

13. AVAILABILITY STATEMENT
Unlimited

14. SECURITY CLASSIFICATION
(This Page)
Unclassified
(This Report)
Unclassified

15. NUMBER OF PAGES

16. PRICE

NRC FORM 335 (2-89)

DATE
FILMED
5/16/94
END